UNIVERSIDAD DE CHILE
FACULTAD DE CIENCIAS FÍSICAS Y MATEMÁTICAS
DEPARTAMENTO DE INGENIERÍA CIVIL

IMPACT OF SHEAR IN COMPUTING P – Y CURVES FOR A RC PILE

MEMORIA PARA OPTAR AL TITULO DE INGENIERO CIVIL

EDUARDO ANTONIO NÚÑEZ PEZO

PROFESOR GUÍA:
LEONARDO MASSONE SÁNCHEZ

MIEMBROS DE LA COMISIÓN:
FERNANDO YÁÑEZ URIBE
ANNE LEMNITZER

SANTIAGO DE CHILE
JUNIO 2013

RESUMEN

Estudios realizados por Stewart et al, 2007, y posteriormente por Lemnitzer et al, 2013, han mostrado que para una pila con restricción al giro en el cabezal (Fixed – Head) los desplazamientos por esfuerzo de corte pueden llegar a contribuir en un 40% de los desplazamientos totales, a nivel de terreno, y sugieren que el efecto de corte influye en la determinación de curvas p – y. De esta forma, se ha utilizado un modelo de interacción corte – flexión para estimar el efecto del corte en la determinación de las curvas p – y, modelo inicialmente propuesto por Massone et al, 2006, para el análisis de muros de H.A, extendiéndolo en este trabajo para el análisis de columnas.

Dada la geometría de la pila, distintas versiones del modelo de interacción se han validado utilizando la respuesta global carga – desplazamiento de ensayos de columnas circulares recopiladas de la base de datos de PEER, 2011, y de Kawashima Lab, 2011, estudiando la respuesta en términos de rigidez, capacidad máxima y desplazamiento al 10% de degradación de capacidad. Estos especímenes fueron seleccionados de forma de observar degradación por corte en la respuesta. Se ha encontrado buena correlación tanto en rigidez como en capacidad, teniendo valores de razón promedio entre el modelo y el ensayo de (V_{mod}/V_{exp}) 0.91 para la capacidad máxima y de (K_{mod}/K_{exp}) 1.3 para la rigidez, con coeficientes de variación de 0.09 y 0.18, respectivamente, usando el modelo de interacción con un perfil calibrado de deformaciones laterales o expansión (ε_x). Al estudiar la degradación, se ha observado buena correlación al utilizar una discretización en la dirección longitudinal con una razón diámetro – largo del elemento (D/h_{st}) igual a 2.0, obteniendo así un valor promedio de ($\delta_{mod}/\delta_{exp}$) 0.86 con un coeficiente de variación de 0.38. El modelo de flexión, por su parte, entrega valores de (V_{mod}/V_{exp}) igual a 1.1 y (K_{mod}/K_{exp}) igual a 1.9. No se consideró el análisis de ($\delta_{mod}/\delta_{exp}$) por no observar degradación en 6 de 10 casos a grandes deformaciones ($\delta_{mod}/\delta_{exp} \gg 2$).

Las curvas p – y fueron determinadas para un ensayo de una pila Fixed – Head, realizado por Stewart et al, 2007, utilizando un procedimiento de ajuste de la respuesta global de un modelo de flexión y a su vez de un modelo de interacción. Se utilizó la forma base de las curvas p – y propuestas por API (1993) para una arcilla dura, como una respuesta trilineal. Los resultados muestran que para la curva p – y ubicada en la superficie de terreno, la razón entre modelo de flexión e interacción es de (p_{u_Flex}/p_{u_inter}) igual a 0.67 para la resistencia última y de (K_{Flex}/K_{inter}) igual a 0.77 para la rigidez inicial. Los desplazamientos por corte contribuyen en un 35% de los desplazamientos totales, para un desplazamiento lateral de 3.0 in a nivel de terreno.

Adicionalmente, se realizaron análisis de sensibilidad, en donde se determinó que el efecto de corte está concentrado entre la superficie de terreno y una profundidad de 2 diámetros (48 in) y además, se mostró que aumentando al doble la armadura transversal en esta zona se logra aumentar la capacidad en un 7%, para un desplazamiento de 3.0 in, y aumentar la ductilidad de la pila en un 50%. En este caso las deformaciones por esfuerzo de corte contribuyen en un 13% de los desplazamientos totales, para un desplazamiento lateral de 6.0 in, que es el punto en donde se observa degradación.

ABSTRACT

Prior studies developed by Stewart et al, 2007, and Lemnitzer et al, 2013, have shown that for a pile with rotation restrained at the top (Fixed – Head), shear displacements can contribute up to 40% of total displacements, at ground line, and suggest that shear effect would affect the calculation of p – y curves. Thus, a shear – flexure interaction model has been used in order to assess the effect of shear in computing p – y curves of the soil, model proposed by Massone et al, 2006, originally formulated for RC walls is extended for column analysis.

The interaction model, with different assumptions have been validated using the total load – displacement response of column tests provided in the database of PEER, 2011, and Kawashima Lab, 2011, studying the response in terms of rigidity, strength and displacement at 10% of strength degradation. The specimens were selected in order to observe shear degradation in the response. It was found good correlation when predicting rigidity and also strength, where the mean values of model over test ratio were (V_{mod}/V_{exp}) 0.91 for strength and (K_{mod}/K_{exp}) 1.3 for rigidity, with standard deviations of 0.09 and 0.18, respectively, using the interaction model with a calibrated profile of lateral strains or expansion (ε_x). It was observed good correlation in degradation when using a longitudinal discretization of diameter – element length ratio (D/h_{st}) of 2, thus obtaining a mean value of ($\delta_{mod}/\delta_{exp}$) 0.86 with a standard deviation of 0.38. Flexure model give values of (V_{mod}/V_{exp}) equal to 1.1 and (K_{mod}/K_{exp}) equal to 1.9. The analysis of ($\delta_{mod}/\delta_{exp}$) is not considered, because shear degradation was not observed in 6 of 10 cases at large displacements ($\delta_{mod}/\delta_{exp} \gg 2$).

The p – y curves were calculated for the Fixed – Head pile test performed by Stewart et al, 2007, using a fitting procedure of the global response of the flexural model and also for the interaction model. The base p – y curves shape proposed by API (1993) for a stiff clay, as a tri – linear response, were used for this purpose. The results show that for the p – y curve located at ground line, the flexure over interaction model ratio is (p_{u_Flex}/p_{u_inter}) equal to 0.67 for ultimate capacity and (K_{Flex}/K_{inter}) equal to 0.77 for initial rigidity. Shear displacements contributed up to 35% of the total displacements, at ground line.

In addition, sensitivity analyses were performed, where it was found that the effect of shear is concentrated between ground line and a pile depth of 2 diameters (48 in). It was also shown that doubling the transverse reinforcement in this zone increases the capacity in 7%, at a lateral displacement of 3.0 in, and ductility is increased in 50%. Shear displacements contribute up to 13%, at a lateral displacement of 6.0 in, where degradation is observed.

AGRADECIMIENTOS

Quiero poner en la cúspide de mis agradecimientos a mi hermosa familia, quienes han visto de cerca este largo proceso y han sido los pilares fundamentales en mi desarrollo como ser humano y como profesional. A mi padre José, por enseñarme que el conocimiento es lo más esencial y por motivarme a superarme a mí mismo; a mi madre Juanita, por darme el cariño y apoyo a la distancia, por estar siempre pendiente de mi bienestar y de que nada me hiciera falta; a mi hermano Daniel y su esposa Jimena por hacerme tío de un niño tan hermoso e inteligente como Josecito y por darme momentos de alegría que me permitieron llevar de mejor manera los momentos más difíciles. Además, quiero agradecer a mis tatas, tíos y tías, primos y primas, con los cuáles viví momentos inolvidables durante estos años, sin ellos nada podría haber sido tan maravilloso como lo fue. Quiero hacer un recuerdo especial a mi querida abuelita Luisa, madre de mi madre, que fue una mujer muy leal y devota a su familia. Me gustaría haber compartido en vida este logro con ella y por eso este trabajo va dedicado a ella en forma muy especial.

Quiero dar mis más cariñosos agradecimientos a dos señoritas hermosas que fueron muy importantes en mi proceso de titulación. A mi polola Adriana, y su pequeña hija Emilia. A Adriana por ser una mujer tan especial, tan culta e interesante, por tener tantas aptitudes y seguir siendo tan humilde, porque además todas nuestras conversaciones son interesantes y porque compartimos una devota pasión por la música. Su amor y su apoyo, la motivación y el soporte que me brindó fueron fundamentales en los momentos más difíciles. A la “Emily” por su encanto, su alegría de niña y sus ojitos despiertos y descubridores y por esos abrazos gritando “Tío Gato!” con alegría. Mis dos niñas me han hecho el hombre más feliz en este último año y medio y espero seguir compartiendo mi vida con ellas siempre.

Quiero agradecer a mis amigos más cercanos, a los de la U y también los de San Fernando, en especial a Oriel Núñez, Juan Pablo Valenzuela, Sebastián Tapia, Javier Salcedo y Jaime Medina, con quienes nos hicimos “yuntas” desde primer año y aún nos seguimos juntando y pasándola bien, y a mis amigos Agustín Guzmán y Cristian Espinoza, a quienes conozco hace más de 10 años y con quienes tuve la oportunidad de convivir en Santiago. Solo ellos saben lo que es llegar sin ni un peso a fin de mes y con el refrigerador y la despensa vacía, ellos también vieron como me quemaba las pestañas estudiando hasta tarde y fueron capaces de hacerme reír cuando estaba cansado y triste, por eso los quiero y porque han sido mis confidentes y consejeros por muchos años.

Quiero agradecer a mi profesor guía, Leonardo Massone, por la oportunidad y por la enorme paciencia que tuvo conmigo en la realización de esta memoria de título. Fue un interesante desafío y agradezco mucho la posibilidad de haber conocido el trabajo de él junto a la Srta. Anne Lemnitzer. Espero que mis aportes en esta memoria les sean de utilidad en futuros trabajos.

Finalmente, quiero decir que ser un alumno de la *fcfm* es una tremenda experiencia. Hay que tener una resistencia enorme, sin duda. Sin embargo, hoy al final de este proceso puedo decir que estoy sumamente satisfecho y orgulloso de haber pasado por estas salas de clase y haber conocido a tanta gente, profesores y compañeros, de haber tenido la oportunidad de estar junto a ellos en la lucha por la educación. Sencillamente, esta gente maravillosa hizo de mi paso por la universidad una experiencia inolvidable.

CONTENTS

INDEX OF FIGURES

INDEX OF TABLES

CHAPTER 1. Introduction

1.1. Introduction

Cast – In – Drilled – Holes (CIDH) shafts are support elements used in highways and bridges. The behavior of these types of structures is controlled by the properties of the shaft and the surrounding soil. For good estimation of the response of these elements, it is necessary to consider the interaction between the shaft and the soil by using a proper model. A pile nonlinear beam – column finite element model along with a p – y curves approach, for the soil, is commonly used to assess this interaction.

Prior test was conducted on a 24 in diameter Fixed – Head pile, with an embedded length of 600 in, in order to predict soil – structure interaction (Stewart et al, 2007) and calculating the p – y curves of the soil using the test profiles. For this case, a uniaxial fiber model was used to model the RC elements. Later, a model that couples the shear and axial – bending behavior was applied for the analysis, using the p – y curves obtained by Stewart et al, 2007. It was found that for a Fixed – Head pile (rotation restrained) the shear displacements are contributing up to 40% of the total displacements, suggesting that nonlinear shear deformations should be considered when modeling a Fixed – Head pile, and that an appropriate sensor layout should be used to capture shear deformation when deriving p – y curves from field measurements (Lemnitzer et al, 2013). A shear – flexure interaction model consists in a macroscopic fiber – based model where the fibers have a panel behavior, i.e., with axial deformations and angular distortions in the plane of the panel (Massone et al, 2006). Therefore, the model can integrate the resistance and rigidity degradation caused by shear (diagonal tension or compression), effect that the uniaxial fiber model does not integrate and may be relevant, depending on the shear – span ratio of the element or the restraining conditions.

The shear – flexure interaction model has been developed and applied for walls (Massone et al, 2006, Massone et al, 2009, Massone, 2010) for different conditions of axial load, longitudinal and transversal reinforcement ratio and shear – span ratios. It has also been extended for its use in beam elements (Galleguillos, 2010, Gotschlich, 2011), and is used here for the analysis of columns.

1.2. Objectives

The main objective of this work is to assess the effect of shear in the calculation of p – y curves for a RC pile test, in terms of the ultimate resistance and initial rigidity of p – y curve. To accomplish this, first, a fiber – based model that couples shear and axial – bending behavior will be validated for RC columns tests, for different shear – span, reinforcement and axial load ratios. The discretization of the cross section is studied for this purpose and the effect of the transversal reinforcement is to be assessed, in terms of confinement and effective shear force. Second, p – y curves should be characterized for a stiff, clayey soil, since the beam – column model will be applied along with the p – y curves approach. Finally, the effect of shear in the calculation of p – y curves will be assessed comparing the results with the ones obtained using a uniaxial fiber model.

1.3. Methodology

To achieve the objectives mentioned above the following steps are followed:

- The constitutive laws for the materials will be defined, for concrete in tension and compression and reinforcement steel. The uniaxial curves available in the literature will be considered here.

- The validity of the shear – flexure interaction model will be studied for its application on RC columns. The validation is performed using the model proposed by Massone et al, 2006, for walls, making an extension for columns. For this purpose, a set of columns tests provided by the PEER, 2011, and Kawashima Lab, 2011, databases are used. The load – displacement responses from the tests will be compared with the ones obtained from the analytical results.

- The constitutive laws should be defined for a stiff, clayey soil, in terms of the p – y curves, i.e., the soil resistance vs. displacement for a uniaxial spring representing a soil element. The API (1993) stiff clay p – y curve will be used for this purpose

- The shear – flexure interaction model will be calibrated to predict the response of a Fixed – Head pile. This calibration is performed using a fitting procedure of the p – y curves, based on a prior full scale test performed by Stewart et al., 2007, on a Fixed – Head pile.

1.4. Scope

CHAPTER 1: Introduction

The motivation of this work is presented along an introduction based on previous research on the shear – flexure interaction model. The objectives and methodology of this work is also presented.

CHAPTER 2: Constitutive Laws of Materials and p – y Curves Characterization

The constitutive laws for concrete and reinforcement steel are defined, based on the models available in the literature. The constitutive laws are defined for the surrounding soil, based on the p – y curves available in the literature. The application on piles is presented.

CHAPTER 3: Shear – Flexure Interaction Model

A detailed description of the flexure and shear – flexure interaction models are provided, based on previous research about the model. The extension of the model for RC columns is detailed in this part.

CHAPTER 4: Analysis of the Shear – Flexure Interaction Model on Columns

The shear – flexure interaction model is analyzed and validated for its application on RC columns, for a different shear – span, reinforcement and axial load ratios, comparing the analytical results with the tests available in the PEER, 2011, and Kawashima Lab, 2011, databases.

CHAPTER 5: Analysis of the Shear – Flexure Interaction Model on a Pile

A fitting procedure is performed to calculate the p – y curves of the surrounding soil, in order to represent the response of a prior full scale test performed on a Fixed – Head pile. The p – y curves are calculated using a flexure and a shear – flexure interaction models. The results are compared in terms of ultimate resistance and initial rigidity of the p – y curves.

CHAPTER 6: Conclusions

The conclusions of this work are presented.

CHAPTER 2. Constitutive Models of Materials and p-y Curves Characterization

2.1. Constitutive Models of the Materials

In this section, the stress – strain relationships for concrete (in tension and compression) and reinforcement steel are defined. These are the commonly used uniaxial relationships for monotonic load. The analysis is yet to be extended for cyclic response.

2.1.1. Constitutive Model for Concrete in Compression

The stress – strain relationships should consider the effects of biaxial compression softening (reduction of the principal stress due to cracking under tensile stress in the orthogonal direction) and tension stiffening (average post-peak tensile stresses in concrete due to the bonding of concrete and reinforcing steel between cracks) to obtain reliable results for the panel behavior, as proposed by Massone et al, 2006.

To describe the stress-strain behavior of concrete in compression, the Thorenfeldt - base curve, calibrated by Collins and Porasz, 1989, Wee et al, 1996, and Carreira and Kuang-Han, 1985, and updated via the introduction of the compression softening parameter proposed by Vecchio and Collins, 1993, is used. The Thorenfeldt base curve has the following expression (eq. 2.1.1):

$$\sigma_c = f_c' \cdot \frac{n \cdot \left(\frac{\varepsilon_c}{\varepsilon_0}\right)}{n - 1 + \left(\frac{\varepsilon_c}{\varepsilon_0}\right)^{n \cdot k}} \tag{2.1.1}$$

Where σ_c and ε_c are the stress and strain of the concrete in compression, respectively. The parameters f_c' and ε_0 are the maximum capacity for compression and the strain at f_c', respectively. Finally, the parameters n and k are shape factors of the ascending and descending curve.

The parameters n and k are proposed by Collins & Porasz, 1989, for relatively high resistance concrete ($f_c' > 20\ MPa$). These parameters have the following expressions (eq. 2.1.2 and 2.1.3)

$$n = 0.8 + \frac{f_c'(MPa)}{17} \tag{2.1.2}$$

$$k = \begin{cases} 1 & if\ 0 \le \varepsilon < \varepsilon_0 \\ 0.67 + \dfrac{f_c'(MPa)}{62} & if\ \varepsilon_0 < \varepsilon \end{cases} \tag{2.1.3}$$

This model intends to represent the panel behavior of a reinforced concrete element. Thus, it is necessary to consider the compression softening effect, which is the reduction of the compressive resistance due to tensile cracks in the orthogonal direction. To include this effect, Vecchio &

Collins, 1993, introduced the reduction factor of the compressive resistance, given by the following expression (eq. 2.1.4):

$$\beta = \frac{1}{0.9 + 0.27 \cdot \frac{\varepsilon_1}{\varepsilon_0}} \tag{2.1.4}$$

Where ε_1 is the principal tensile strain and the ratio $\varepsilon_1/\varepsilon_0$ is considered positive. The stress – strain relationship for concrete in compression is shown in Figure 2.1. The effect of parameter β is also shown in the same figure.

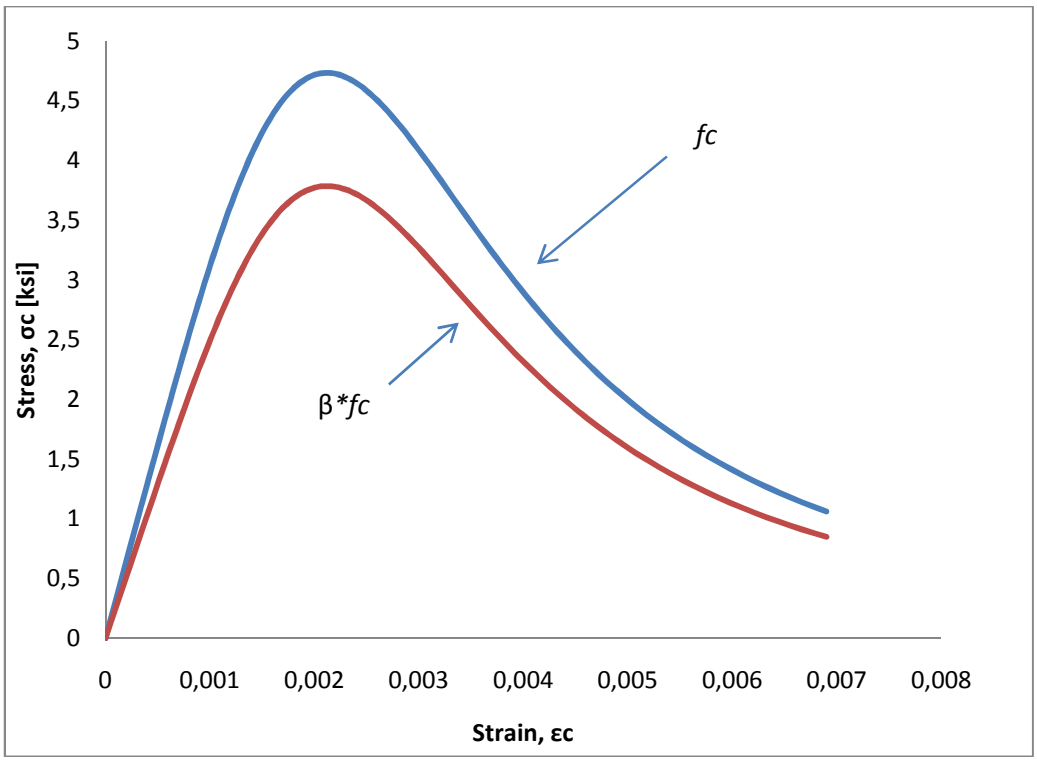

Figure 2.1: Concrete in compression model, Collins & Porasz (1989). Effect of parameter $\boldsymbol{\beta}$. $\boldsymbol{f'_c = 4.7\ [ksi]}$, $\boldsymbol{\varepsilon_0 = 0.00230}$, $\boldsymbol{\beta = 0.8}$

The value of ε_0 is calculated using the equation proposed by Wee et al, 1996, as recommended by Massone et al, 2006, and depends only on the peak compressive stress of concrete f'_c.

$$\varepsilon_0 = 0.00078 \cdot (f'_c(MPa))^{1/4} \tag{2.1.5}$$

2.1.2. Constitutive Model for Concrete in Tension

The model proposed by Belarbi & Hsu, 1994, is used to describe the behavior of concrete in tension, and also, to describe the interaction between the reinforcement bars and concrete on cracks (tension stiffening effect). The behavior of concrete in tension is described by the following expressions (eq.2.1.6):

$$\sigma_c = \begin{cases} E_c \cdot \varepsilon_c & if \ \ \varepsilon_c \leq \varepsilon_{cr} \\ f_{cr} \cdot \left(\frac{\varepsilon_{cr}}{\varepsilon_c}\right)^{\beta} & if \ \varepsilon_c > \varepsilon_{cr} \end{cases} \tag{2.1.6}$$

Where σ_c and ε_c are the tensile stress and strain of reinforced concrete, respectively. The parameters f_{cr} and ε_{cr} are the cracking stress and strain. The elastic modulus E_c and the cracking stress and strain f_{cr} and ε_{cr}, can be calculated using the following expressions proposed by Belarbi & Hsu, 1994:

$$E_c = 3917 \cdot \sqrt{f_c'(MPa)} \tag{2.1.7}$$

$$f_{cr} = 0.313 \cdot \sqrt{f_c'(MPa)} \tag{2.1.8}$$

$$\varepsilon_{cr} = 0.00008 \tag{2.1.9}$$

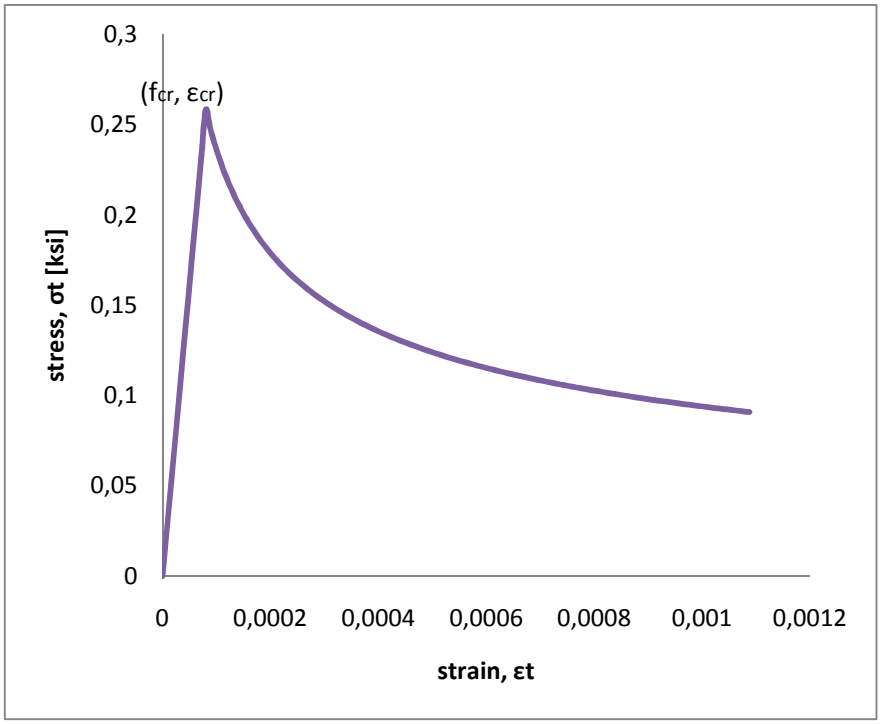

Figure 2.2: Concrete in tension model. Belarbi & Hsu (1994). $\mathbf{f_{cr} = 0.256}$, $\boldsymbol{\beta = 0.4}$

The parameter β (eq. 2.1.6) controls the ability to redistribute the stresses in the concrete after cracking. The test specimens conducted by Belarbi & Hsu (1994) had reinforcing bars in the longitudinal direction, making the redistribution possible. Belarbi & Hsu (1994) recommend using a value of $\beta = 0.4$, based on the experiments.

2.1.3. Constitutive Model for Confined Concrete

To describe the behavior of confined concrete, the model proposed by Saatcioglu & Razvi, 1992, is used. The model proposes an ascending parabolic branch, followed by a descending linear branch. A constant residual strength is assumed beyond this branch at 20% of peak stress.

Saatcioglu & Razvi studied different types of lateral reinforcement (from poorly to well reinforced columns), along with different column geometries, and obtained the following expressions to calculate the confined concrete strength for circular columns with spiral reinforcement (eq. 2.1.10, 2.1.11 and 2.1.12):

$$f'_{cc} = f'_{co} + k_1 f_l \tag{2.1.10}$$

$$k_1 = 6.7\,(f_l)^{-0.17} \tag{2.1.11}$$

$$f_l = \frac{2A_s f_{yt}}{b_c s} \tag{2.1.12}$$

Where f'_{cc} and f'_{co} are the confined concrete and plain concrete strengths, respectively, k_1 is a coefficient depending on the poison ratio and the effective lateral pressure (f_l). The parameters A_s and f_{yt} are the area and the yielding stress of the lateral reinforcement. The parameters b_c and s corresponds to the diameter of the spiral (measured center to center of the hoop bar) and the hoop pitch, respectively.

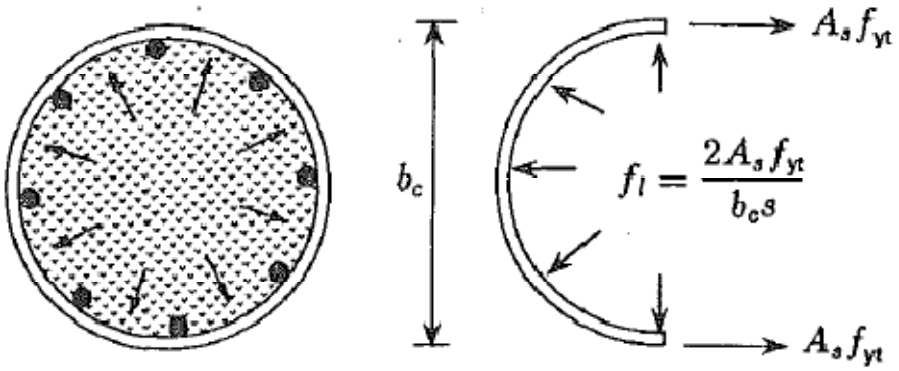

Figure 2.3: Lateral pressure in circular columns. Saatcioglu & Razvi (1992).

The confinement also enhances the ductility of concrete and this effect is considered in the Saatcioglu & Razvi, 1992, model. They observed that the confined concrete strength is, also, reached at a higher strain level, and have little strength decay in post – peak. Saatcioglu & Razvi, 1992, proposes the following expressions to calculate this effect:

$$\varepsilon_1 = \varepsilon_{01}(1 + 5K) \tag{2.1.13}$$

$$K = \frac{k_1 f_l}{f'_c} \tag{2.1.14}$$

Where ε_1, corresponds to the strain at f'_{cc} (confined concrete), $\varepsilon_{01}$is the strain at f'_c (plain concrete), k_1 and f_l were defined in eq. 2.1.11 and 2.1.12, respectively. The effect of confinement, in terms of strength and strain capacity, is shown in Figure 2.4:

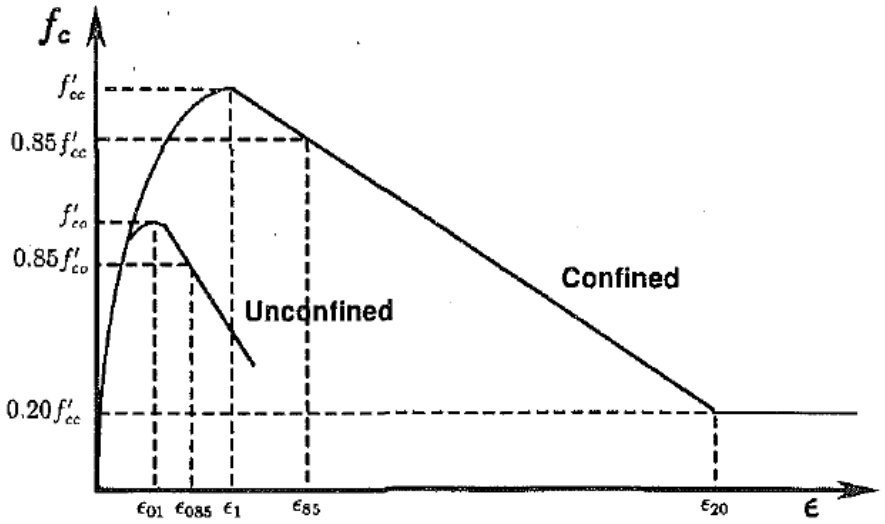

Figure 2.4: Effect of confinement on concrete. Saatcioglu & Razvi, 1992.

Finally, the strain corresponding to a strength loss of 15% is calculated using the following expression:

$$\varepsilon_{85} = 260\rho\varepsilon_1 + \varepsilon_{085} \tag{2.1.15}$$

Where ε_{085}, corresponds to the strain for a strength loss of 15% on plain concrete, ρ corresponds to the transverse reinforcement ratio and $\varepsilon_1$was defined in eq. 2.1.13.

Saatcioglu & Razvi, 1992, model is not implemented in OpenSees. Thus, the parameters n and k are adjusted to fit the Collins & Porasz, 1989, model to the Saatcioglu & Razvi, 1992, model, as shown in Figure 2.5.

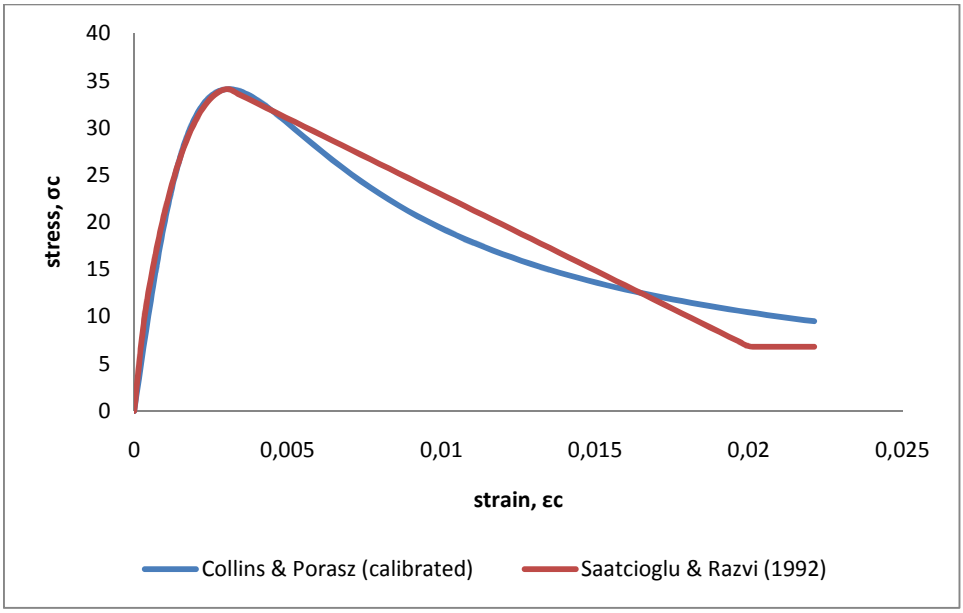

Figure 2.5: Collins and Porasz model calibrated to Saatcioglu & Razvi (1992) model.

2.1.4. Constitutive Model for Reinforcing Steel

The reinforcing steel is modeled using the curved proposed by Menegotto & Pinto, 1973, as recommended by Massone et al, 2006. This model is characterized by two asymptotes, one with a slope E_0 (Modulus of Elasticity) and another with slope $E_1 = bE_0$, where b is the strain hardening ratio. The curve of transition between these two asymptotes is governed by the parameter R (curvature). The cyclic behavior is not considered in this model, i.e., only the monotonic branch is considered for the analysis. The stress – strain relationship for reinforcement steel is shown in Figure 2.6.

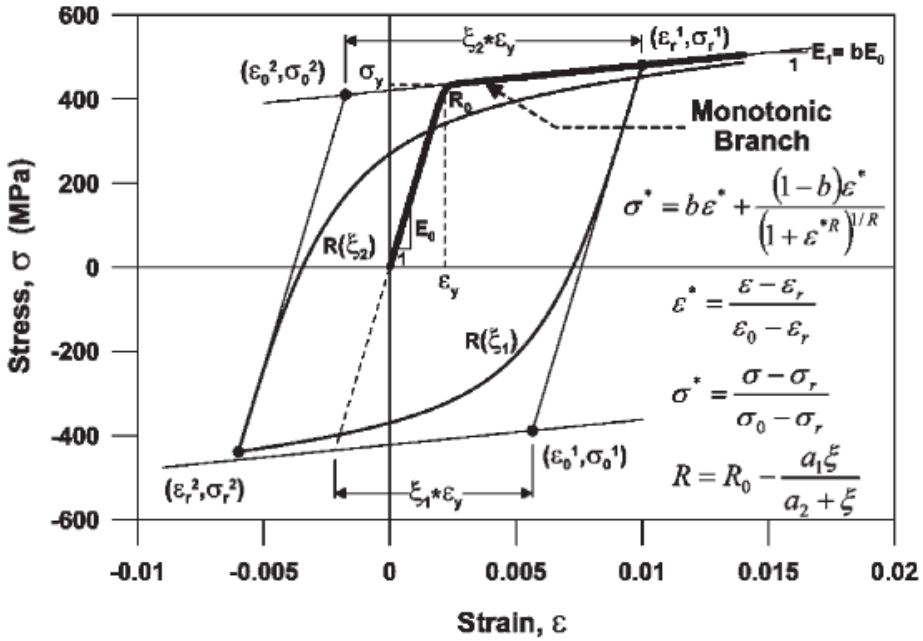

Figure 2.6: Reinforcing steel model. Menegotto & Pinto (1973).

This model is corrected in order to consider the redistribution of stresses after cracking of concrete under tensile. Therefore, the nominal yielding stress of the reinforcement is reduced to 91%, which is the effective yielding stress of bars embedded by concrete. The parameter R_0 is calculated by the following expressions proposed by Belarbi & Hsu (1994):

$$R_0 = \frac{1}{9 \cdot B - 0.2} \leq 25 \tag{2.1.16}$$

$$B = \frac{1}{\rho} \cdot \left(\frac{f_{cr}}{\sigma_y}\right)^{1.5} \tag{2.1.17}$$

Where f_{cr} is the cracking stress of concrete, ρ is the longitudinal reinforcement ratio and σ_y is the yielding stress of steel.

2.2. Characterization of p – y curves

The p – y curves are the relationships between the displacement (y) and the soil resistance (p) of an element of soil. This is an extension of the linear elastic Winkler model expressing the nonlinear soil deformations through the use of nonlinear p – y springs. The p – y curves have been extensively used to model laterally loaded piles, using finite element models as shown in Figure 2.7, where the soil springs are attached to the prescribed nodes of the concrete structure. This procedure intends to represent the soil – structure interaction.

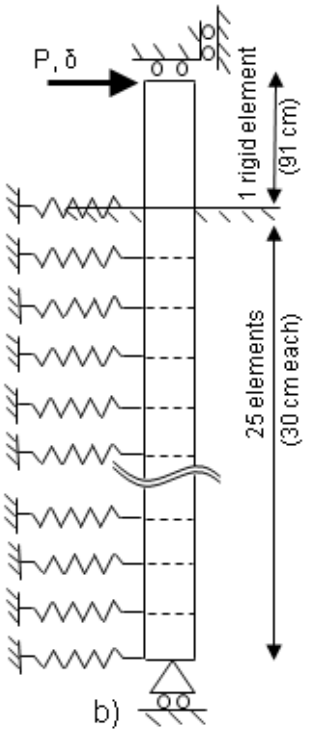

Figure 2.7: Pile Model with p – y approach. Lemnitzer et al, 2013.

There are many types of p – y curves. In fact, there is a single p – y curve to each type of soil, depending on its composition and density, state of stresses, confinement, and other material properties. In general, the p – y curves can be classified in ductile and brittle, as shown in Figure 2.8.

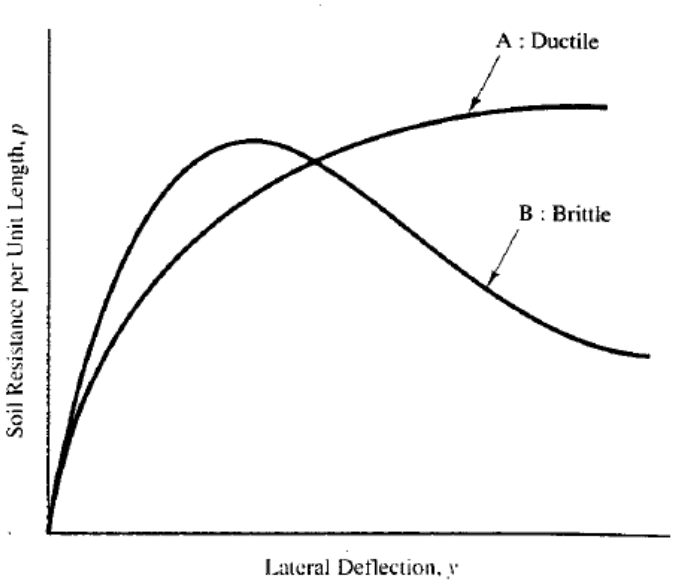

Figure 2.8: Types of p - y curves. Coduto, D, 2001.

The API (1993) proposes equations to calculate the p – y curves for different types of soil. In the following section it is described the shape of p – y curve selected for the present work.

2.2.1. Shape of p – y curves

The type of soil of the site of testing, for the Fixed – Head pile studied in this work, consist of mostly silty clays, for the upper 50 ft. (twice the length of the Fixed – Head pile), therefore, the soil is assumed to have a stiff clay behavior (Stewart et al, 2007). The API (1993) proposes the following equations to describe the p – y curves for a stiff clay.

$$\frac{p}{p_u} = \begin{cases} 0.5\left(\frac{y}{y_c}\right)^{0.25} & , \ y/y_c \leq 16 \\ 1.0 & , \ y/y_c \geq 16 \end{cases} \tag{2.1.1}$$

$$y_c = 2.5\varepsilon_c D \tag{2.1.2}$$

Where p_u and y_c denote ultimate resistance and the deflection at one – half of the ultimate resistance. The parameters ε_c and D denote the strain that occurs at one half of the maximum stress and the pile diameter, respectively. The value of the ultimate resistance is depending on the pile depth, and it is assumed a linear distribution of p_u, as follows.

$$p_u = \begin{cases} \left(3 + \frac{\gamma z}{c} + \frac{Jz}{D}\right) cD & 0 < z < z_r \\ 9cD & z \geq z_r \end{cases} \quad (2.1.3)$$

$$z_r = \frac{6D}{\left(\frac{\gamma D}{c} + J\right)} \quad (2.1.4)$$

Where γ and c denote the unit weight and the undrained shear strength of the soil. The empirical parameter J is taken as 0.5 for soft clays and 0.25 for medium stiff clays, as recommended by Matlock, 1970. The parameter z_r denotes the depth below soil surface to bottom of reduced resistance zone where p_u decreases. The shape of the p – y curve finally obtained is shown in Figure 2.9.

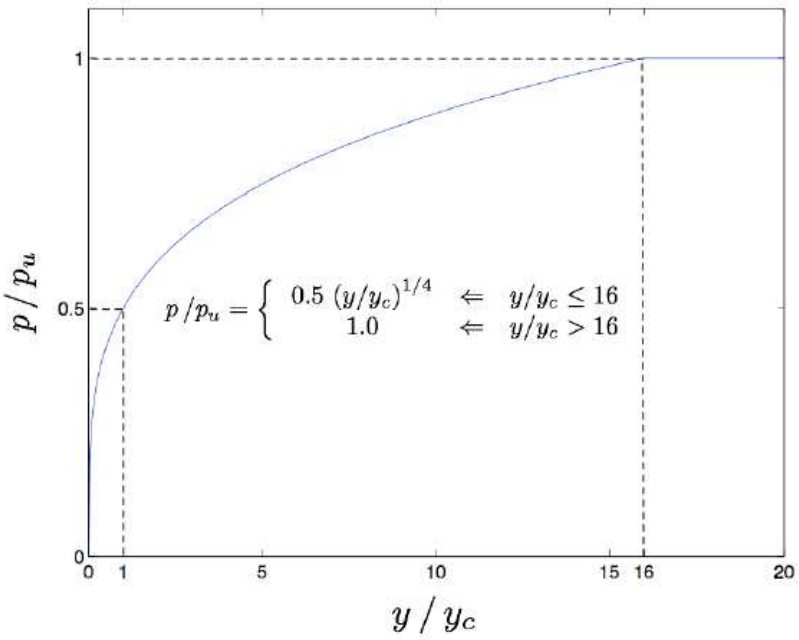

Figure 2.9: Shape of p - y curves for a stiff clay, Stewart et al, 2007.

2.2.2. Implementation of the p – y curves

The Fixed Head pile model along with the p – y approach is implemented in OpenSees (OpenSees, http://opensees.berkeley.edu). It is intended to incorporate the soil behavior by using uniaxial springs having the p – y relationships described in equation 2.2.1. The p – y curve is implemented as a tri-linear response to approximate the nonlinear prescribed p – y curves by the API (1993). The procedure is the following:

a) The y axis is divided in three intervals. The first goes from 0 to a value of y_c, representing the first portion of the p – y curve. The second interval goes from y_c to $16y_c$, where the ultimate strength p_u is reached. Finally, the third interval goes from $16y_c$ to $20y_c$, where the soil resistance is constant and equal to p_u.

b) A continuous least squares method is applied in each interval, as following:

- The error function to be minimized is:

$$E = \int_{y_1}^{y_2} \left(f(y) - (my + n)\right)^2 dy \tag{2.1.5}$$

Deriving with respect to m and n and equalizing to zero, then solving for m and n, the following expressions are obtained:

$$m = \frac{2\int_{y_1}^{y_2} 2f(y)y\,dy - (y_1 + y_2)\int_{y_1}^{y_2} 2f(y)\,dy}{\frac{4}{3}({y_2}^3 - {y_1}^3) - ({y_2}^2 - {y_1}^2)(y_1 + y_2)} \tag{2.1.6}$$

$$n = \frac{1}{2(y_2 - y_1)}\left(\int_{y_1}^{y_2} 2f(y)\,dy - ({y_2}^2 - {y_1}^2)m\right) \tag{2.1.7}$$

- In the first interval, the linear approximation is forced to have $n = 0$. Thus, a different expression is obtained for m.

$$m = \frac{\int_0^{y_1} 2f(y)y\,dy}{\frac{2}{3}{y_1}^3} \tag{2.1.8}$$

- For the third interval it is assumed to have a constant soil resistance, which is the soil resistance obtained in the second interval at $y = 16y_c$.

c) The function $f(y)$ of equations 2.2.5 to 2.2.8 is the same of equation 2.2.1. Thus, the previous integrals are calculated and give the following expressions:

$$\int_{y_1}^{y_2} 2f(y)y\,dy = \frac{4}{9}p_u{y_c}^2\left(\left(\frac{y_2}{y_c}\right)^{\frac{9}{4}} - \left(\frac{y_1}{y_c}\right)^{\frac{9}{4}}\right) \tag{2.1.9}$$

$$\int_{y_1}^{y_2} 2f(y)\,dy = \frac{4}{5}p_u y_c\left(\left(\frac{y_2}{y_c}\right)^{\frac{5}{4}} - \left(\frac{y_1}{y_c}\right)^{\frac{5}{4}}\right) \tag{2.1.10}$$

$$\int_0^{y_1} 2f(y)\,dy = \frac{4}{5}p_u y_c\left(\frac{y_1}{y_c}\right)^{\frac{5}{4}} \tag{2.1.11}$$

Finally, a tri-linear fit is obtained for the API (1993) recommended p – y curves as shown in Figure 2.10. The same procedure is repeated for each node of the model, which has attached a spring with a particular p – y relationship.

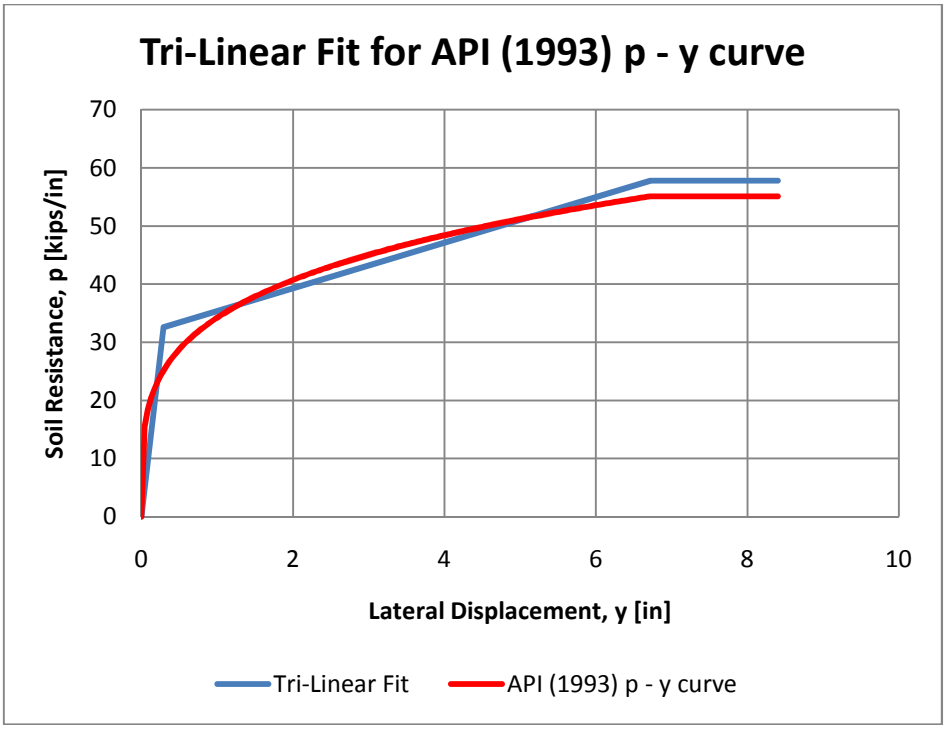

Figure 2.10: Tri-Linear fit for API (1993) p – y curve.

CHAPTER 3. Shear – Flexure Interaction Model

3.1 Flexure Model Description

The flexure model corresponds to a simple case of non – linear analysis. In this model, the element (column or pile) is divided into regular elements along its length (in the longitudinal direction), which are connected to nodes. Each element is divided in a certain number of fibers (in the transverse direction). Every fiber is represented by a single spring (Figure 3.1) having a uniaxial behavior. In bi – dimensional analysis, each element has 3 degrees of freedom per node (2 displacements and 1 rotation), which are associated to strains via interpolation functions and the Bernoulli hypothesis (plane sections remain plane after load). These strains do not represent shear deformations, but only flexural.

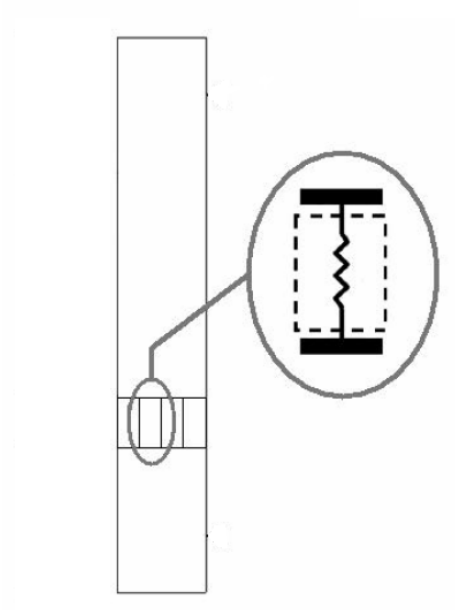

Figure 3.1: Column discretization. Uniaxial fiber model (after Gotschlich, 2011).

Given the fibers strains, the stresses can be calculated via the constitutive laws of materials (concrete and steel) and, given the element geometry, the forces and moments can be calculated. Shear force is calculated from equilibrium. Thus, for a given displacement (on the top of the column) the deformations are iterated to reproduce that displacement (for a fixed tolerance), and the load is finally calculated, for the load pattern previously selected.

3.2 Shear – Flexure Interaction Model Description

The Shear – Flexure Interaction Model corresponds to a macroscopic biaxial fiber model that couples the axial – bending behavior with the shear behavior of a reinforced concrete (RC) element. This model considers every fiber to have a panel behavior, i.e., to have axial strains and also angular distortions in the plane of the element. This is an extension of the flexure model, by adding an additional lateral spring to the fiber, as shown in Figure 3.2.

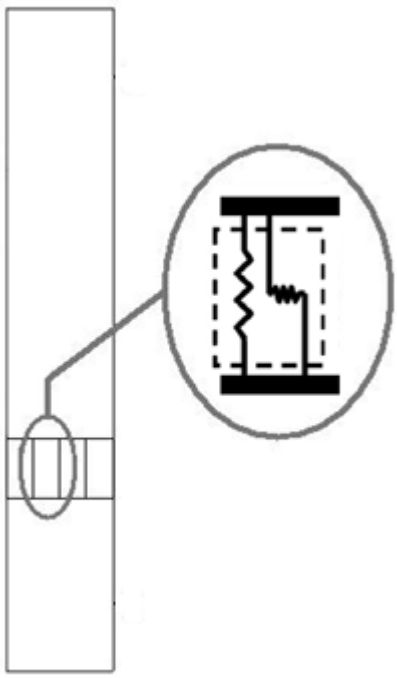

Figure 3.2: Column discretization. Shear - Flexure biaxial fiber model (after Gotschlich, 2011).

The column is divided, in the longitudinal direction, in elements of defined length which are divided, as well, in horizontal fibers having a panel behavior. In the interaction model, it is assumed that the rotations are concentrated in a single point (called center of rotation) located at a distance $c \cdot h$, where h is the total length of the fiber element and c is a constant less than 1. Experimental calibrations in wall specimens have shown that rotations are concentrated at $0.4 \cdot h$. In beams, a value of $0.5 \cdot h$ has shown good results (Galleguillos, 2010; Gotschlich, 2011). It is assumed that the rotations are concentrated at $0.5 \cdot h$ for the case of columns. Each element possesses six degrees of freedom (two displacements and one rotation at both ends of the element). The element is shown in Figure 3.3.

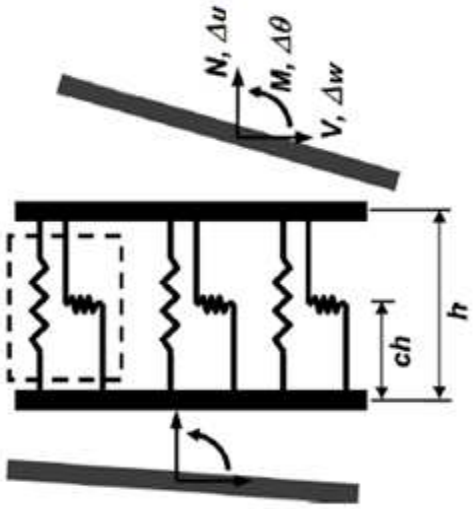

Figure 3.3: Shear - Flexure interaction element. Massone et al, 2006.

Assuming that the Bernoulli hypothesis is true (that plain sections remain plane after deformation), and that the shear strain is uniform along the entire section, the angular distortion (γ_{xy}) and the longitudinal axial strain (ε_y) are calculated for all the strips, based on the prescribed degrees of freedom for the current analysis step. Accordingly, each strip has two input variables ε_y and γ_{xy}, based on the element deformations. The transverse strain (ε_x) is initially estimated in order to complete the definition of the strain field. Then, using the constitutive laws of materials and the geometric properties the stress field and forces can be determined.

For calculating the unknown ε_x, there are two methods to proceed. The first is assuming that the transverse axial stress is zero ($\sigma_x = 0$), which is consistent with the boundary conditions at the sides of the column with no transverse load applied over its height. Then, the procedure is to iterate the value of ε_x in order to achieve horizontal equilibrium. This method has shown good prediction when modeling slender walls, but discrepancies are observed when modeling walls with shear – span ratios less than 1.0 (Massone et al, 2006). The second method corresponds to give calibrated values of ε_x to the model, which has shown improvements on the prediction when modeling short walls (Massone et al, 2009). This procedure does not need iterations.

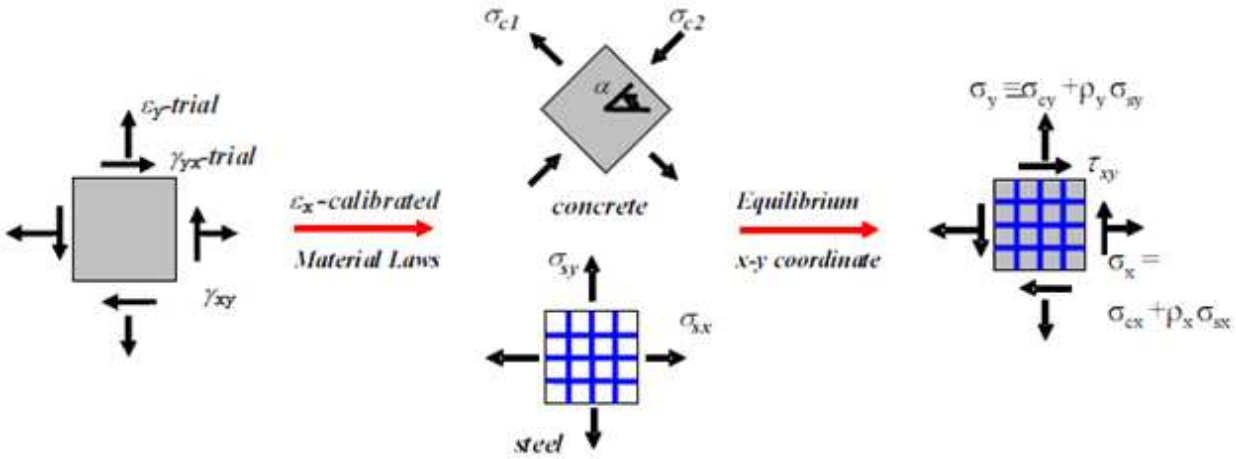

Figure 3.4: Strain field to resultant stress field. Procedure. Massone et al, 2009.

The procedure to obtain the stress field, from the strain field is shown in the Figure 3.4, and it is similar for both cases ($\sigma_x = 0$ and ε_x calibrated). In the first case (zero transverse stress), the value of ε_x has to be estimated first. Then, assuming that the principal strain directions coincide with the principal stress directions, the stresses are calculated for the concrete and reinforcement steel, in the principal directions, using the uniaxial constitutive models discussed in section 2.1. Later, the stresses are calculated for x and y directions, thus obtaining the stress field associated to the initially given strain field (ε_x, ε_y and γ_{xy}). In this step, the hypothesis $\sigma_x = 0$ is verified, for a prescribed tolerance; if the equation is satisfied then the next element is analyzed, else the value of ε_x has to be modified, repeating the procedure until the equation is satisfied, for the given tolerance. For the case of ε_x calibrated, the iterative procedure is not necessary, obtaining directly the stress field with a non zero value of σ_x.

The analysis is performed via displacement control. A displacement is imposed at the top of the column, and the strain and stress field is calculated and also the force that produces the displacement, using the procedure described above. The procedure is repeated for every increment of displacement, and the load – displacement profiles can be obtained from the analysis.

In the case of imposing the value of transverse strains, it is needed a calibrated profile. Massone et al, 2009, calibrated an average strain profile for short walls with rotation restrained at both ends, from experimental data. Later, Massone, 2010, calibrated expressions for ε_x, using 2D finite element models, for cantilever and double curvature configurations. The calibration has shown good correlation in predicting both the magnitude and distribution of the transverse strain, compared to experimental data, and has also shown good results when modeling beams (Galleguillos, 2010, Gotschlich, 2011). The expressions found for the maximum transverse strain are:

Cantilever:

$$\varepsilon_{x,max} = 0.0055 \cdot (100 \cdot \rho_h + 0.25)^{-0.44} \cdot (100 \cdot \delta)^{1.4} \tag{3.2.1}$$

Double Curvature:

$$\varepsilon_{x,max} = 0.0033 \cdot \left(100 \cdot \rho_h + 0.25\right)^{-0.53} \cdot \left(\frac{h_w}{l_w} + 0.5\right)^{0.47} \cdot \left(\frac{100N}{f'_c A_g} + 5\right)^{0.25} \cdot (100 \cdot \delta)^{1.4} \tag{3.2.2}$$

Where ρ_h is the transverse reinforcement ratio, $\delta = \Delta / h_w$ is the element drift, where Δ is the lateral displacement and h_w the height of the wall. The parameter l_w corresponds to the wall length, N is the applied axial load, f'_c the concrete compressive strength and $A_g$the total cross sectional area.

The maximum value of ε_x is located at different heights, depending if the configuration is cantilever or double curvature. For cantilever configuration, $\varepsilon_{x,max}$ is located at $0.38 \cdot h_w$ from

the maximum moment point; and for double curvature configuration, $\varepsilon_{x,max}$ is located at $0.5 \cdot h_w$. The height varies with the displacement, but such variation is neglected for simplicity. Thus, the following expressions were obtained for the shape of the average transverse strain:

Cantilever:

$$\frac{\varepsilon_x(y)}{\varepsilon_{x,max}} = \begin{cases} sin^{0.75}\left(\frac{y}{0.76h_w}\pi\right) & si\ 0 \le y \le 0.38h_w \\ sin^{0.75}\left(\frac{(y+0.24h_w)}{1.24h_w}\pi\right) & si\ 0.38h_w \le y \le h_w \end{cases} \quad (3.2.3)$$

Double Curvature:

$$\frac{\varepsilon_x(y)}{\varepsilon_{x,max}} = \left\{sin^{0.75}\left(\frac{y}{h_w}\pi\right)\right. \quad (3.2.4)$$

Where y, is the relative position in the wall measured from the support.

3.3 Column Discretization

The Shear – Flexure Interaction Model has been validated for walls (Massone et al, 2006) and beams (Galleguillos, 2010, Gotschlich, 2011). The elements modeled had rectangular cross sections, unlike the columns studied in the present work, which are all circular cross sectional elements with spiral reinforcement (See section 4.1). Because the model is implemented for rectangular sections (Figure 3.5), the columns cross sections are transformed into equivalent rectangular sections, calculating the plain and confined concrete and reinforcement steel areas as indicated in sections 3.3.1 and 3.3.2.

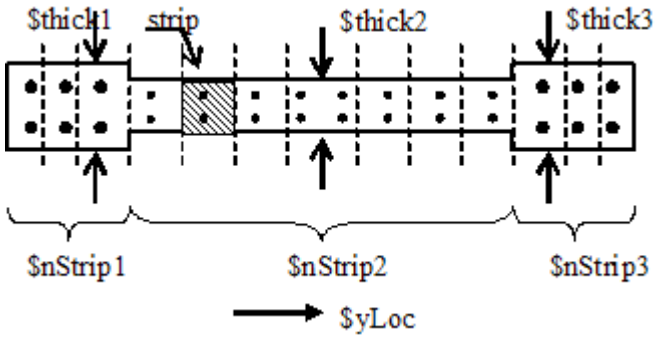

Figure 3.5: Geometric parameters for walls. Shear - Flexure Interaction Model. (OpenSees, 2011).

3.3.1. Confined and Plain Concrete Areas

The concrete areas are calculated using the integral of the circumference, with the limits of integration depending on the number of strips prescribed. Some parameters have been defined for calculating these areas (Figure 3.6). The procedure is the following:

a) First, the strip width (dw) is calculated. A uniform width is used for this case, thus, $dw = {}^{D}/_{N}$, where D is the column diameter and N is the prescribed number of strips (8 or 16 strips).

b) A set of coordinates is defined (x_i), which represents the start and ending of every strip. The coordinates are calculated as following:

$$x_i = -\frac{D}{2} + dw \cdot i \tag{3.3.1}$$

Where i goes from 1 to $N + 1$, and represents the dashed lines on Figure 3.6. These values are used as the limits of integration of the circumference area. Notice that $x_i = 0$ corresponds to the center of the cross section, thus, the left side of the cross section has $x_i < 0$ and the right side has $x_i > 0$.

c) For a strip i, the areas are calculated using the integral of the circumference. The area for confined concrete for the ith strip (A_{cci}) is:

$$A_{cci} = 2 \cdot \int_{x_i}^{x_{i+1}} \sqrt{\left(\frac{d}{2}\right)^2 - x^2}\ dx \tag{3.3.2}$$

Then, polar coordinates are used to solve the integral, thus having $x = {}^{d}/_{2}\ sin\,\theta$ and $dx = {}^{d}/_{2}\ cos\,\theta\ d\theta$. Finally, the area is given by eq. 3.3.3:

$$A_{cci} = 2\left(\frac{d}{2}\right)^2 \cdot \left(\frac{\theta_{i+1} - \theta_i}{2} + \frac{1}{4}(\sin 2\theta_{i+1} - \sin 2\theta_i)\right) \tag{3.3.3}$$

Where $\theta_i = \sin^{-1} {}^{2x_i}/_{d}$, is the relationship between the Cartesian and polar coordinates.

d) The plain concrete area for the ith strip (A_{ci}) is calculated subtracting the confined concrete area (A_{cci}) to the total area of the ith strip (A_{ti}). The total concrete area of the strip is calculated using the eq. 3.3.3 replacing the value of d for D:

$$A_{ti} = 2\left(\frac{D}{2}\right)^2 \cdot \left(\frac{\theta_{i+1} - \theta_i}{2} + \frac{1}{4}(\sin 2\theta_{i+1} - \sin 2\theta_i)\right) \tag{3.3.4}$$

Where $\theta_i = \sin^{-1} {}^{2x_i}/_{D}$. Finally, the plain concrete area for the ith is given by the following equation:

$$A_{ci} = A_{ti} - A_{cci} \tag{3.3.5}$$

e) Special attention should be put on the borders, when $|x_i| > d$, i.e., when one of the dashed lines on Figure 3.6 is outside the confined area. Two cases can be identified:

- Both x_i and x_{i+1} are outside the confined area. In this case, the confined concrete area is zero ($A_{cci} = 0$) and the plain concrete area (A_{ci}) is equal to the area given by eq. 3.3.4.

- One coordinate, for instance x_i, is outside the confined area and the other (x_{i+1}) is inside the confined area. In this case, the value of x_i in eq. 3.3.2 should be replaced by $-d$ or d, depending if it is in the left side or the right side of the column, respectively.

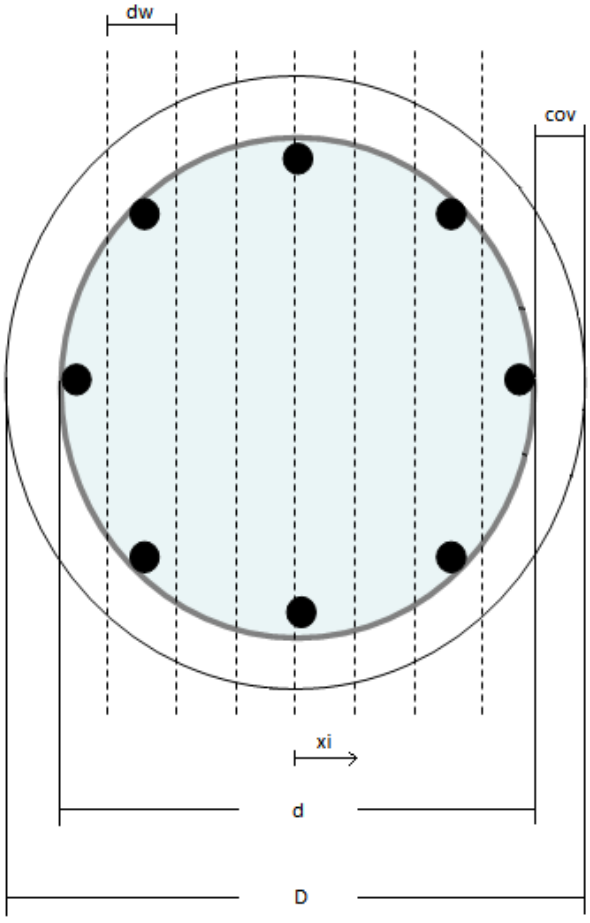

Figure 3.6: Definition of confined and plain concrete areas for the i-th fiber

3.3.2. Longitudinal Reinforcement Areas

The longitudinal reinforcement area for each strip is calculated assuming that there is a uniform and continuous distribution in a circumference of diameter d, i.e., instead of calculating the areas of longitudinal reinforcement using the real coordinates of each bar a circular distribution is assumed, and the calculations are direct. The procedure is the following:

a) First, an equivalent linear density is calculated using the following expression:

$$\rho_l = \frac{A_s}{\pi d} \tag{3.3.6}$$

Where ρ_l is the linear density, A_s is the total longitudinal reinforcement, and d is the diameter of the confined area.

b) Then, the distribution of the reinforcement is defined with a *1-D* curve as following:

$$\vec{r} = \frac{d}{2} \cdot (\cos\theta\,, \sin\theta) \tag{3.3.7}$$

$$\frac{d\vec{r}}{d\theta} = \frac{d}{2} \cdot (-\sin\theta\,, \cos\theta) \tag{3.3.8}$$

c) The area is calculated using the following arc length integral:

$$L = \int_{\theta_1}^{\theta_2} \left\| \frac{d\vec{r}}{d\theta} \right\| d\theta = \frac{d}{2} \cdot (\theta_i - \theta_{i+1}) \tag{3.3.9}$$

Where $\theta_i = cos^{-1}\, {}^{2x_i}/_{d}$ and $\theta_{i+1} = cos^{-1}\, {}^{2x_{i+1}}/_{d}$, and the set of coordinates x_i were defined in eq. 3.3.1. Notice the order of appearance of θ_i and θ_{i+1} in eq. 3.3.9. The order of these terms is that because, when $x_{i+1} > x_i$ then $\theta_{i+1} < \theta_i$.

d) Finally, the longitudinal reinforcement area for the ith strip (A_{si}) is calculated using the following expression:

$$A_{si} = \rho_l \cdot d \cdot (\theta_i - \theta_{i+1}) \tag{3.3.10}$$

e) Special attention should be put on the borders, when $|x_i| > d$, i.e., when one of the dashed lines on Figure 3.7 is outside the confined area. Two cases can be identified:

- Both x_i and x_{i+1} are outside the confined area. In this case, a value of $A_{si} = 0.01 \cdot A_s$ is assigned. The model needs a reinforcement steel area for each fiber, because, if no area is assigned, the model does not give good results or does not converges. Thus, it was decided to assign a 1% of the total reinforcement area (A_s).

- One coordinate, for instance x_{i+1}, is outside the confined area and the other (x_i) is inside the confined area. In this case, the value of θ_{i+1} in eq. 3.3.10 should be replaced by 0.

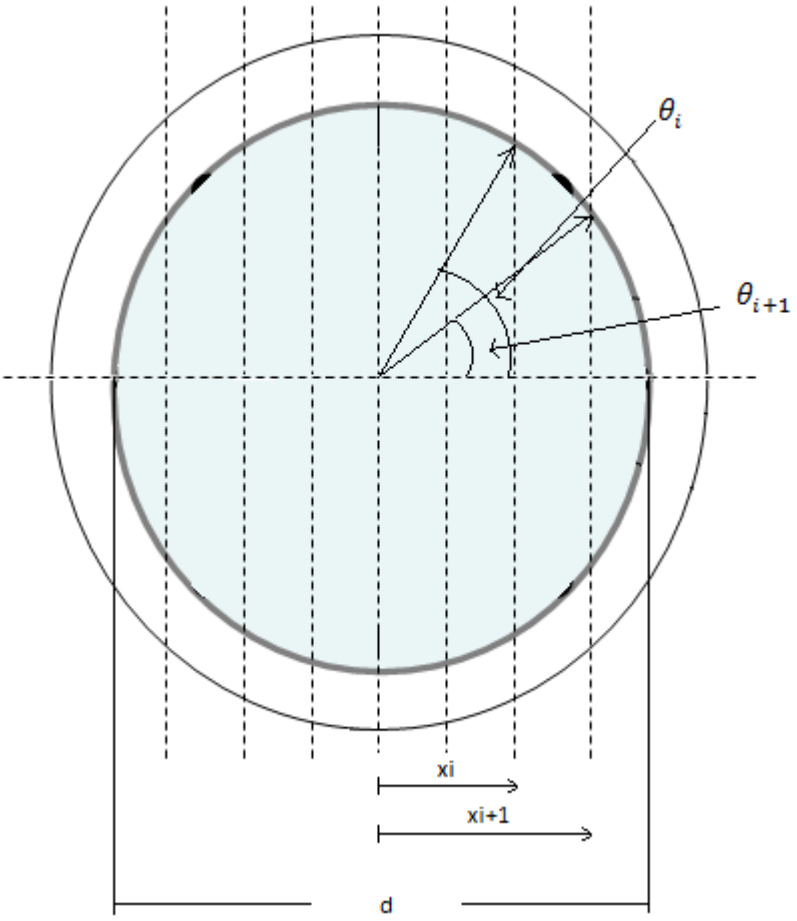

Figure 3.7: Definition of the Reinforcement Steel areas for the i-th fiber

CHAPTER 4. Analysis of Shear – Flexure Interaction Model on Columns

4.1 Tests Description

The tests are collected from the PEER (Pacific Earthquake Engineering Research) database, (PEER spd, 2011). A set of 8 columns were selected for the study. The database provides the material properties, geometry of the entire element and reinforcement, and gives the load – displacement response for every test. The tests are separated in categories, depending on the type of failure they showed in the laboratory, and they are also separated according to the test characteristics. Two additional columns were found in the Kawashima Earthquake Engineering Laboratory database of the Tokyo Institute of Technology, corresponding to the Specimens 13 and 14 (Kawashima Lab, 2011)

The Table 4.1 shows the full information of the column specimens selected for the analysis. The specimens were selected according to obtain shear degradation on the load – displacement response, thus, the shear – flexure interaction model could be validated with the test results.

Table 4.1: Properties of the columns used in the analyses.

Specimen				Geometry				Transverse Reinforcement			Longitudinal Reinforcement		Axial Load	Material Properties		
ID N°	REFERENCE	Type	Failure Type	*hc* [mm]	*D* [mm]	*M/VD*	*D/hst*[1]	Bar	ρt[2] %	Concrete Cover [mm]	Bar	ρl %	*N/f'cAg* %	*f'c* [MPa]	*fyt* [MPa]	*fyl* [MPa]
SPEC1	Benzoni and Priestley, 1994, S1	Cantilever	Flexure - Shear	914.5	610	1.5	5.3	Spiral ϕ6.4 @ 76.2 mm	0.28	15.9	12 ϕ12.7	0.52	5.7	30	361	462
SPEC2	Benzoni and Priestley, 1994, S2	Cantilever	Flexure - Shear	914.5	610	1.5	5.3	Spiral ϕ6.4 @ 127 mm	0.17	15.9	24 ϕ12.7	1.04	5.7	30	361	462
SPEC3	McDaniel, 1997, S1	Cantilever	Shear	1219.2	609.6	2	4.0	Spiral ϕ4.9 @ 101.6 mm	0.13	18.6	20 ϕ15.9	1.36	0.2	29.8	200	454
SPEC4	McDaniel, 1997, S1-2	Cantilever	Shear	1219.2	609.6	2	4.0	Spiral ϕ4.9 @ 101.6 mm	0.13	18.6	21 ϕ15.9	1.36	0.2	26.8	200	454
SPEC5	McDaniel, 1997, S2	Cantilever	Shear	1219.2	609.6	2	4.0	Spiral ϕ4.9 @ 101.6 mm	0.13	18.6	21 ϕ15.9	1.36	0.2	31.2	200	437.6
SPEC6	Petrovski & Ristic, 1984, M2E1	Cantilever	Flexure - Shear	900	307	2.93	2.7	Spiral ϕ6 @ 75 mm	0.63	36	12 ϕ12	1.83	5.5	35.9	240	240
SPEC7	Petrovski & Ristic, 1984, M2E2	Cantilever	Flexure - Shear	895	307	2.92	2.7	Spiral ϕ6 @ 75 mm	0.63	36	12 ϕ12	1.83	10	34.4	240	240
SPEC8	Wong et al, 1990, S2	Cantilever	Flexure - Shear	800	400	2	4.0	Spiral ϕ6 @ 65 mm	0.47	18	20 ϕ16	3.2	39	37	340	475
SPEC9	Yoneda, Kashima & Shoji - tp021	Cantilever	not - reported	1350	400	3.38	2.4	Spiral ϕ6 @ 150 mm	0.26	70	12 ϕ16	1.89	4.9	30	363	374
SPEC10	Yoneda, Kashima & Shoji - tp024	Cantilever	not - reported	1350	400	3.38	2.4	Spiral ϕ6 @ 150 mm	0.13	70	12 ϕ16	1.89	4.9	30	363	374

[1] D/hst ratio for the 8 elements along the column length discretization.

[2] ρt corresponds to the volumetric transverse reinforcement ratio, calculated as the volume of transverse reinforcement over the confined concrete volume. It is calculated as $\rho_t = 4A_s/sb_c$, where $A_s$is the area of the hoop bar, s is the hoop vertical spacement and b_c is the confined area diameter, measured center to center of the hoop bar.

4.2 Analysis of Columns response

The analyses performed on the specimens described on section 4.1 can be classified on the different types of discretization used (longitudinal and transverse directions), and also different types of models:

1. Types of models:

    a. Flexure Model (see Section 3.1).
    b. Shear – Flexure Interaction Model with $\sigma_x = 0$ (see Section 0)
    c. Shear – Flexure Interaction Model with ε_x calibrated (see Section 0)

2. Types of discretization:

    a. Continuous Reinforcement with 8 fibers in the transverse direction (see Section 3.3).
    b. Continuous Reinforcement with 16 fibers in the transverse direction (see Section 3.3). This discretization is used in order to assess the effect of strip refinement.
    c. Fixed number of 8 elements on the longitudinal direction. The ε_x calibrated model permits only 8 elements in the longitudinal direction. This discretization was recommended by Massone et al, 2006, because it showed to give better predictions on post – peak curve for walls. Then, an 8 elements discretization is used along the $\sigma_x = 0$ model and Flexure model in order to make comparisons.
    d. Fixed value of $D/h_{st} = 2$ ratio, where D is the column diameter and h_{st} is the length of the element. This discretization has been selected in order to represent the observations on the Fixed – Head pile studied by Stewart et al, 2007. Post test excavations revealed shear cracks and concrete spalling along apparent compression struts within 1.5 pile diameters below ground surface (Lemnitzer et al, 2013). Thus, the element length was selected to be one – half of each specimen diameter in order to better observe the shear behavior.

All discretizations and types of models were applied for each specimen, thus obtaining a total of 8 models for each column as shown in Table 4.2.

Table 4.2: Summary of models applied to each specimen.

Transverse Discretization	Longitudinal Discretization	Model
8 Fibers	$\frac{D}{h_{st}} = 2$	$\sigma_x = 0$
	8 Elements	$\sigma_x = 0$ ε_x calibrated Flexure
16 Fibers	$\frac{D}{h_{st}} = 2$	$\sigma_x = 0$
	8 Elements	$\sigma_x = 0$ ε_x calibrated Flexure

The load – displacement responses obtained from the analysis are compared against the test data in order to assess the validity of different implementations of the interaction model in the analysis of columns. The overall responses are compared, and also they are compared statistically, in terms of the maximum capacity, rigidity at 60% of capacity and degradation displacement at 10% of capacity loss. The results are discussed in the following sections.

4.2.1. Analysis of Columns. Maximum Capacity.

The maximum capacity is one of the parameters studied for the analysis of columns. The parameter studied for each model is the distribution of the maximum lateral load obtained from the analysis ($V_{max.\ Model}$) over the maximum lateral load of the test ($V_{max.\ Test}$), i.e:

$$\hat{v} = \frac{V_{max.\ Model}}{V_{max.\ Test}} \qquad (4.3.1)$$

The distribution of $\hat{v}$ is shown in Figures 4.1, 4.2, 4.3 and 4.4, for all the types of analysis and discretizations. It can be observed that the shear – flexure interaction model is underestimating the maximum capacity of columns, whether the procedure of $\sigma_x = 0$ or ε_x calibrated is used. However, the ε_x calibrated model has mean $\hat{v}$ value closer to 1.0 ($\hat{v}$ gives a mean value of 0.92 when modeling with 16 fibers) than the $\sigma_x = 0$ procedure ($\hat{v}$ gives a mean value of 0.84 when using 8 elements in the longitudinal direction, and 0.86 when using a constant $D/h_{st} = 2$ ratio, both for a 16 fibers discretization). The flexure model is giving mean values of $\hat{v}$ equal to 1.00 and 1.10 for 8 and 16 fibers, respectively. Nevertheless, the flexure model shows a higher dispersion of the data than using any of the shear – flexure interaction models. The flexure model shows a standard deviation of 0.19, whereas the Shear – Flexure interaction model is showing about half of such standard deviation (0.10, 0.11 and 0.09 for $\sigma_x = 0$ with 8 elements in the longitudinal direction, $\sigma_x = 0$ with a constant $D/h_{st} = 2$ ratio and ε_x calibrated, respectively).

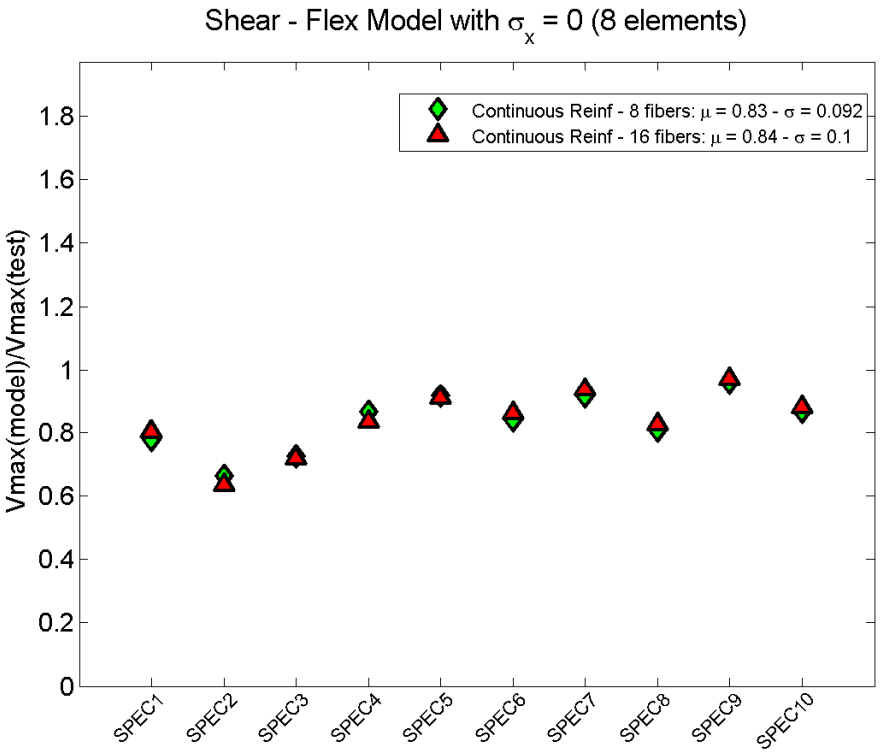

Figure 4.1: Maximum capacity. Shear – Flexure interaction model with $\boldsymbol{\sigma_x = 0}$, and 8 elements in the longitudinal direction.

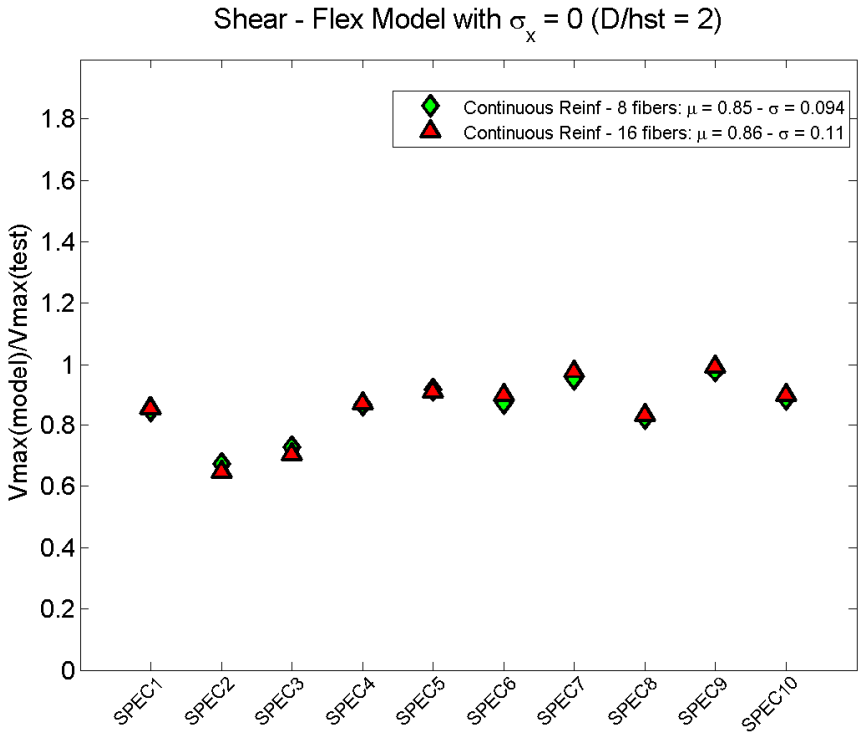

Figure 4.2: Maximum capacity. Shear – Flexure interaction model with $\boldsymbol{\sigma_x = 0}$, and a constant $\boldsymbol{D/h_{st} = 2}$ ratio.

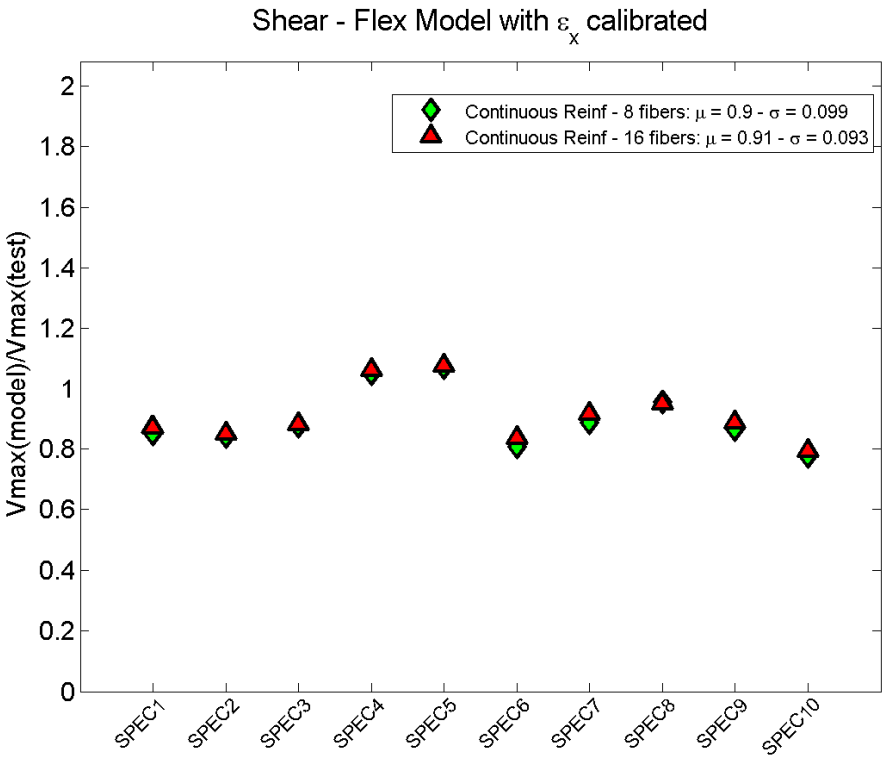

Figure 4.3: Maximum capacity. Shear – Flexure interaction model with $\boldsymbol{\varepsilon_x}$ calibrated (8 element in the longitudinal direction)

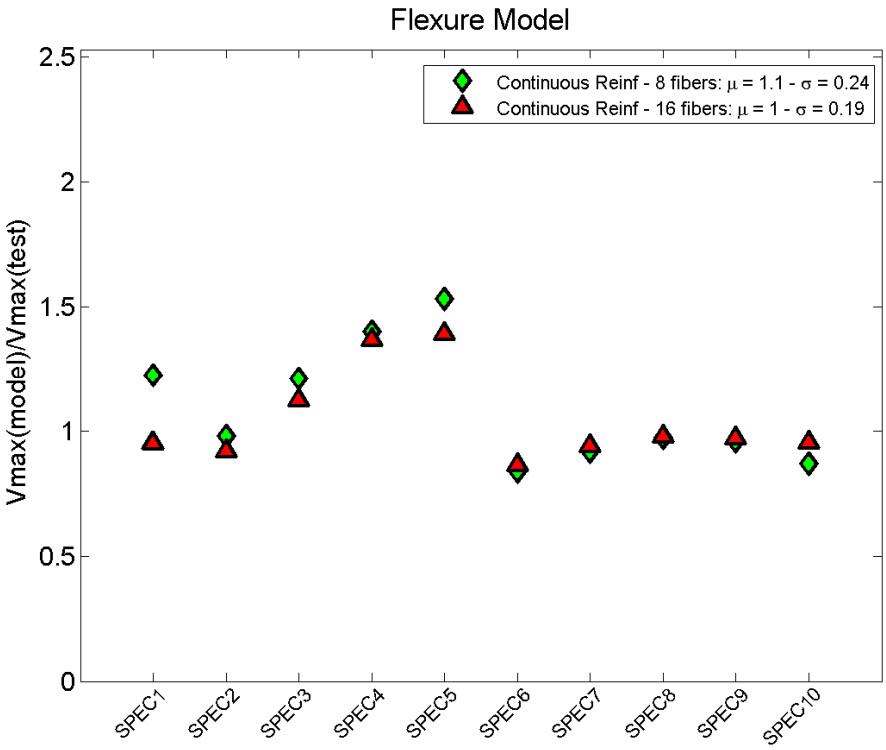

Figure 4.4: Maximum capacity. Flexure model (8 elements in the longitudinal direction).

4.2.2. Analysis of Columns. Rigidity at 60% of Maximum Capacity.

The rigidity at 60% of maximum capacity is other of the parameters studied for the analysis of columns. The parameter studied for each model is the distribution of the secant rigidity at 60% of maximum lateral load obtained from the analysis ($K60_{\,Model}$) over the secant rigidity at 60% of maximum lateral load of the test ($K60_{\,Test}$), i.e.:

$$\hat{k} = \frac{K60_{\,Model}}{K60_{\,Test}} \tag{4.3.2}$$

The distribution of $\hat{k}$ is shown in Figures 4.5, 4.6, 4.7 and 4.8, for all the types of analysis and discretizations. It can be observed that the Shear – Flexure interaction model with ε_x calibrated $\hat{k}$ closer to 1.0 than the other models ($\hat{k}$ is giving a mean value of 1.3 for 8 and 16 fibers discretization). The other models give higher mean values of $\hat{k}$ (1.7 for $\sigma_x = 0$ and 8 elements in the longitudinal direction; 1.7 for $\sigma_x = 0$ and a constant $D/h_{st} = 2$ ratio; and 1.9 for the Flexure Model, all for a 16 fibers discretization). Relatively low dispersion is observed for the parameter $\hat{k}$ (0.17 for $\sigma_x = 0$ with 8 elements in the longitudinal direction; 0.17 for $\sigma_x = 0$ and a constant $D/h_{st} = 2$ ratio; 0.18 for Shear – Flexure model with ε_x calibrated and 0.19 for the Flexure model, all for a 16 fibers discretization). The 8 fibers and the 16 fibers discretization (in the transverse direction) give similar results for all models.

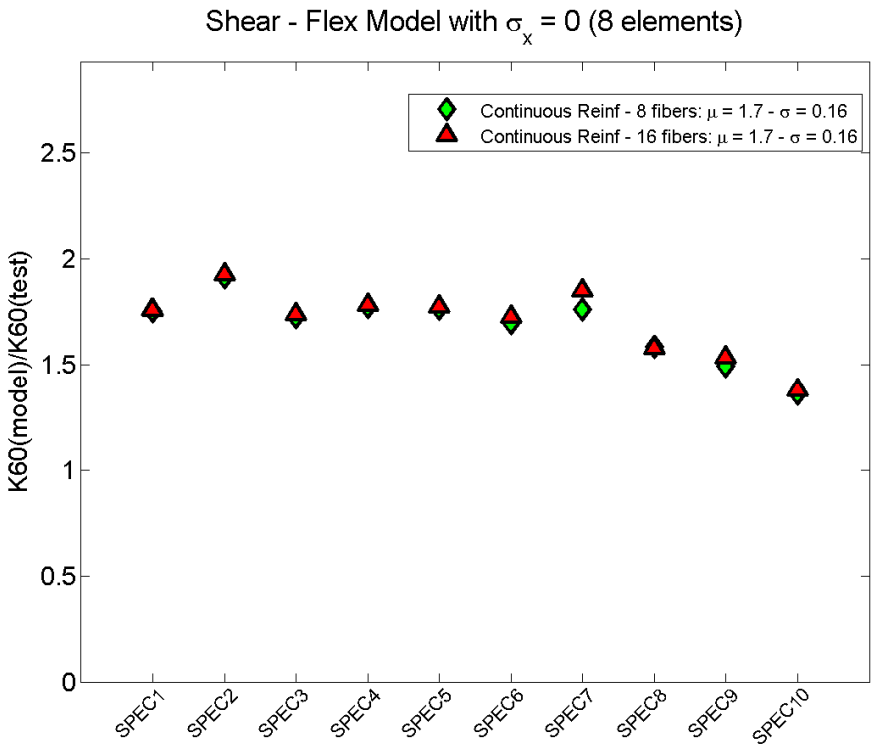

Figure 4.5: Rigidity at 60% of maximum capacity. Shear – Flexure interaction model with $\boldsymbol{\sigma_x = 0}$, and 8 elements in the longitudinal direction.

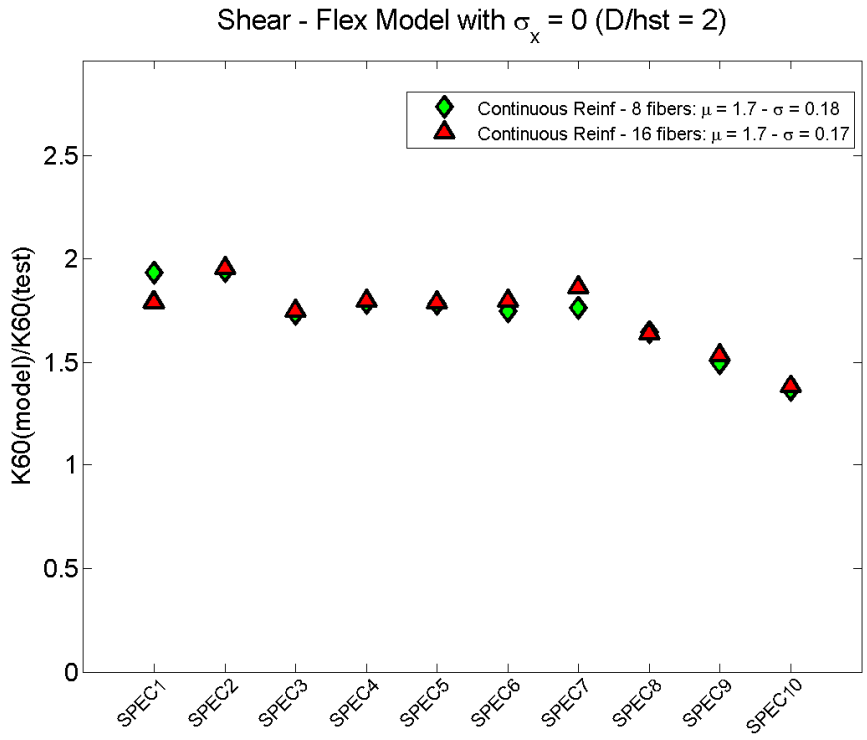

Figure 4.6: Rigidity at 60% of maximum capacity. Shear – Flexure interaction model with $\boldsymbol{\sigma_x = 0}$, and a constant $\boldsymbol{D/h_{st} = 2}$ ratio.

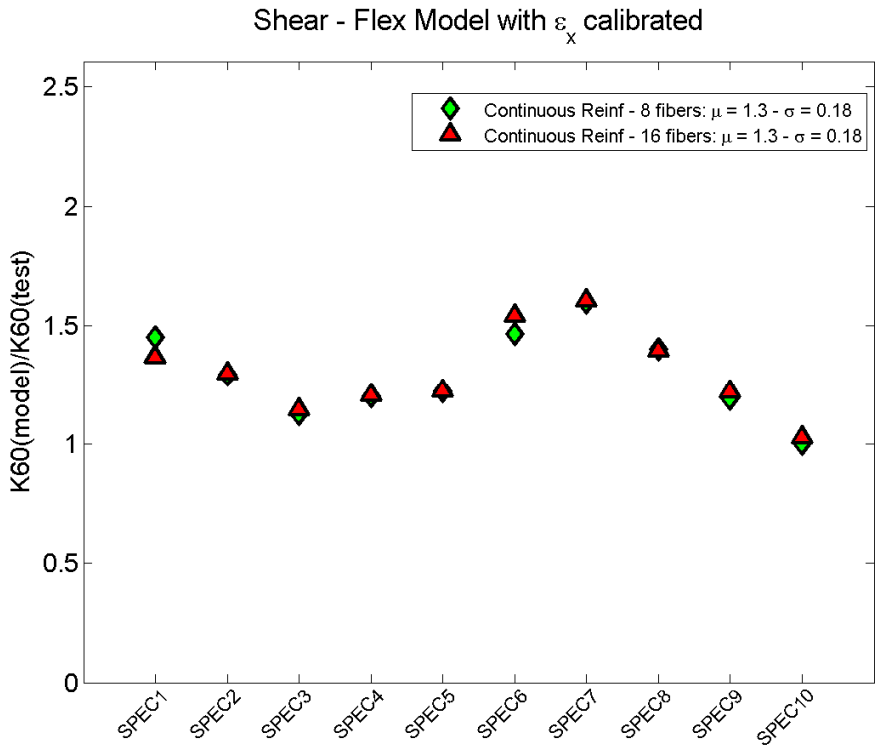

Figure 4.7: Rigidity at 60% of maximum capacity. Shear – Flexure interaction model with $\boldsymbol{\varepsilon_x}$ calibrated (8 elements in the longitudinal direction).

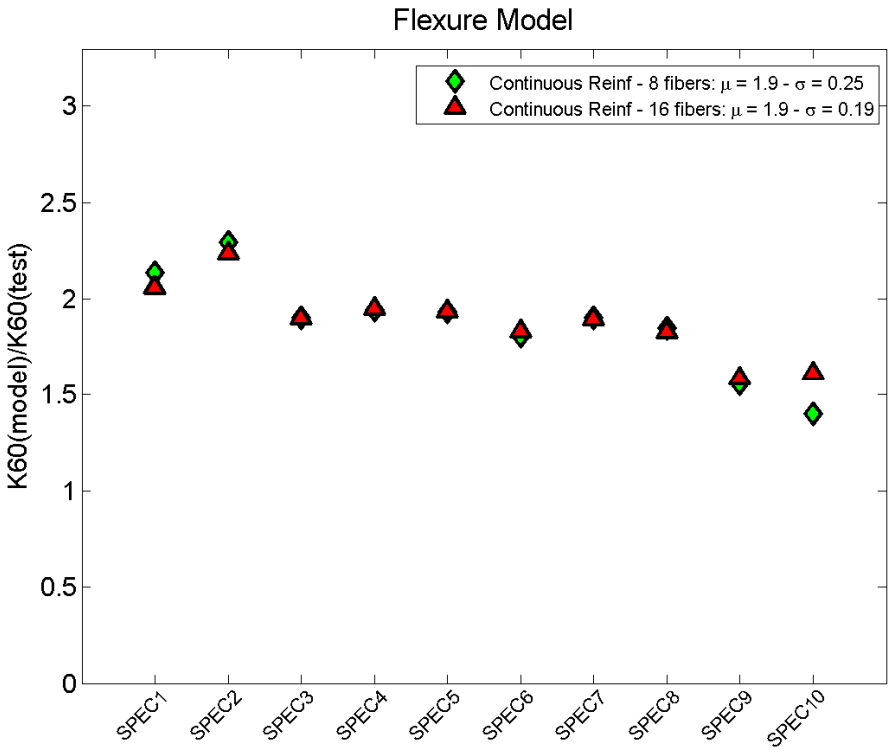

Figure 4.8: Rigidity at 60% of maximum capacity. Flexure model (8 elements in the longitudinal direction).

4.2.3. Analysis of Columns. Displacement at 10% of Capacity Loss.

The Displacement at 10% of Capacity Loss is the third of the parameters studied for the analysis of columns. The parameter studied for each model is the displacement at 10% of capacity loss obtained from the analysis ($D10_{Model}$) over the same parameter obtained from the test ($D10_{Test}$), i.e.:

$$\hat{d} = \frac{D10_{Model}}{D10_{Test}} \tag{4.3.3}$$

The distribution of $\hat{d}$ (Figure 4.9) is shown for the interaction model with $\sigma_x = 0$ and a constant $D/h_{st} = 2$ ratio. Interaction models with 8 elements in the longitudinal direction showed too fast degradation due to damage localization. The flexure model is, by definition, a model that does not incorporates shear degradation, so it is not considered in the analysis of $\hat{d}$.

The $\sigma_x = 0$ with a constant $D/h_{st} = 2$ ratio is giving a mean value of $\hat{d}$ of 0.83 for an 8 fibers discretization, and 0.86 for a 16 fibers discretization. Most of the specimens give values of $\hat{d}$ between 0.5 and 1, except for specimens 4 and 5, that give values $\hat{d}$ near to 1.5 (for both discretizations). A possible reason is the low amount of transverse reinforcement provided to specimens 4 and 5. In the model, the transverse reinforcement confines the concrete raising the concrete strength in approximately 4% with a consequent raise of ε_c of approximately 20% (Table 4.3), for both specimens, according to the Saatcioglu & Razvi, 1992, model. A sensitivity

analysis is performed in these two specimens in order to assess the effect of neglecting confinement when low transverse reinforcement is used in the columns (Figure 4.10 and Figure 4.11). The results show that using only the unconfined concrete model in Specimens 4 and 5 has little effect on the estimation of maximum capacity and rigidity. Nevertheless, it can be noticed that the prediction on degradation is improved for these cases, by neglecting the effect of confinement. However, in these cases the test was finished with a low number of cycles, thus it is possible that degradation is not well shown in the load – displacement response and is not possible to make conclusions due to lack of information.

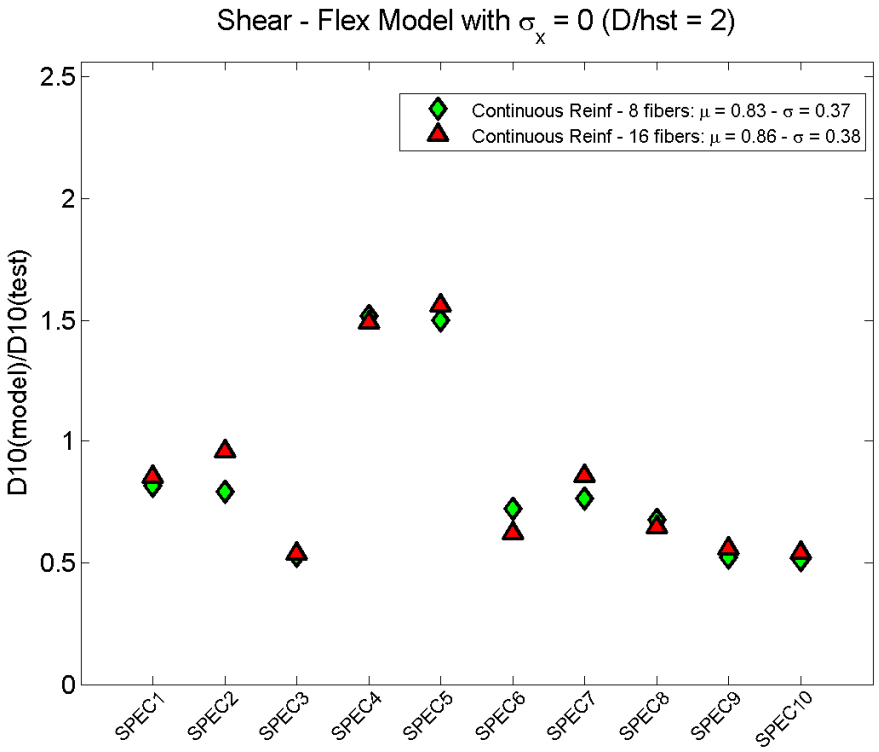

Figure 4.9: Displacement at 10% of capacity loss. Shear – Flexure interaction model with $\boldsymbol{\sigma_x = 0}$, and a constant $\boldsymbol{D/h_{st} = 2}$ ratio.

Table 4.3: Properties of Specimens 4 and 5.

	Specimen 4	Specimen 5
f'_c [MPa]	26.8	31.2
f'_{cc} [MPa]	28.0	32.4
ε_c	0.00177	0.00184
ε_{cc}	0.00218	0.00220

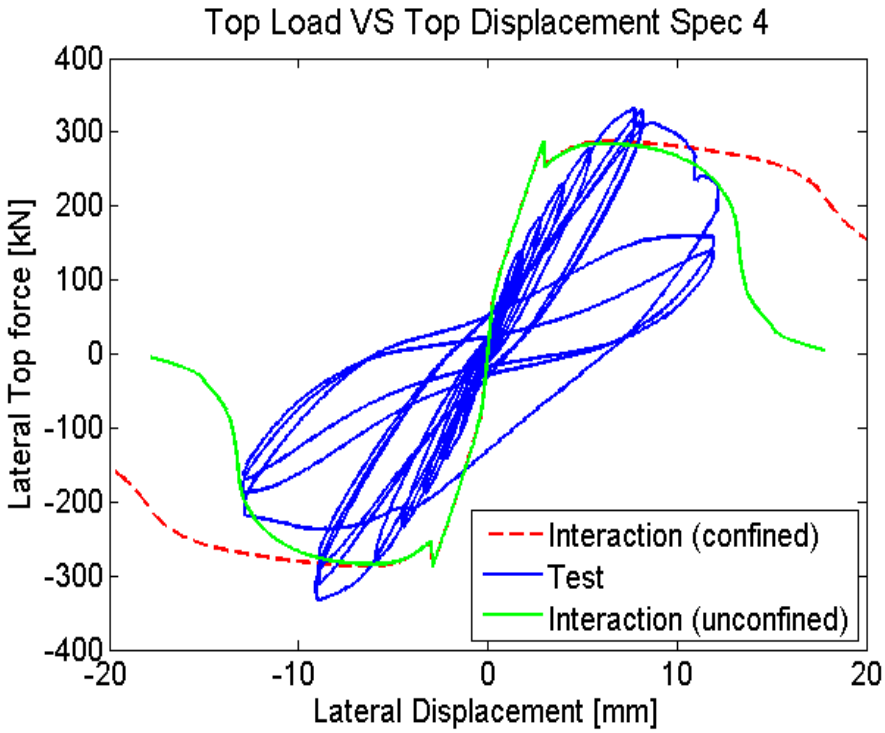

Figure 4.10: Comparison of load – displacement responses of Specimen 4, considering confined concrete model and neglecting the effect of confinement.

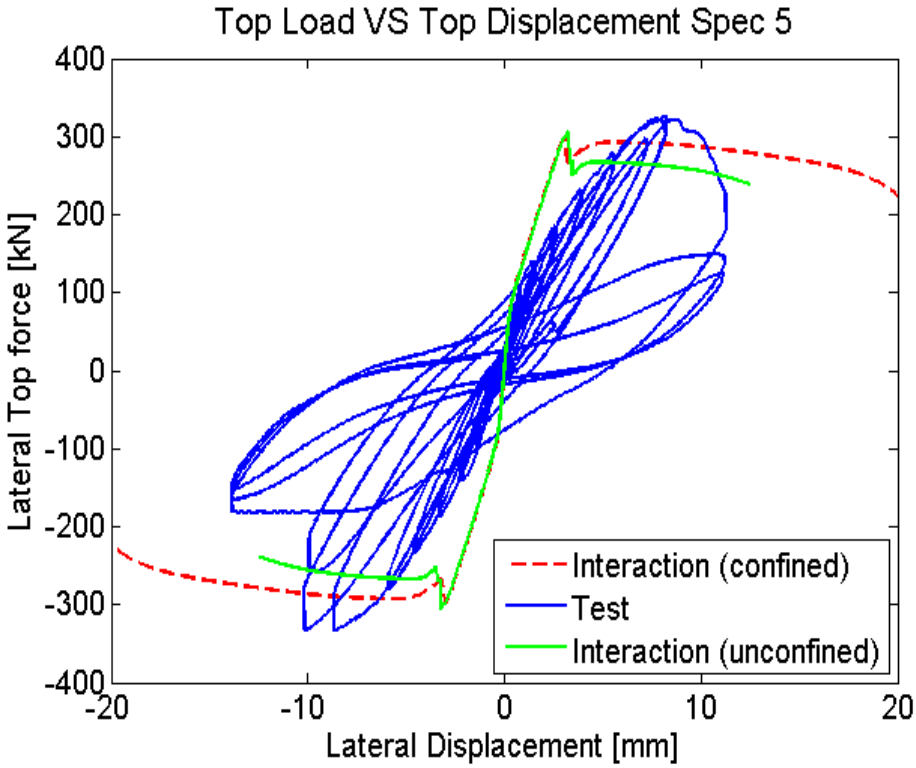

Figure 4.11: Comparison of load – displacement responses of Specimen 5, considering confined concrete model and neglecting the effect of confinement.

4.2.4. Analysis of Columns. Transverse Strain for model $\sigma_x = 0$.

The transverse strain (ε_x) has also been studied for the model with $\sigma_x = 0$, and a constant $D/h_{st} = 2$ ratio, using a 16 fibers discretization. The maximum value of ε_x for each fiber of every specimen is shown in Figure 4.12. It can be observed that in all cases there are fibers with ε_x beyond the yielding strain of steel. Nevertheless, most of the fibers show lower values of ε_x than 0.0021. The percentage of fibers with $\varepsilon_x > 0.0021$ is related to the shear – span ratio according to Table 4.4 and Figure 4.13. A lower shear – span ratio gives a higher percentage of fibers with $\varepsilon_x > 0.0021$. In section 4.3 sensitivity analyses related to transverse reinforcement are performed, where low impact was observed in terms of maximum capacity and degradation displacement, for these specimens.

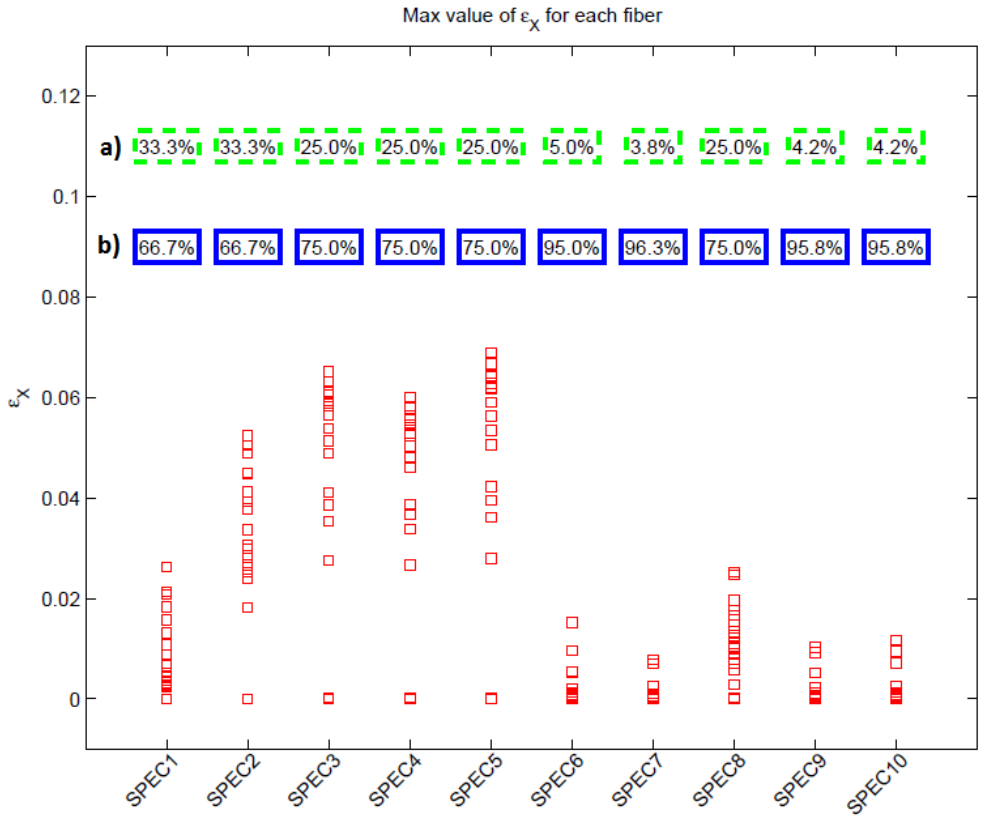

Figure 4.12: Maximum value of transverse strain ($\boldsymbol{\varepsilon_x}$) of each fiber, for all specimens. The percentages in the boxes represent a) the percentage of fibers with $\boldsymbol{\varepsilon_x > 0.0021}$ and b) the percentage of fibers with $\boldsymbol{\varepsilon_x < 0.0021}$.

Table 4.4: Shear – span ratios and percentage of fibers with $\boldsymbol{\varepsilon_x > \varepsilon_y}$, for every specimen.

ID N°	*M/VD*	*Fibers with* $\varepsilon_x > \varepsilon_y$ [%]
SPEC1	1.5	33.3
SPEC2	1.5	33.3
SPEC3	2	25.0
SPEC4	2	25.0
SPEC5	2	25.0
SPEC7	2.92	3.8
SPEC6	2.93	5.0
SPEC8	2	25.0
SPEC9	3.38	4.2
SPEC10	3.38	4.2

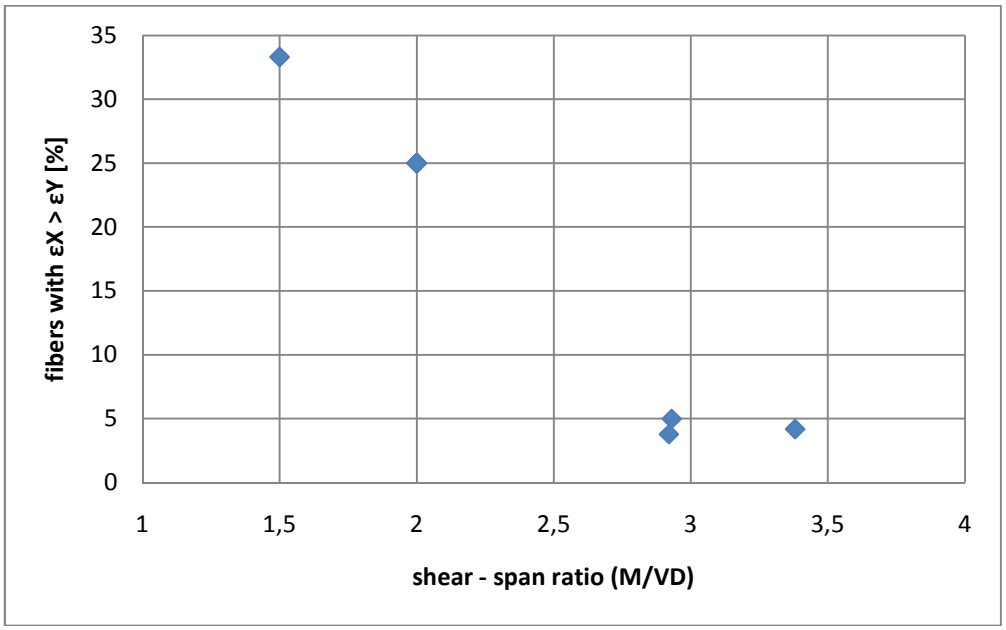

Figure 4.13: Percentage of fibers with $\boldsymbol{\varepsilon_x > \varepsilon_y}$ vs shear – span ratio.

Two different stages have also been studied. The values of $\boldsymbol{\varepsilon_x}$ were studied at maximum capacity of the load – displacement response, and also at 1% of column drift. Most of the specimens do not show yielding in $\boldsymbol{\varepsilon_x}$, at maximum capacity (Figure 4.14). At 1% of drift it is observed a higher number of fibers with yielding, were shorter columns show a higher percentage of fibers with $\boldsymbol{\varepsilon_x} > 0.0021$ (Figure 4.15). Similar results are obtained when comparing the percentage of fibers with $\boldsymbol{\varepsilon_x} > 0.0021$ to the shear – span ratio, as shown in Figures 4.16 and 4.17. The fibers with yielding were found to correspond to the element near to the support (with displacement and rotation restrained), were higher stresses and strains are expected.

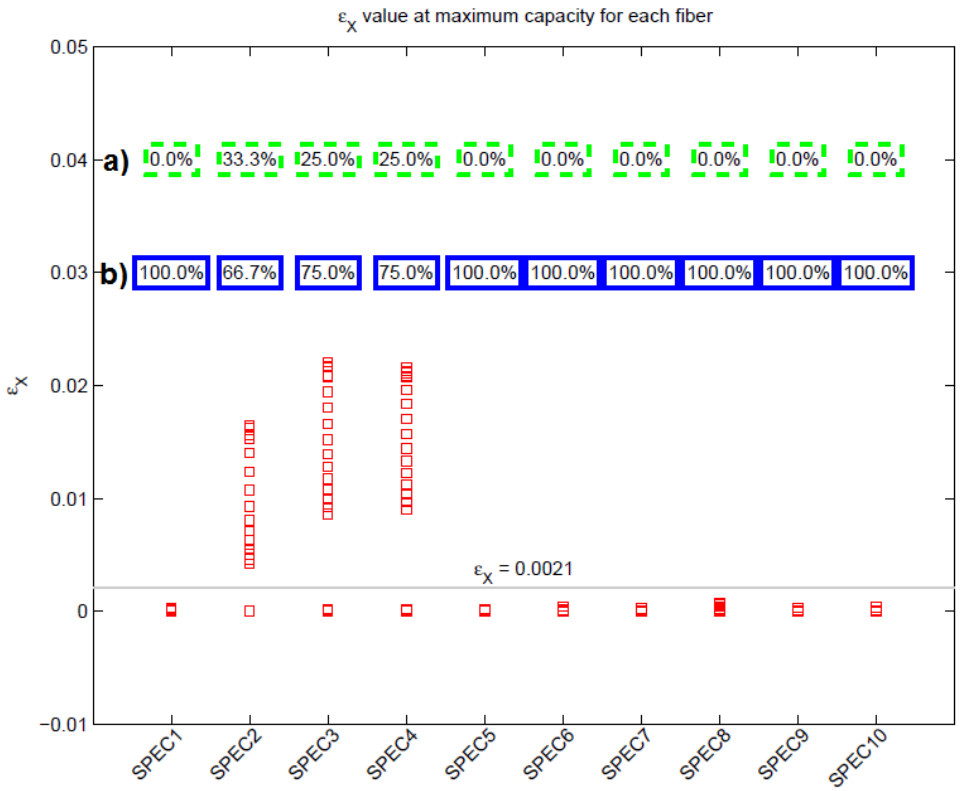

Figure 4.14: Values of $\boldsymbol{\varepsilon_x}$ at maximum capacity for each fiber. The percentages in the boxes represent a) the percentage of fibers with $\boldsymbol{\varepsilon_x > 0.0021}$ and b) the percentage of fibers with $\boldsymbol{\varepsilon_x < 0.0021}$.

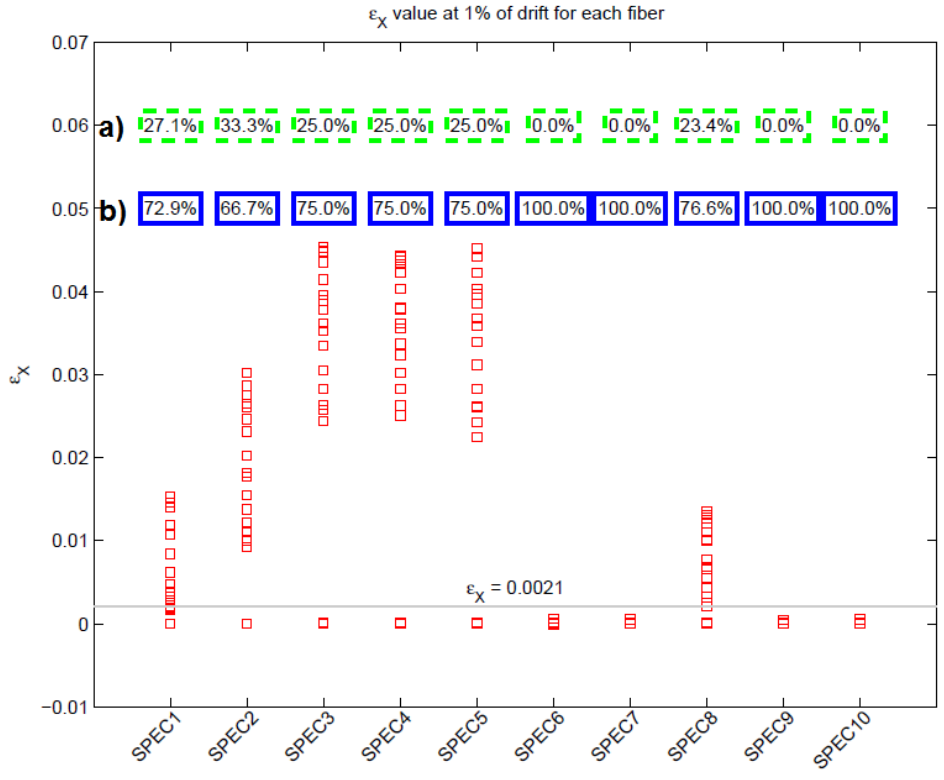

Figure 4.15: Values of $\boldsymbol{\varepsilon_x}$ at 1% of column drift for each fiber. The percentages in the boxes represent a) the percentage of fibers with $\boldsymbol{\varepsilon_x > 0.0021}$ and b) the percentage of fibers with $\boldsymbol{\varepsilon_x < 0.0021}$.

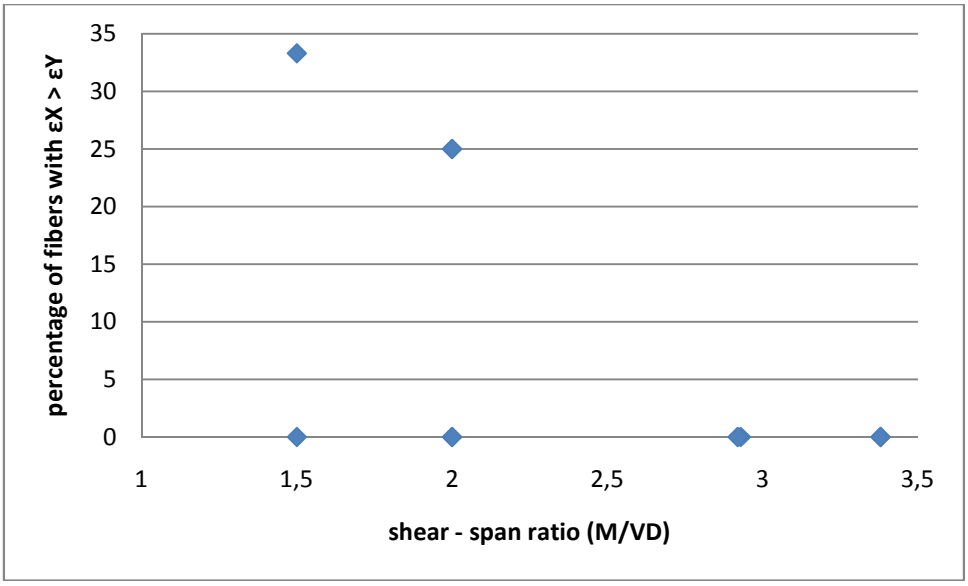

Figure 4.16: Percentage of fibers with $\boldsymbol{\varepsilon_x > \varepsilon_y}$ vs shear – span ratio. Values at maximum capacity.

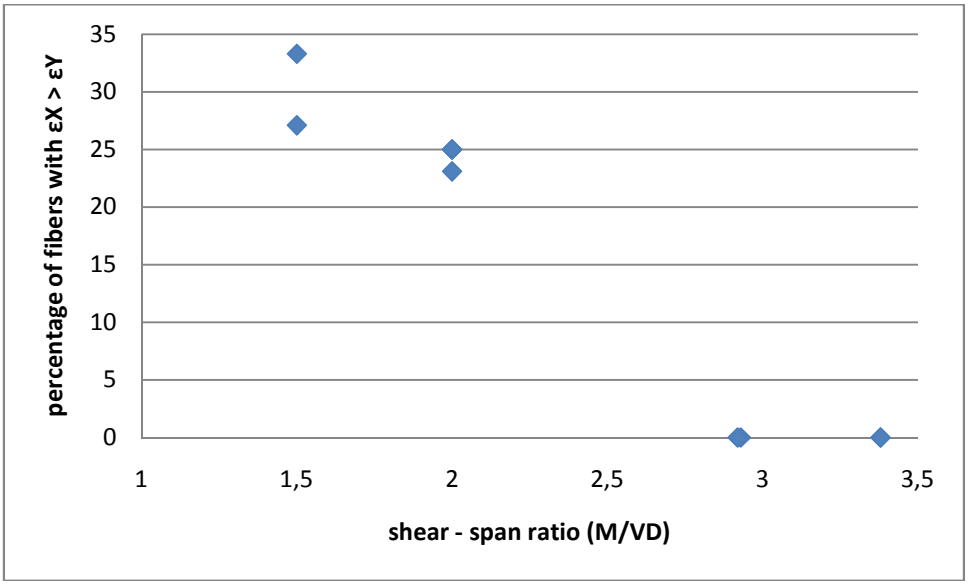

Figure 4.17: Percentage of fibers with $\boldsymbol{\varepsilon_x > \varepsilon_y}$ vs shear – span ratio. Values at 1% of lateral drift.

4.3 Sensitivity Analysis

Sensitivity analyses were performed in order to assess the effect of selected parameters in the response of the shear – flexure model. The parameters selected were the confinement effectiveness, in terms of the effective lateral pressure (f_l, see section 2.1) and the amount of transverse reinforcement, in terms of the transverse reinforcement ratio (ρ_t).

4.3.1. Sensitivity Analysis of Confinement Effectiveness

The effect of confinement is assessed by comparing two values of the lateral effective pressure, given by the Saatcioglu & Razvi, 1992, model. This parameter is studied because

transverse reinforcement contributes to both confinement and shear resistance, therefore, confinement effectiveness could be affected. It is considered for the analysis the 100% and the 50% of f_l (equation 2.1.12). This has the same effect on the parameters n and k for the Collins & Porasz, 1989, model, discussed in section 2.1.3. The analysis is run for all the specimens. The base model used for this analysis corresponds to the Shear – Flexure interaction with 8 fibers, using the ε_x calibrated procedure (see Section 0). A statistical analysis is performed on two parameters, 1) maximum capacity, and 2) degradation displacement at 10% of capacity loss. This is shown on Figures 4.18 and 4.19.

Confinement has little effect on capacity. For a 50% of confinement, capacity is, on average, 1% lower than the case with 100% of confinement, with low dispersion. It can be seen that confinement has little effect on degradation for most of the specimens, except for specimens 1 and 8, where degradation displacement is about 30% lower than the case with 100% of confinement (Figure 4.19).

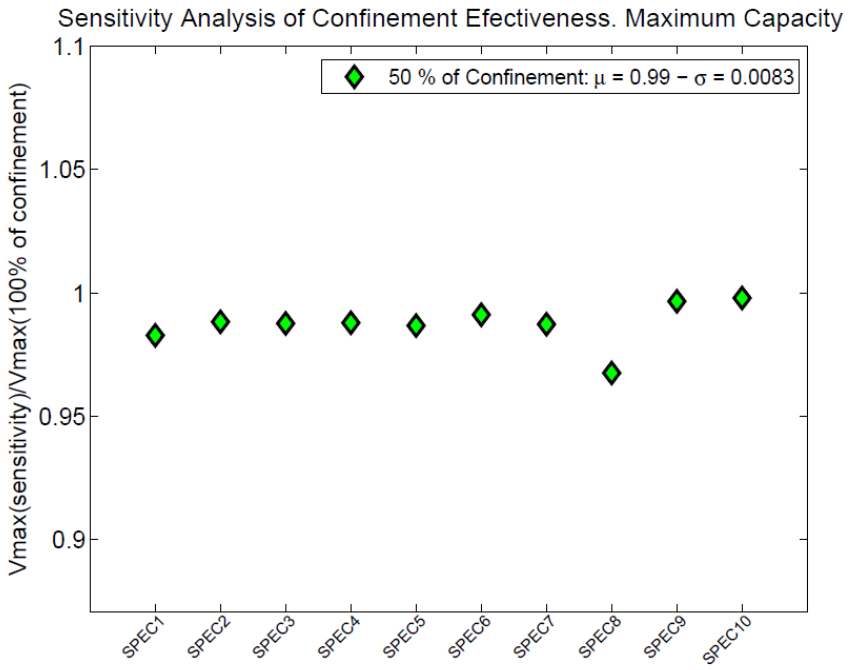

Figure 4.18: Sensitivity analysis of confinement. Maximum capacity statistics.

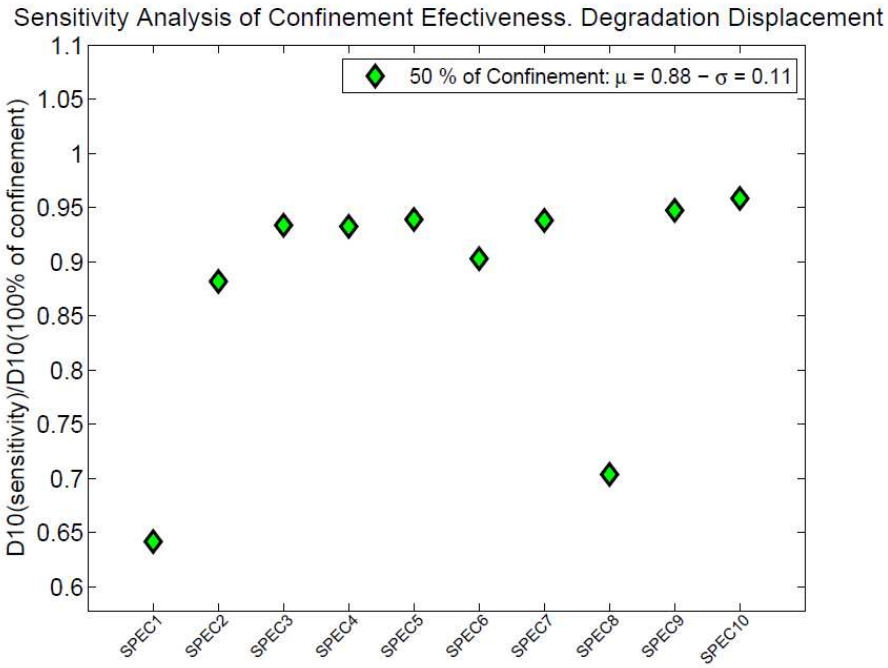

Figure 4.19: Sensitivity analysis of confinement. Degradation displacement Statistics.

4.3.2. Sensitivity Analysis of Lateral Reinforcement

The amount of lateral reinforcement is studied because in circular columns with spiral reinforcement, the projection of reinforcement in the direction of displacement is less than 100% of the nominal area, due to the hoop curvature. The effect of the amount of lateral reinforcement is assessed by comparing the base model (Shear – Flexure with 8 fibers, using ε_x calibrated procedure), with a 100% of transverse reinforcement ratio (ρ_t), against two different values of transverse reinforcement ratio, 50% and 150% of ρ_t. All other parameters remain constant. Figures 4.20 and 4.21 show a statistical analysis performed on two parameters, 1) maximum capacity, 2) and degradation displacement at 10% of capacity loss.

The effect of the amount of lateral reinforcement is shown for the shear – flexure interaction model with ε_x calibrated. It can be seen that this parameter has little effect on capacity and ductility. The average maximum capacity and degradation displacement, have little differences (lower than 1% for all cases) comparing to the 100% of lateral reinforcement.

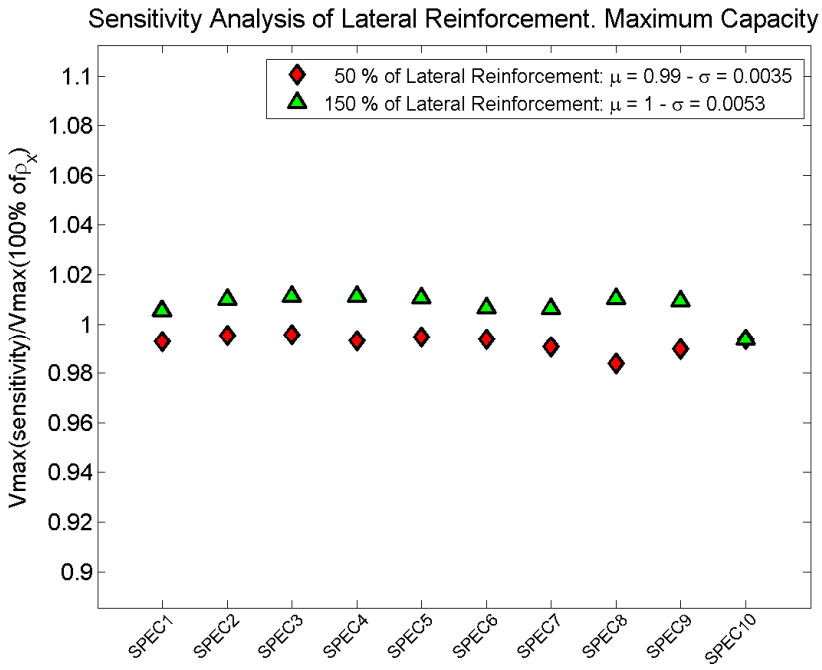

Figure 4.20: Sensitivity analysis of lateral reinforcement. Maximum capacity statistics.

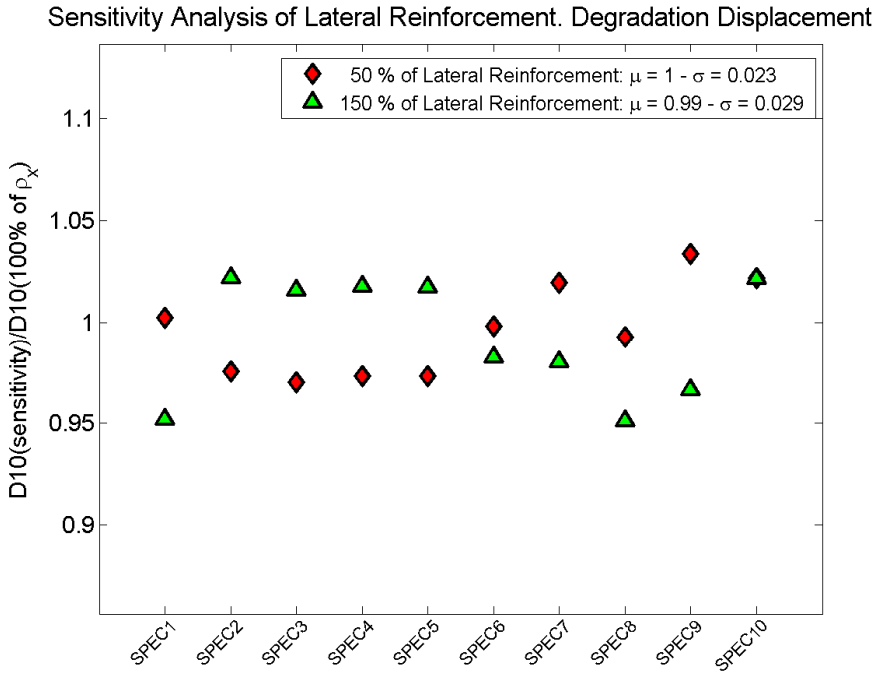

Figure 4.21: Sensitivity analysis of confinement. Degradation displacement statistics.

CHAPTER 5. Analysis of Shear – Flexure Interaction Model on a Pile

5.1 Background

The principal objective of this work is to assess the effect of pile shear deformations on p – y curves (Section 2.2). To achieve this, the load – displacement response of a fixed – head pile test performed by Stewart et al, 2007, is used. Prior studies performed by Lemnitzer et al, 2013, on the fixed – head pile, showed that shear displacements can contribute up to 40% of the total displacements, when modeling the pile using the interaction model along with the p – y approach. Therefore, shear deformations have an influence on the total displacements finally calculated and ultimately may significantly influence the p – y curves. The analyses performed by Lemnitzer et al, 2013, used p – y curves obtained from prior large scale testing on the site, for similar boundary conditions. Nevertheless, the p – y curves were derived by Stewart et al, 2007, such that good correlation was observed with a flexure model. This gives an adjustment for the load – displacement response obtained by the flexural model, but shows discrepancies when using the interaction model (Figure 5.1).

A fitting procedure is performed to obtain the p – y curves adjusting the load -displacement response of the interaction model to the load – displacement response of the test. The characterization of the p – y curves used for this purpose, was discussed in section 2.2. The flexure model is also used to model the structure, in order to compare the p – y curves obtained using a uniaxial fiber model against the p – y curves obtained using a model that incorporates shear deformations.

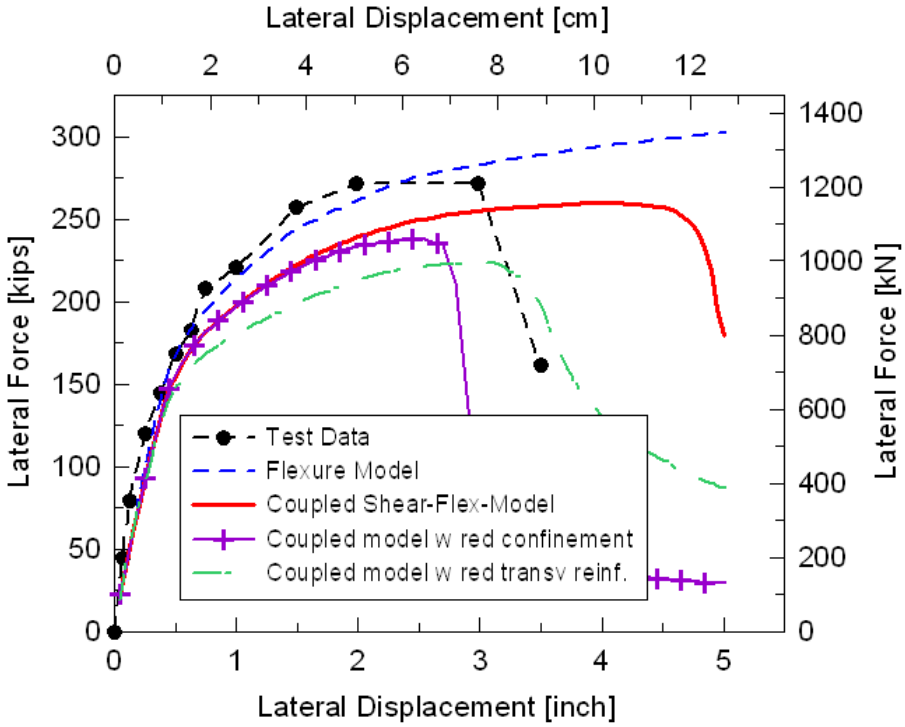

Figure 5.1: Load – Displacement profiles for Fixed - Head pile using p - y curves derived by Stewart et al, 2007. Lemnitzer et al, 2013.

5.2 Test Description. Pile and Model Properties

The experimental studies were conducted by Stewart et al, 2007, for a 0.61 m. diameter Fixed – Head pile. The shaft was designed using a 28 MPa concrete mix, however, cylinder tests gave values of f'_c between 30 and 36 MPa. The longitudinal reinforcement consists of 8 #9 bars ($d_b = 29$ mm) A706, Grade 60 steel, with a measured yield stress of 483 MPa. Transverse reinforcement was a 48 cm diameter spirals made of #5 bars ($d_b = 16$ mm) spaced at 11 cm pitch over the length of the pile. The clear concrete cover was 6 cm. The length of the pile is 7.5 m. (25 ft or 300 in).

The values incorporated in the model were an average plain concrete strength of $f'_c = 32$ MPa, at a concrete strain of $\varepsilon_c = 0.0023$. The confined concrete properties were calculated using the Saatcioglu & Razvi, 1992, model, and resulted in a confined concrete strength of $f'_{cc} = 51$ MPa at a concrete strain of $\varepsilon_{cc} = 0.0089$. The yield stress for reinforcement is taken as $f_y = 439$ MPa, with a strain hardening ratio of $b = 0.008$ for the Menegotto & Pinto, 1973, model. The material models used for the analysis were discussed in section 2.1.

A constant $D/h_{st} = 2$ ratio was assumed for the longitudinal discretization, which led to 25 elements along its length ($h_{st} = 30$ cm). The continuous reinforcement with 16 fibers was assumed for the transverse discretization. The decision was taken based on the results of section 4.2. The $\sigma_x = 0$ procedure of analysis was elected, although, the ε_x calibrated procedure gave better results, it needs a calibrated ε_x profile and there is no calibration for the transverse strain on piles.

5.3 Soil Parameters and p – y curves implementation

In 2001, a large suite of geotechnical tests were performed in the site of testing (Wallace et al, 2001). In summary, the soil profile can be described as (Stewart et al, 2007):

- (0 to ~5 ft) Rubble and fill
- (~5 to ~21 ft) Silty clay, PI ~15, 60% fines, lower-bound OCR from 3.5 to 5.9, 2 ft thick silty sand interbed at ~10 ft
- (~21 to ~24 ft) Medium- to fine-grained silty sand/sandy silt, PI ~12, 30% fines
- (~24 to ~48 ft) Silty clay, PI ~13 to ~14,
- (> ~48 ft) Medium sand, water bearing (water table is at ~48 ft)

The construction of the p – y curves is based on the API (1993) recommendations, as discussed in section 2.2. It can be seen that the soil profile consist of essentially silty clays for the upper 50 ft, therefore, it has been assumed that the shaft is embedded in a soil with a clay behavior. Thus, the parameters selected to define the API (1993) p – y curves are (Stewart et al, 2007) $\gamma = 125$ pcf, $c = 3900$ psf, $J = 0.25$ and $\varepsilon_{50} = 0.007$.

To implement the p – y curves it has been assumed the exponential shape recommended in the API (1993), and incorporated in OpenSees as a tri – linear model as described in section 2.2. In order to study the shear effect on p – y curves, two parameters has been selected: the undrained shear strength of the soil (c) and the deflection at one – half of the ultimate resistance (y_c). Both

parameters are multiplied by factors in order to adjust the load – displacements responses given by flexure and shear – flexure models, to the test responses, as following:

$$c^* = N_c \cdot c \tag{5.3.1}$$

$$y_c{}^* = N_y \cdot y_c \tag{5.3.2}$$

The values of N_c and N_y are changed in order to fit the overall load – displacement response to the test response, so the curves are compared graphically. First, the value of N_c is changed in order to adjust the ultimate strength of the pile; and then the value of N_y is changed in order to adjust the rigidity and strength degradation (if exists) of the pile.

5.4 Analysis of Pile response and effect of shear on p – y curves

5.4.1. Results for the Flexure Model.

The first step of the analysis was studying the response of the pile given by the flexure model. The parameters N_c and N_y, were adjusted in order to fit the load - displacement response of the flexure model to the test response. It can be noticed that the flexure model has a good adjustment for the initial stiffness and strength, however, the model does not show strength degradation, associated to shear failures on the pile (Figure 5.2). The curve is shown along the load – displacement response obtained by Lemnitzer et al, 2013, in order to make comparisons. The parameters $\hat{v}$ and $\hat{k}$ defined in eq. 4.3.1 and 4.3.2, respectively, are calculated for these cases (Table 5.1), where $\hat{v}$ is calculated considering the responses before 3 in (before strength degradation of the test). Parameter $\hat{d}$ (eq. 4.3.3) is not considered because flexure models do not show strength degradation. It can be observed that both models are good when predicting strength and predicting rigidity.

Table 5.1: Values of $\hat{\mathbf{v}}$ and $\hat{\mathbf{k}}$ calculated for flexures models of Lemnitzer et al, 2013, and calibrated p – y curves.

	Lemnitzer et al, 2013	Flexure model (calibrated p – y curves)
$\hat{v}$	1.04	1.03
$\hat{k}$	0.99	1.02

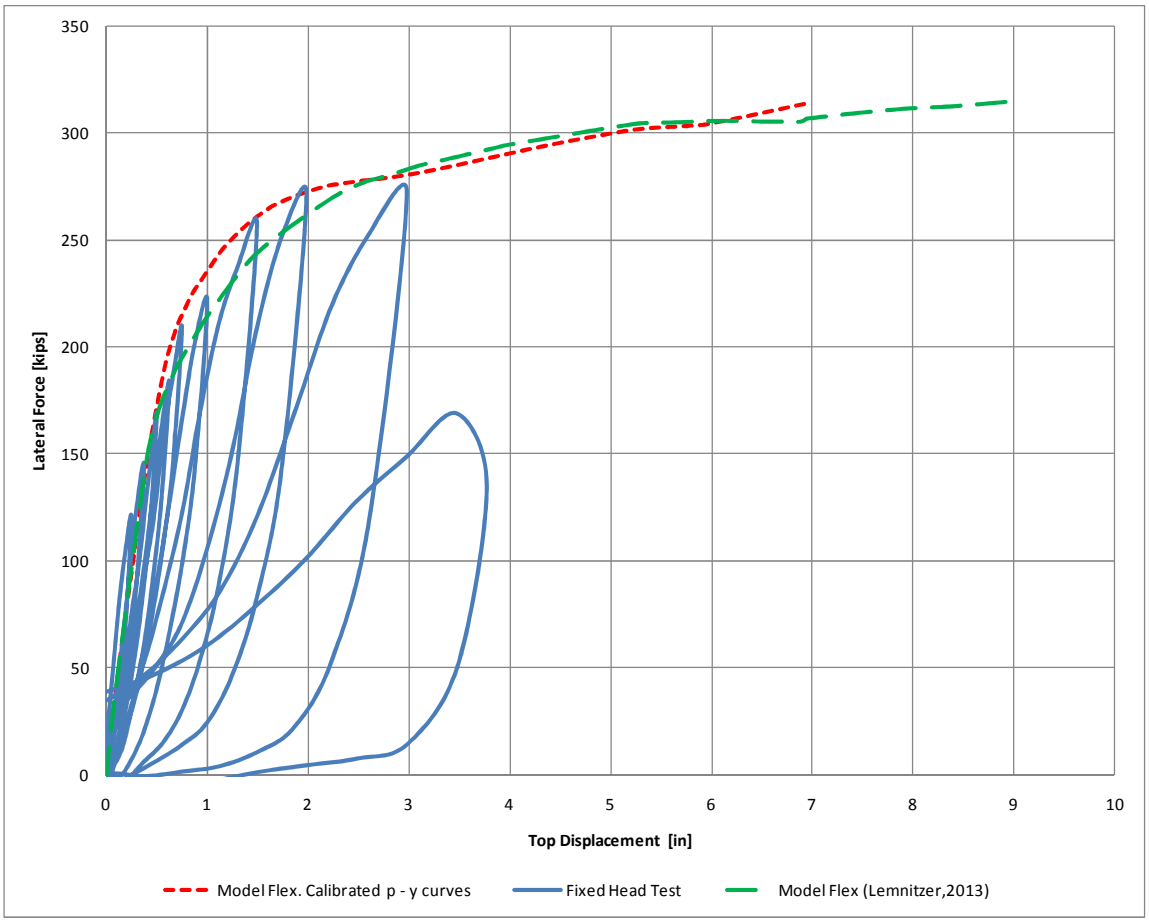

Figure 5.2: Load - Displacement responses for Fixed - Head pile. p - y curves adjusted for the Flexure model.

The values of p_u and y_c obtained are compared to the ones used by Lemnitzer et al, 2013, (Table 5.2). The values of p_u obtained from the analysis are higher along the pile depth, where differences of about 10% are found at 0 in, 20% at 24 in (1 pile diameter) and 23% at 48 in (2 pile diameters). The value of y_c obtained is 57% higher to the value used by Lemnitzer et al, 2013. Nevertheless, p – y relationships have little differences on initial stiffness as shown in Table 5.3, where a difference of about 1% was found for the superficial layer. The p – y relationships are shown for different depths in Figure 5.3 for both models.

It is important to notice that the pile test response show displacements until about 3.5 in (Figure 5.2) and the p – y curve obtained by Lemnitzer, 2013, for the superficial layer ($Z = 0$ in), is practically identical to the p – y curve obtained in the present work, until the same displacement, being the actual calibration about 10% higher at $y = y_c$, and also shows lower rigidity for $y > y_c$ (Figure 5.3). Similar behavior is observed in the global response, suggesting that pile behavior is controlled by the p – y curve at $Z = 0$ in.

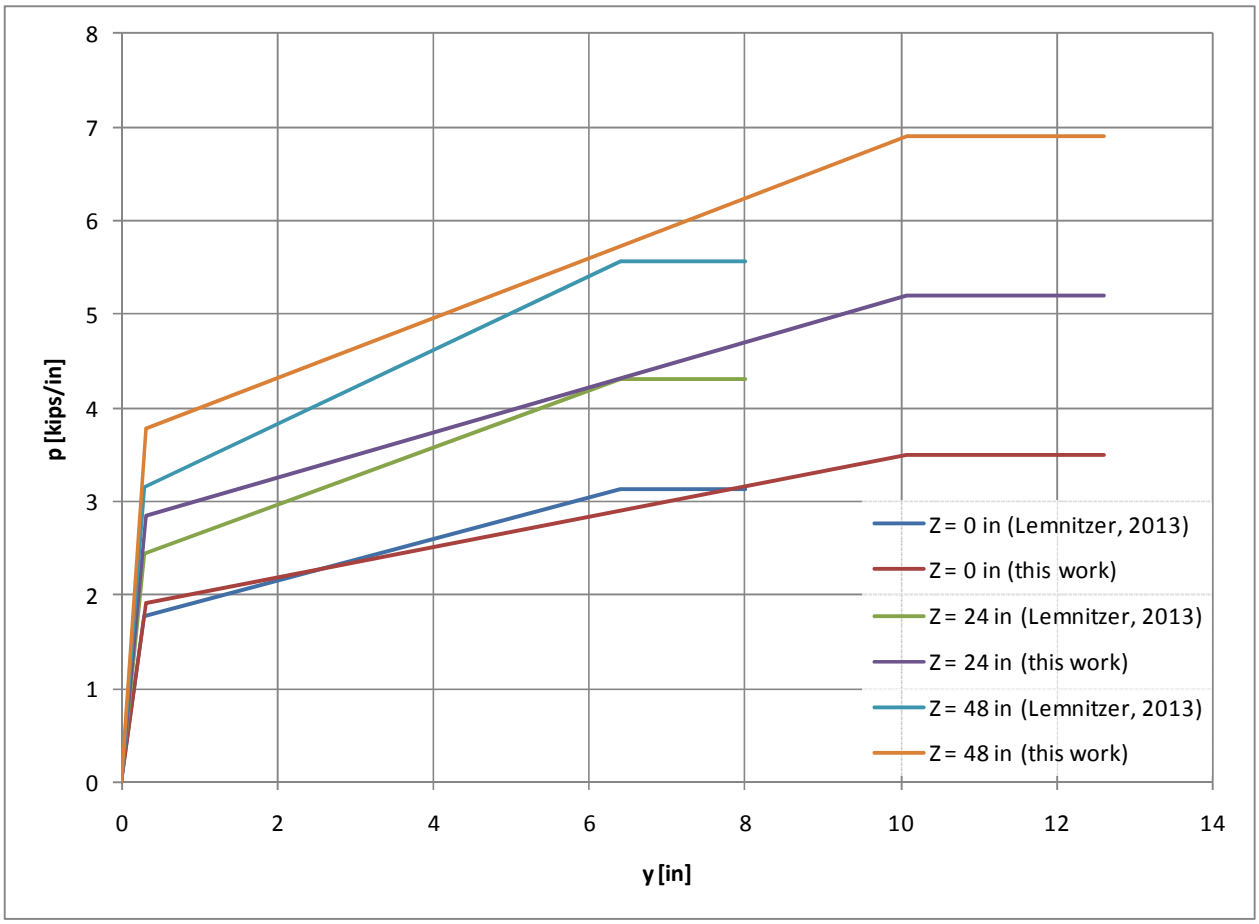

Figure 5.3: Comparison of p – y curves deduced using the fitting procedure for the flexure model against the p – y curves used by Lemnitzer et al, 2013.

Table 5.2: Comparison of $\mathbf{p_u}$ and $\mathbf{y_c}$ obtained using the fitting procedure and the ones used by Lemnitzer et al, 2013.

	Lemnitzer et al, 2013.		Flexure p - y curves	
Depth[in]	pu [kips/in]	yc [in]	pu [kips/in]	yc [in]
0	2.988	0.400	3.315	0.630
12	2.988	0.400	4.123	0.630
24	4.104	0.400	4.932	0.630
36	4.104	0.400	5.740	0.630
48	5.310	0.400	6.548	0.630
60	5.310	0.400	7.357	0.630
72	6.246	0.400	8.165	0.630
84	6.246	0.400	8.973	0.630
96	6.714	0.400	9.782	0.630
108	7.200	0.400	9.945	0.630
120	7.200	0.400	9.945	0.630

Table 5.3: Comparison of initial rigidity (K) and ultimate resistance (pu) of the p – y curves used by (1) Lemnitzer et al, 2013, against the p – y curves deduced using the fitting procedure for the flexure model (2).

Z [in]	K1 [kips/in^2]	K2 [kips/in^2]	pu1 [kips]	pu2 [kips]	K1/K2	pu1/pu2
0	6.18	6.12	3.13	3.49	1.01	0.90
24	8.49	9.10	4.30	5.19	0.93	0.83
48	10.98	12.09	5.57	6.90	0.91	0.81

5.4.2. Results for the Shear - Flexure Interaction Model.

The second step of the analysis was studying the response of the pile given by the interaction model. The parameters N_c and N_y, were adjusted in order to fit the load - displacement response of the shear – flexure interaction model to the test response (see Figure 5.4). The interaction model has a good adjustment for strength, initial stiffness and strength degradation, in terms of parameters $\hat{v}$, $\hat{k}$ and $\hat{d}$ shown in Table 5.4.

Table 5.4: Parameters $\hat{\mathbf{v}}$, $\hat{\mathbf{k}}$ and $\hat{\mathbf{d}}$, for the interaction model along the calibrated p – y curves.

	Interaction model (calibrated p – y curves)
$\hat{v}$	1.02
$\hat{k}$	1.03
$\hat{d}$	1.04

Finally, the flexure and interaction curves, obtained using the fitting procedure, are compared in Figure 5.5. It can be observed that both models give similar results for the ascending curve, between 0 in. and 3 in. of lateral displacement. Then, the flexure model keeps ascending while the interaction model shows strength degradation beyond the 3 in. of lateral displacement.

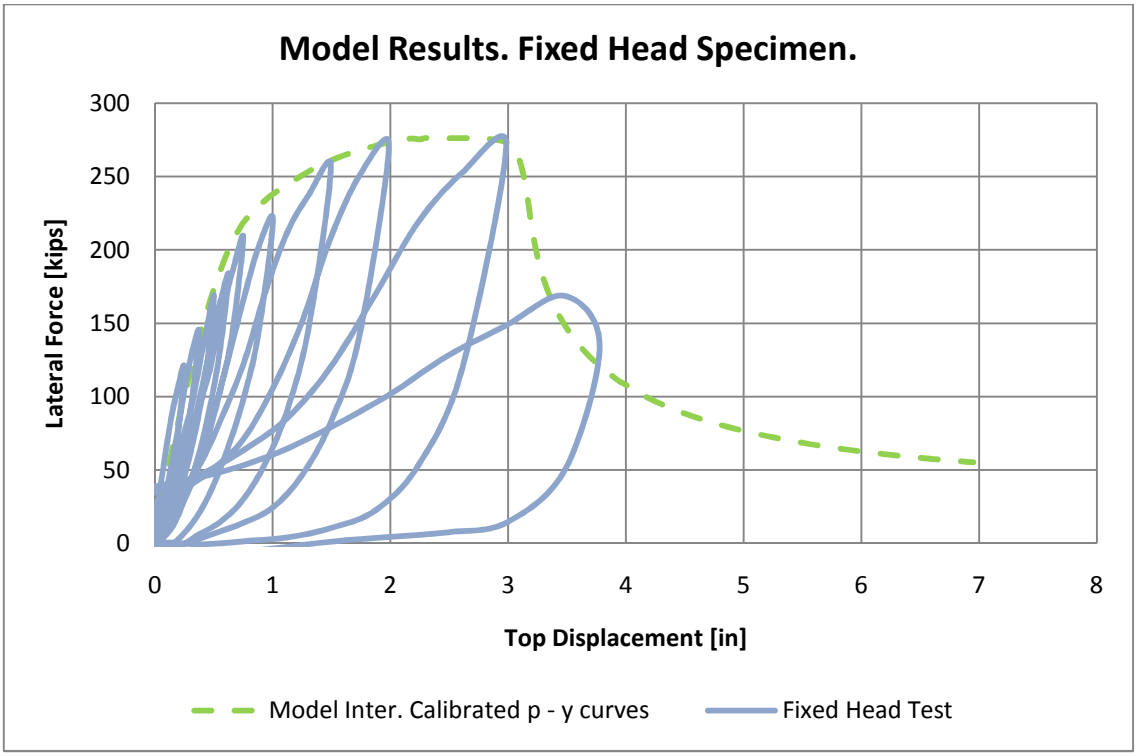

Figure 5.4: Load - Displacement profiles for Fixed - Head pile. p - y curves adjusted for the Shear - Flexure (***S – F***) Interaction model.

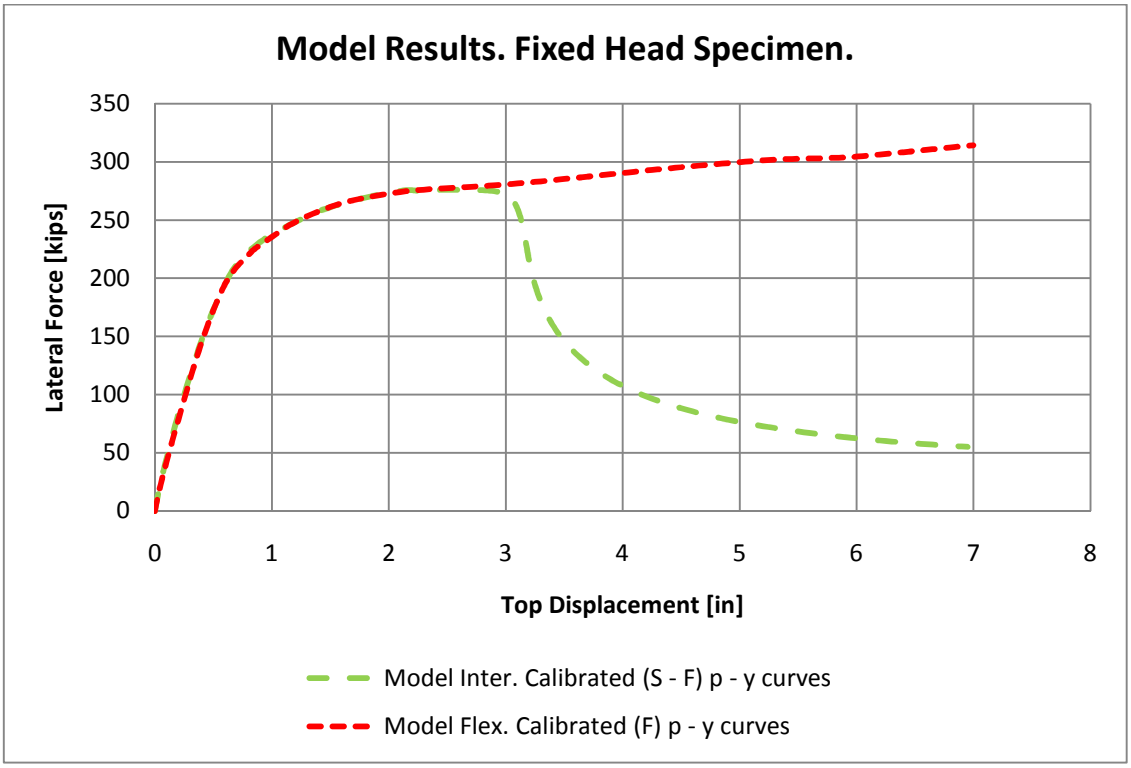

Figure 5.5: Comparison of load – displacement responses of flexure and interaction models for the Fixed – Head pile.

5.4.3. Effect of Shear on the p – y curves.

The parameters N_c and N_y, defined in eq. 5.3.1 and 5.3.2, were adjusted to fit the load – displacement responses of the flexure and the shear – flexure interaction models, to the load – displacement response of the Fixed – Head test performed by Stewart et al, 2007. Figure 5.6 shows flexure and interaction models using the p – y curves calibrated for flexure model (***F*** p – y curves). The interaction model gives lower initial rigidity and strength than flexure, thus, it is expected that p – y curves calibrated for the interaction model (***S – F*** p – y curves) should have higher initial stiffness and ultimate resistance than the ***F*** p – y curves. The values of N_c and N_y finally obtained are shown in Table 5.5, and applying the new values (c^* and $y_c{}^*$, eqs. 5.3.1 and 5.3.2, respectively) to the shape of p – y curves recommended in the API (1993), different p – y relationships are obtained as shown in Figure 5.7 as tri – linear responses. (Note: It is important to make the difference between the p – y curves calibrated for flexure model, ***F*** p – y curves, and the p – y curves calibrated for the interaction model, ***S – F*** p – y curves).

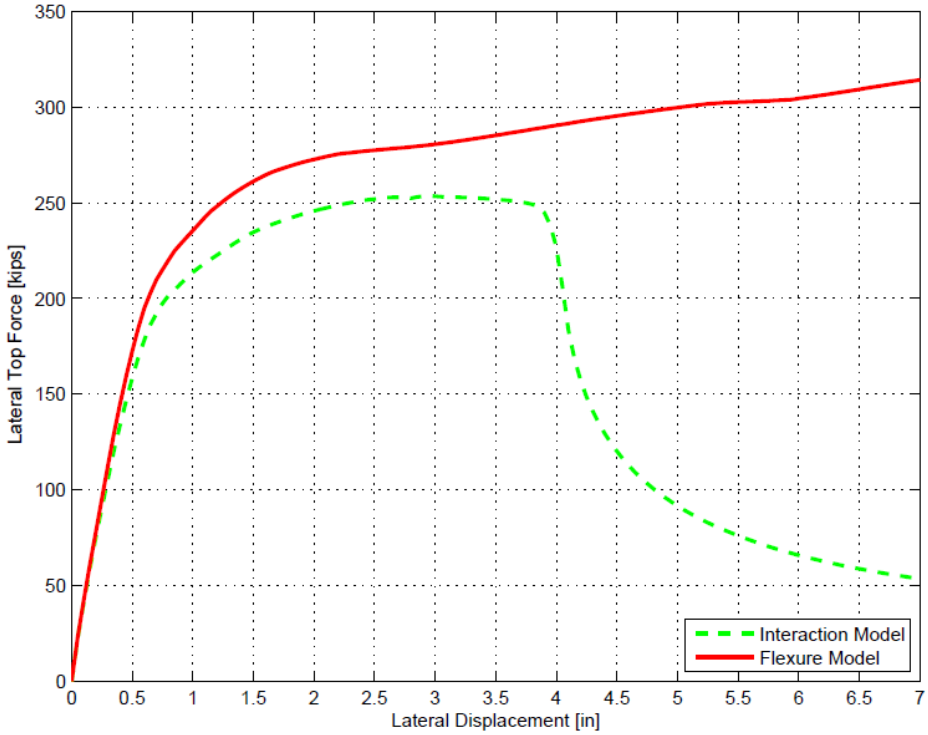

Figure 5.6: Load – displacement responses for flexure and interaction models obtained using the ***F*** p – y curves.

Table 5.5: Values of $\mathbf{N_c}$, $\mathbf{N_y}$, **c** and $\mathbf{y_c}$ obtained for the Flexure (***F***) and Shear – Flexure (***S – F***) Interaction Models.

	N_c	N_y	c [kips/in^2]	y_c [in]
Flexure (*F*) Model	1.7	1.5	0.0460	0.630
Shear – Flexure (*S* - *F*) Model	2.5	1.6	0.0677	0.714

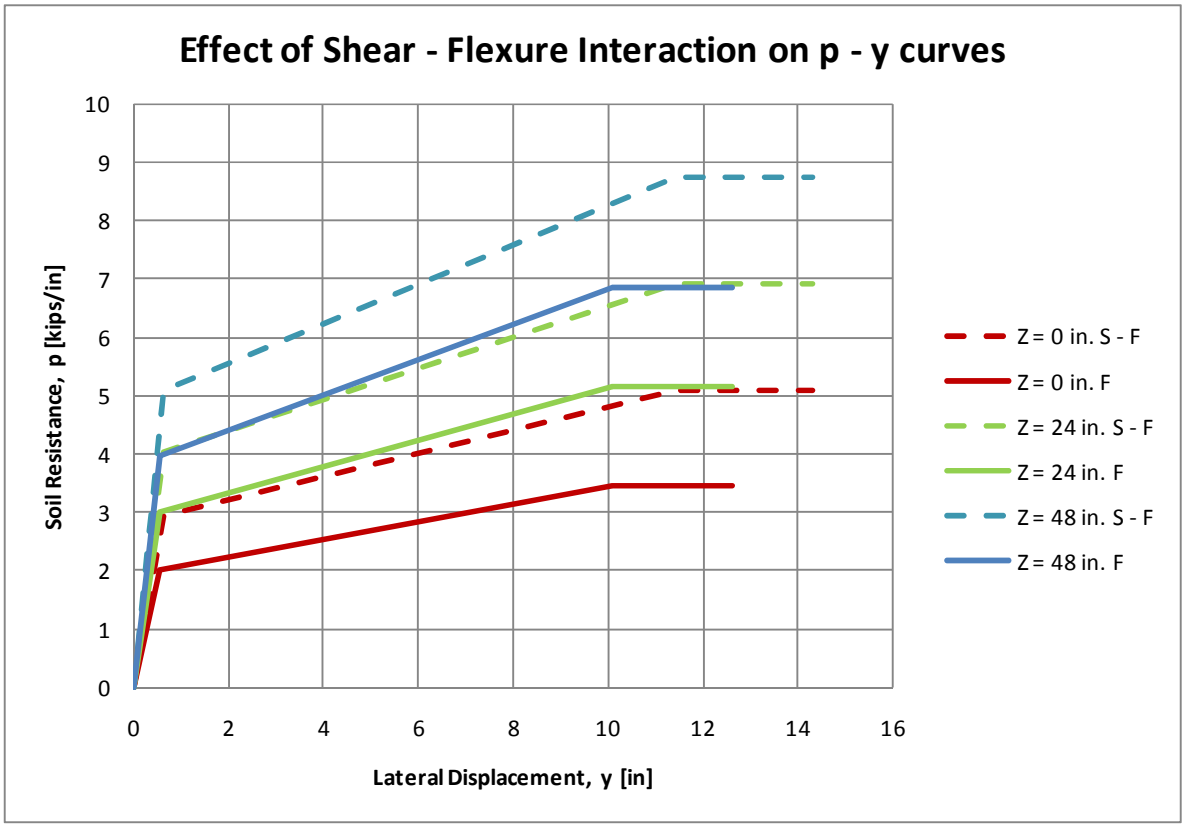

Figure 5.7: Comparison of p – y curves obtained using Flexure (***F***) and Shear – Flexure (***S – F***) Models.

The p – y curves are shown for the ground line (Z = 0 in.) and for a depth of 1 and 2 pile diameters (24 in and 48 in, respectively). The ***S – F*** p – y curves (dashed lines) show higher ultimate resistance than the ***F*** p – y curves (continuous lines). The initial stiffness of the ***S – F*** p – y curves is also higher than the ***F*** p – y curves, as shown in Table 5.6.

Table 5.6: Comparison of the initial stiffness and ultimate resistance of the p - y curves obtained by the Shear – Flexure (***S – F***) and Flexure (***F***) Models.

Z [in]	K (***S – F***) [kips/in^2]	K (***F***) [kips/in^2]	pu (***S – F***) [kips/in]	pu (***F***) [kips/in]	K (***S – F***)/K (***F***) [%]	pu (***S – F***)/pu (***F***) [%]
0	4.6	3.5	5.1	3.5	129.8	147.1
24	6.2	5.2	6.9	5.1	118.5	134.3
48	7.8	6.9	8.7	6.8	112.8	127.8

It can be observed that the difference of about 10% of capacity, in the global response, between the flexure and interaction models at 3.0 in of lateral displacement (Figure 5.6) result in a difference of p_u of 47%, for the superficial curve (Z = 0 in) and a difference of initial stiffness of about 30%. The differences for the superficial p – y curve at 3.0 in of lateral displacement are about 40% (Table 5.7).

Table 5.7: Comparison of the soil resistance at 3.0 in of lateral displacement, for the superficial p – y curve (Z = 0 in)

Z [in]	p(y = 3 in) ***S - F*** [kips/in]	p(y = 3 in) ***F*** [kips/in]	***S-F/F*** [%]
0	3.4	2.4	141.6

The parameter c affects the distribution of $p_u(z)$ (equation 2.2.3) and the value of z_r (equation 2.2.4). This effect is shown in Figure 5.8. The interaction model gives higher values for $p_u(z)$ than the Flexure model, just as predicted by Lemnitzer et al, 2013. It should be highlighted that the influence of shear is expected to be concentrated at the top of the pile, thus, the $p_u(z)$ distribution presented is not necessarily a real representation of the soil behavior for deeper levels. The influence of shear in depth is studied in 5.5.1.

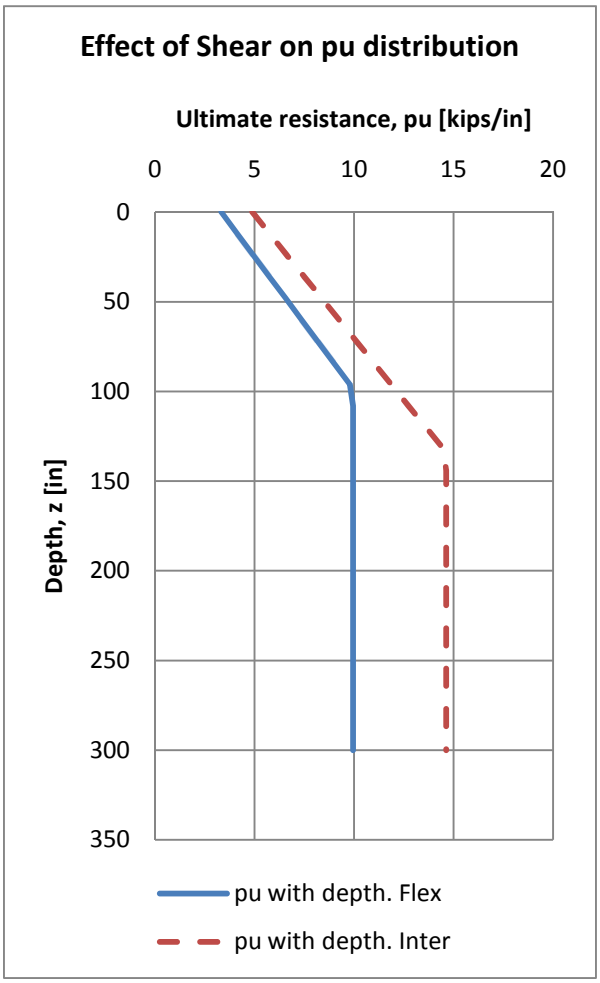

Figure 5.8: Effect of Shear on $\mathbf{p_u}$ distribution.

5.4.4. Displacement Profiles.

In the previous study developed by Lemnitzer et al, 2013, the displacement profiles threw that shear displacements are concentrated right below ground line (up to about 24 in depth, or 1 pile diameter) and were nearly zero at other locations, contributing up to 40% of total displacements, for a lateral displacement of 5.0 in at which the load – displacement response obtained using the interaction model starts showing strength degradation. Therefore, the effect on p – y curves is expected to be located essentially on the upper 1 pile diameter.

The displacement profiles obtained in the present work are shown in Figure 5.10. The shear displacements are concentrated between the ground line and a pile depth of approximately 24 in (1 pile diameter), and are negligible at lower depths. The flexural displacements can be observed between the ground line and a pile depth of 120 in (approximately 5 pile depths). The shear displacements are contributing up to 35% to the total lateral displacement, at lateral top displacement of 3.0 in where strength degradation is observed in the global response (Figure 5.4). The flexural displacements account for up to 65% of the total displacements at the same displacement level. These results are obtained from the interaction model along the ***S – F*** p – y curves.

5.4.5. Moment and Shear Profiles.

The moment profile (Figure 5.11) shows that the yielding occurs at two locations, just below ground line in negative bending and approximately at 66 in (near to 3 pile diameters) of depth in positive bending, for a lateral displacement of 3.0 in. Bending moment approaches zero at depths below 200 in (about 8 pile diameters). Thus, two plastic hinges are developed during loading at the locations mentioned above. The longitudinal stress – strain response ($\sigma_y - \varepsilon_y$) for the extreme fibers of each section, shows that yielding occurs at two locations, just below ground line at 6 in and at 66 in (roughly 3 pile diameters), confirming the results observed in the moment profiles (Figure 5.13). At the same displacement level, the nominal capacity is reached at a depth of approximately 66 in. The yielding and nominal moments were computed as 450 and 565 kN-m, respectively (3975 and 5000 kips-in, according to Lemnitzer et al, 2013, based on a section analysis using in-situ shaft properties). Moment profiles obtained by using the flexure model are similar to the interaction model profiles (Figure 5.12). It is also observed yielding at two points (just below ground line in negative bending and at 66 in. of depth in positive bending), and nominal capacity is reached at 66 in, for a lateral displacement of 3.0 in. Also bending moment approaches zero at depths below 200 in.

The shear profile shows that the nominal shear strength is reached at the ground interface for a lateral top displacement of 3.0 in, which is consistent with the results obtained by Lemnitzer et al, 2013. This is also observed in the shear profile obtained with the flexure model. It should be noted that on the field, extensive shear cracks were observed at the pile – cap interface (Figure 5.9). The nominal shear strength was computed as 950 kN (214 kips, Lemnitzer et al, 2013, using the ATC – 32 (1996) recommendations for circular cross sections.

$$V_s = \frac{\pi}{2}\frac{A_{sp} f_{yh} D'}{s} \tag{5.4.1}$$

.

$$V_c = 0.166\sqrt{f'_c}A_e \quad (5.4.2)$$

$$V_n = V_s + V_c \quad (5.4.3)$$

Where D' is the diameter of the hoop reinforcement measured to the hoop centerline (50.8 cm), s is the vertical hoops spacing (11.4 cm), f_{yh} is the yield strength of the hoops (483 MPa for fixed head), A_{sp} is cross-sectional area of the hoop (2 cm^2), A_e is the effective shear area of the shaft (2918.6 cm^2) and f'_c is the concrete compressive strength (32.4 MPa), V_s denotes the shear strength due to transverse reinforcement, V_c represents the concrete shear strength and V_n is the nominal shear strength of the section. The results are also obtained from the interaction model along the ***S – F*** p – y curves.

Figure 5.9: Shear cracks observed after excavation. Lemnitzer et al ,2013.

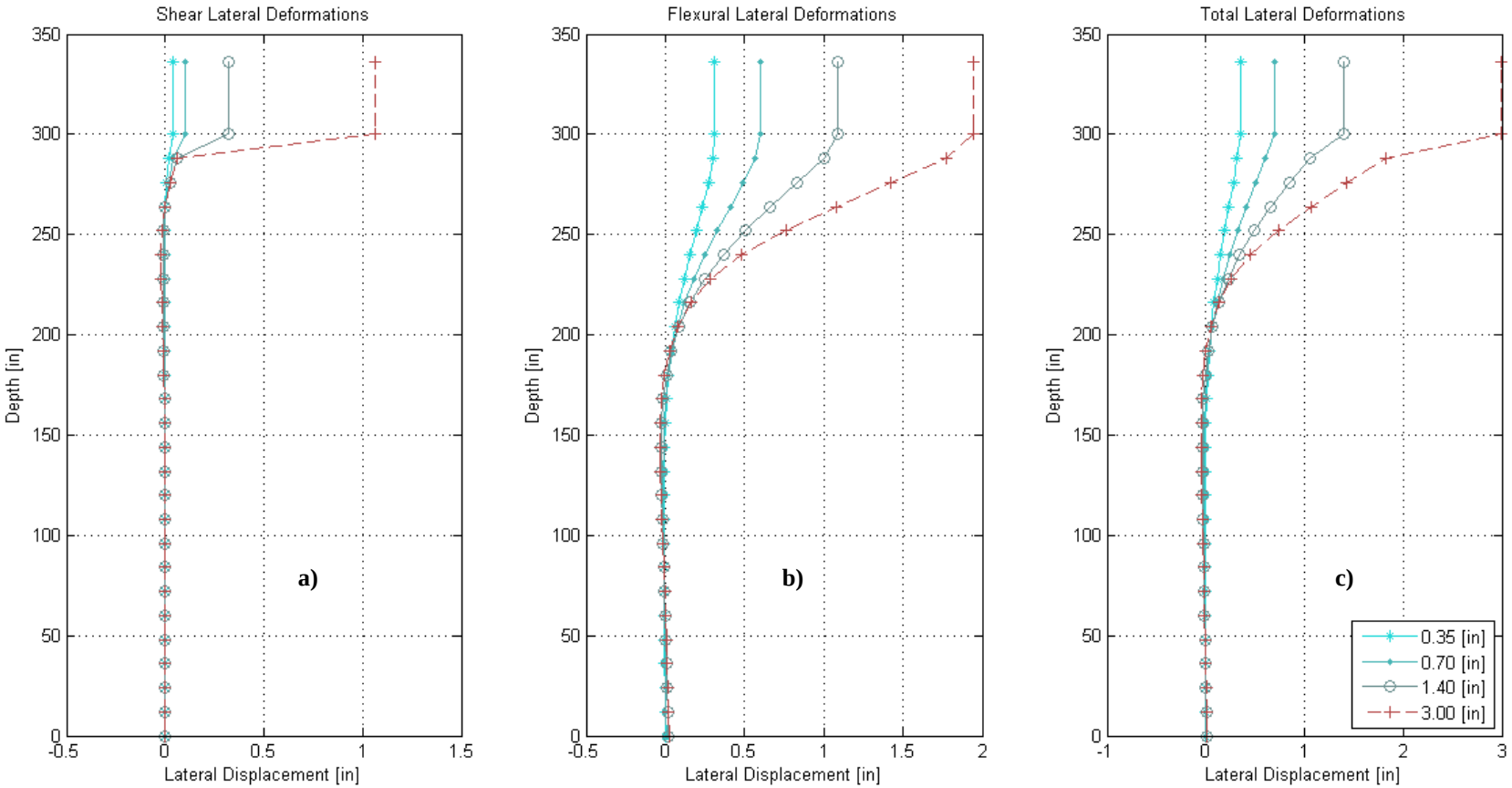

Figure 5.10: Displacement profiles for different top displacement levels. Interaction model.

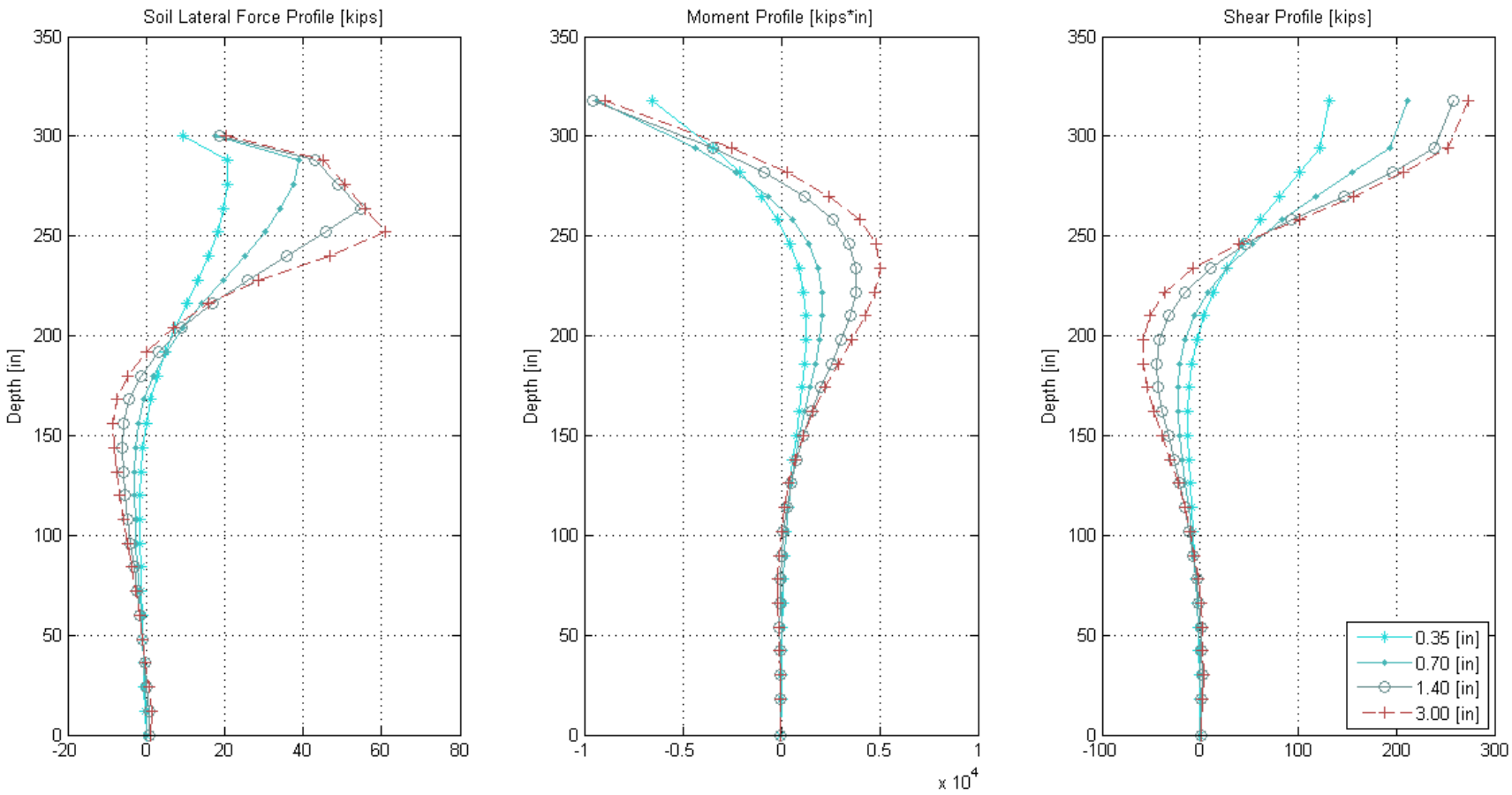

Figure 5.11: Reaction profiles for different top displacement levels. Interaction model.

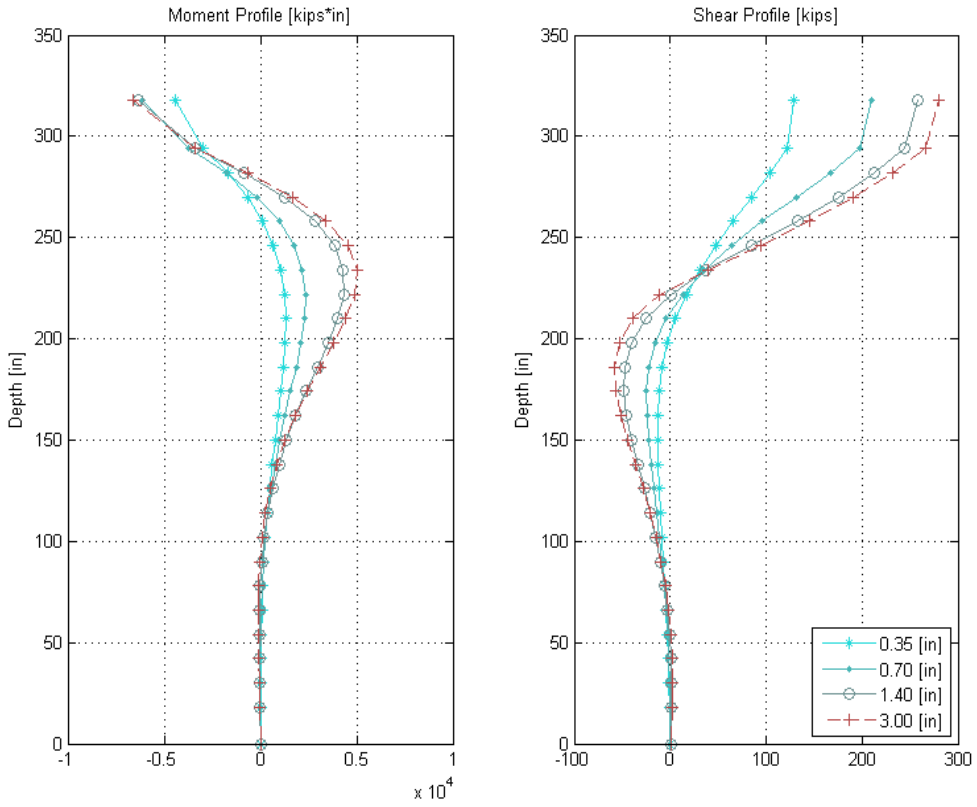

Figure 5.12: Reaction profiles for different top displacement levels. Flexure model.

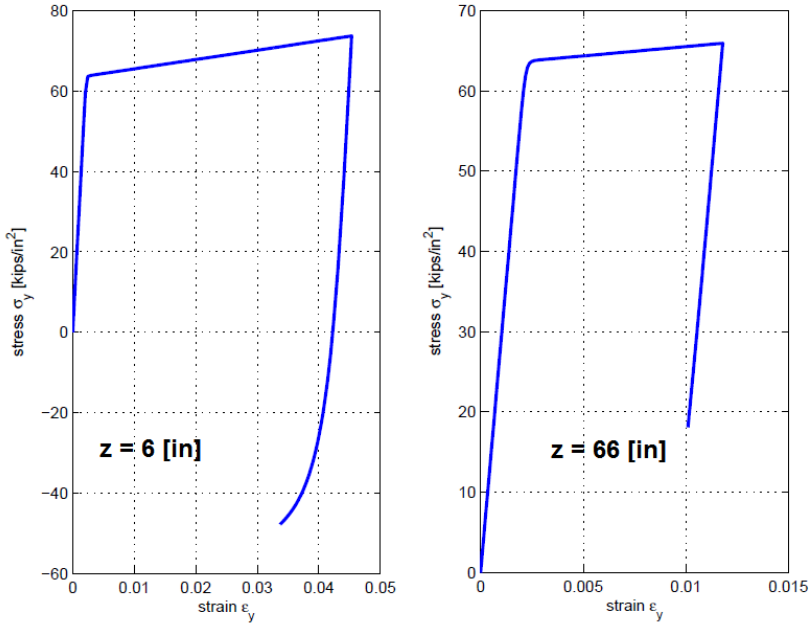

Figure 5.13: Longitudinal stress - strain response for extreme fibers with yielding.

5.5. Sensitivity Analysis

Sensitivity analyses have been performed in order to estimate the impact of some parameters in the prediction of p – y curves. The idea is to give more general information about the effect of shear on p – y curves for other pile characteristics. The parameters selected are: 1) Influence of p – y curves in depth, 2) longitudinal reinforcement ratio of the pile, 3) soil quality, 4) pile diameter, 5) pile – cap interface rigidity and 6) lateral reinforcement of the pile.

5.5.1. Influence of p – y curves in depth

Shear displacements are concentrated only in a shallow layer of 1 pile diameter (24 in.), as discussed in the previous section. Therefore, it is expected that the effect of shear in p – y curves should be concentrated just below the ground line as well, given that the shear displacements below that point are near to zero. To assess this, the interaction model has been used along the p – y curves calculated either with the interaction and the flexure models. The p – y curves of the upper soil springs are the ones calculated with the shear – flexure model (***S – F***), and the following springs are modeled using the p – y curves obtained with the flexure model (***F***). Some cases are analyzed: ***S – F*** p – y curves are used between ground line and 1) ground line (only the first spring has a ***S – F*** p – y curve), 2) 12 in., 3) 24 in. (1 pile diameter), 4) 36 in., 5) 48 in. (2 pile diameters), 6) 60 in., and 7) the bottom line (all the springs use ***S – F*** p – y curves). The results are shown in Figure 5.14.

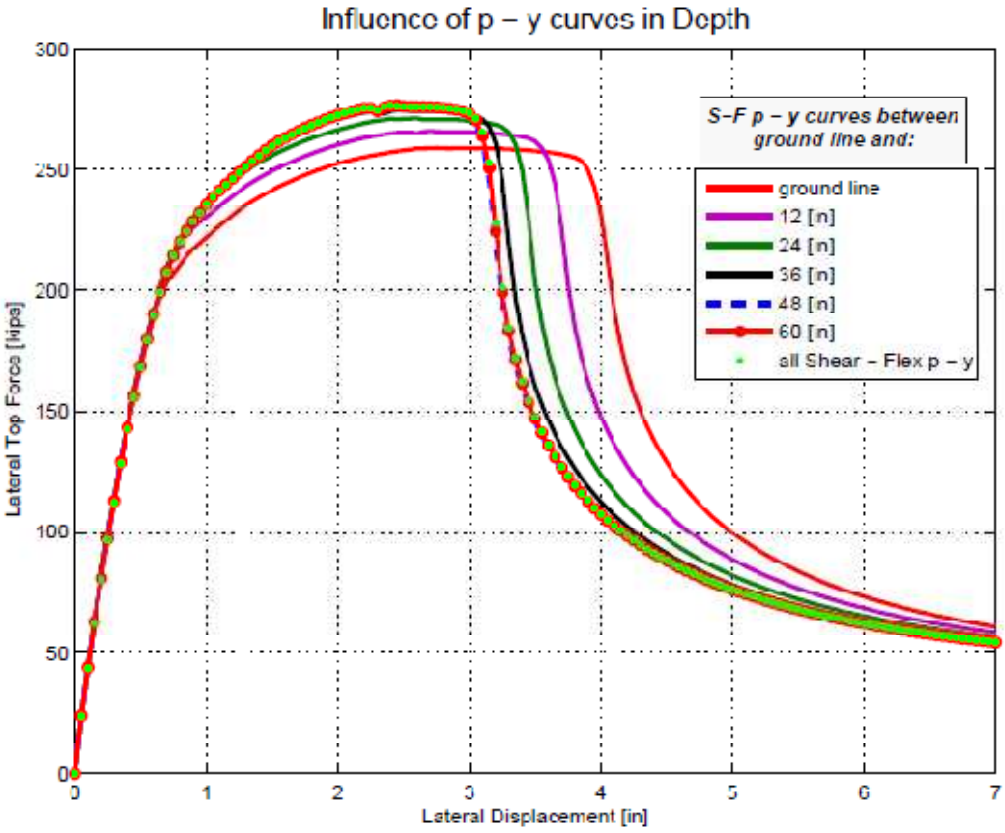

Figure 5.14: Influence of p - y curves in Depth.

The ***S – F*** p – y curves are used on the soil springs from the ground line, to a depth of 2.5 pile diameters. As the ***S – F*** p – y curves are used on deeper soil springs, the load – displacement response becomes more similar to the one obtained using the ***S – F*** p – y curves for all the springs. Initial stiffness is well predicted by only using an ***S – F*** spring at ground line. It can be also observed that the strength is well predicted when using ***S – F*** p – y curves between ground line and a depth of 36 in. having a little overestimation of ductility. The overall load – displacement response calculated using ***S – F*** p – y curves between ground line and a depth 48 in. shows no differences with the response calculated using the ***S – F*** p – y curves along the total pile length. The results suggests the following: 1) The initial stiffness of the pile response is controlled by the p – y curve located at Z = 0 in, 2) the effect of shear on p – y curves is concentrated between ground line and a depth of 2 pile diameters (48 in) and 3) the contribution of p – y curves of deeper levels is negligible.

5.5.2. Longitudinal Reinforcement Ratio

Two different values of ρ_l were used, 50% and 150% of the provided longitudinal reinforcement of the fixed – head pile studied in Stewart et al, 2007. All other parameters remained constant.

When reducing the longitudinal reinforcement to a 50%, the pile has lower yielding and nominal moments (1945 kips-in and 2418 kips-in, respectively, based on a sectional analysis of the new configuration), thus a more flexural response is expected. First, the flexure (***F***) p – y curves of the base model were used in the analysis. The load – displacement response of the interaction model showed about 10% lower strength than flexure response and showed strength degradation at 5.5 in of lateral displacement (Figure 5.15, before fit). Then, the p – y curves were adjusted to fit the interaction model response to the flexure model response, and finally the impact on the p – y curves was evaluated. Results showed that shear – displacements are contributing up to 30% of the total displacements (for a total lateral displacement of 4.5 in, where strength degradation is observed in Figure 5.15, after fit). The effect of shear on the p – y curves is shown in Figure 5.16.

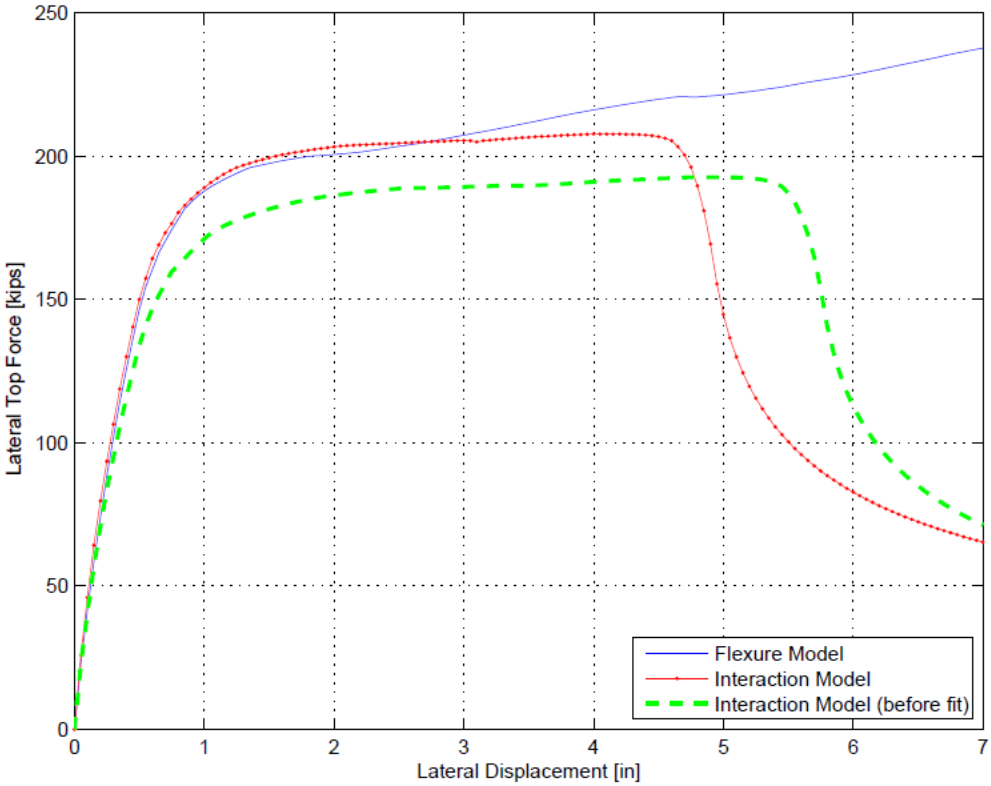

Figure 5.15: Load – displacement response of interaction model fitted to flexure model response. 50% of longitudinal reinforcement.

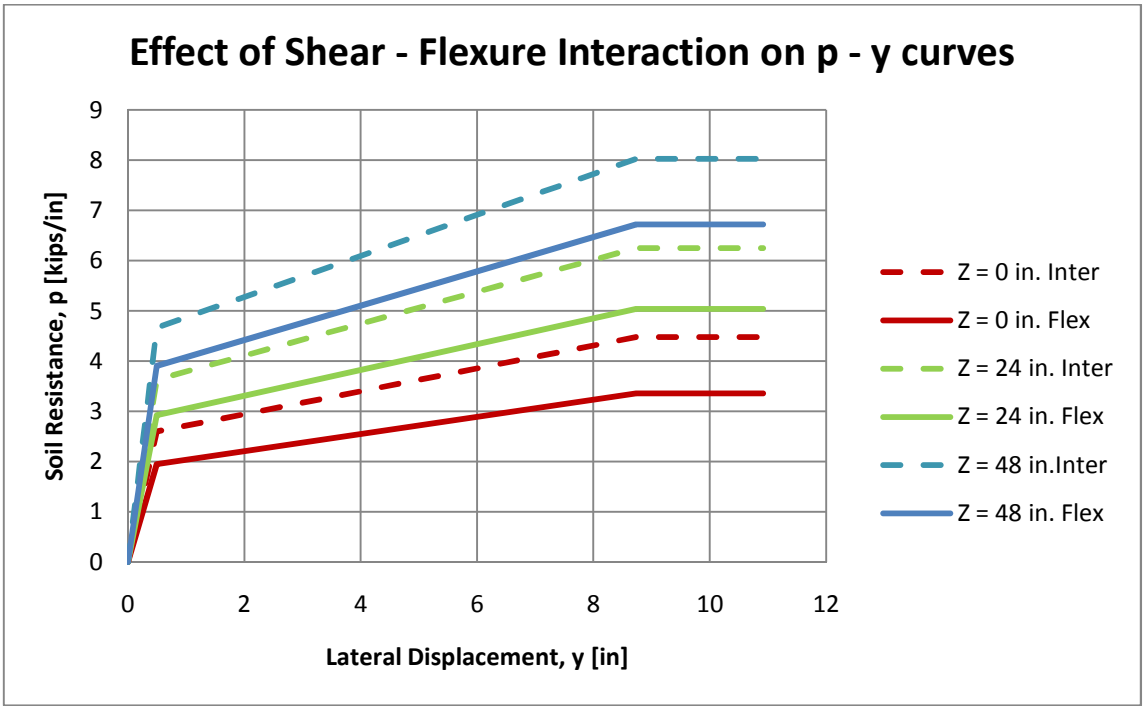

Figure 5.16: Comparison of p – y curves for interaction and flexure models. Sensitivity analysis for 50% of Longitudinal Reinforcement.

The p – y curves for the shear – flexure model (***S – F***) show higher initial stiffness and ultimate resistance, as shown for the ground line and a depth of 1 and 2 pile diameters in Table 5.8. It should be noticed that a difference of strength of about 10% at 4.5 in of lateral displacement between interaction model response (before fit) and flexure model response (Figure 5.15), results in a difference of p_u of about 33% for the superficial spring.

Table 5.8: Comparison of the initial stiffness and ultimate resistance of the p - y curves obtained by the Shear – Flexure (S-F) and Flexure (F) Models. Sensitivity analysis for 50% of Longitudinal Reinforcement Ratio.

Z [in]	K (***S – F***) [kips/in^2]	K (***F***) [kips/in^2]	pu (***S – F***) [kips]	pu (***F***) [kips]	K (***S – F***)/K (***F***) [%]	pu (***S – F***)/pu (***F***) [%]
0	5.2	3.9	4.5	3.4	133.3	133.3
24	7.3	5.9	6.3	5.0	124.1	124.1
48	9.4	7.9	8.0	6.7	119.4	119.4

When using 150% of longitudinal reinforcement, the pile has higher yielding and nominal moments (4781 kips-in and 6000 kips-in, respectively, based on a sectional analysis of the new configuration), thus a higher influence of shear is expected. The same procedure used in the model with 50% of reinforcement is applied, obtaining that shear displacement are contributing up to 35% of the total displacements, for a lateral displacement of 2.3 in, where strength degradation is observed according to Figure 5.17. The effect of shear on p – y relations are shown in Figure 5.18.

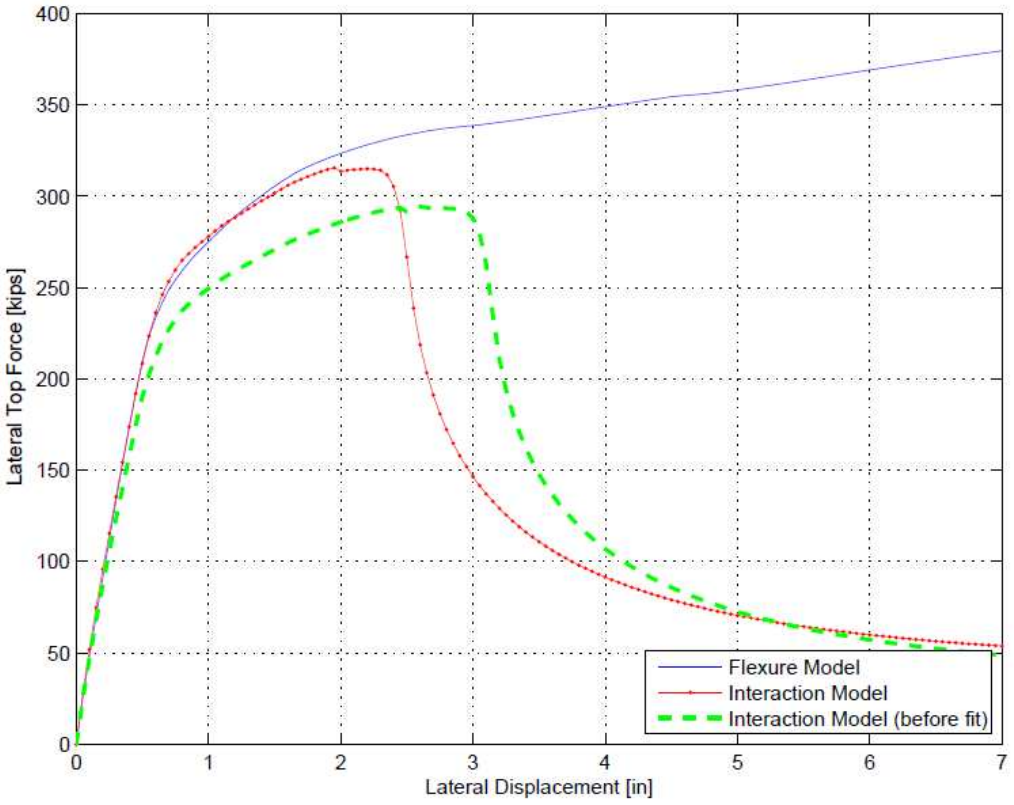

Figure 5.17: Load – displacement response of interaction model fitted to flexure model response. 150% of longitudinal reinforcement.

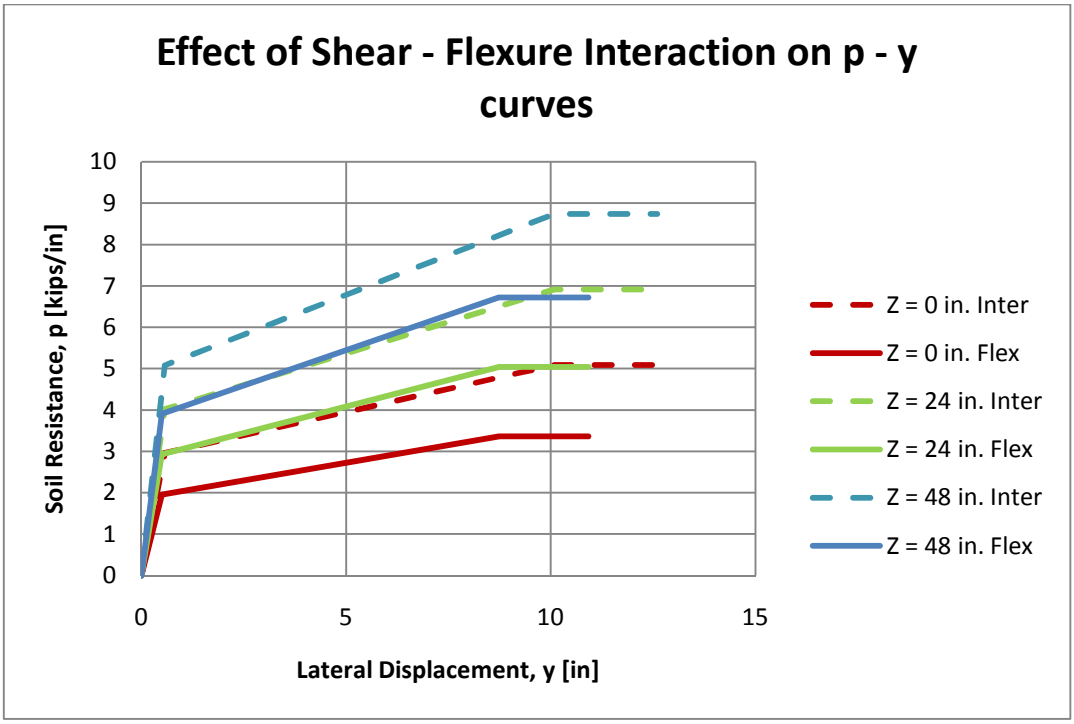

Figure 5.18: Comparison of p – y curves for interaction and flexure models. Sensitivity analysis for 150% of Longitudinal Reinforcement.

The flexure and interaction p – y curves are compared in terms of initial stiffness and ultimate resistance in Table 5.9. In this case, differences of 10% of strength between the interaction model response (Figure 5.17, before fit) and the flexure model response, result in a difference of ultimate resistance (p_u) of 50% for the superficial spring after calibration.

Table 5.9: Comparison of the initial stiffness and ultimate resistance of the p - y curves obtained by the Shear – Flexure (S-F) and Flexure (F) Models. Sensitivity analysis for 150% of Longitudinal Reinforcement Ratio.

Z [in]	K (***S – F***) [kips/in^2]	K (***F***) [kips/in^2]	pu (***S – F***) [kips]	pu (***F***) [kips]	K (***S – F***)/K (***F***) [%]	pu (***S – F***)/pu (***F***) [%]
0	5.2	3.9	5.1	3.4	131.3	151.5
24	7.0	5.9	6.9	5.0	118.9	137.2
48	8.9	7.9	8.7	6.7	112.7	130.1

The impact of shear on the p – y curves in terms of ultimate resistance is higher when a larger amount of longitudinal reinforcement is disposed. Nevertheless, it is observed that the effect on initial stiffness is similar for both cases (about 30% of difference on the superficial spring, for 50% and 150% of longitudinal reinforcement).

5.5.3. Soil Quality

In this case, "softer" p – y relations have been used in order to assess the effect of soil quality on the response. This was done by amplifying the value of N_y obtained in the base flexure model by 4 (reducing stiffness of p – y relations), and reducing by one half the value of N_c (reducing ultimate resistance of p – y relations). The values of N_c, N_y, c and y_c are shown in Table 5.10. Results showed that shear displacements are contributing up to a 19% of the total displacements, for a lateral top displacement of 7.8 in, where strength degradation is observed in Figure 5.19, suggesting that p – y relations should be influenced by shear. In addition, load – displacement response for the interaction model is still showing a strength difference of about 10% compared to flexure model, suggesting that exists degradation caused by shear. The differences between the base model and the p – y relations used in the sensitivity analysis can be observed in Figure 5.20.

Table 5.10: Values of $\mathbf{N_c}$, $\mathbf{N_y}$, **c** and $\mathbf{y_c}$ used in the sensitivity analysis of soil quality.

N_c	N_y	c [kips/in^2]	y_c [in]
0.85	6.0	0.0230	2.52

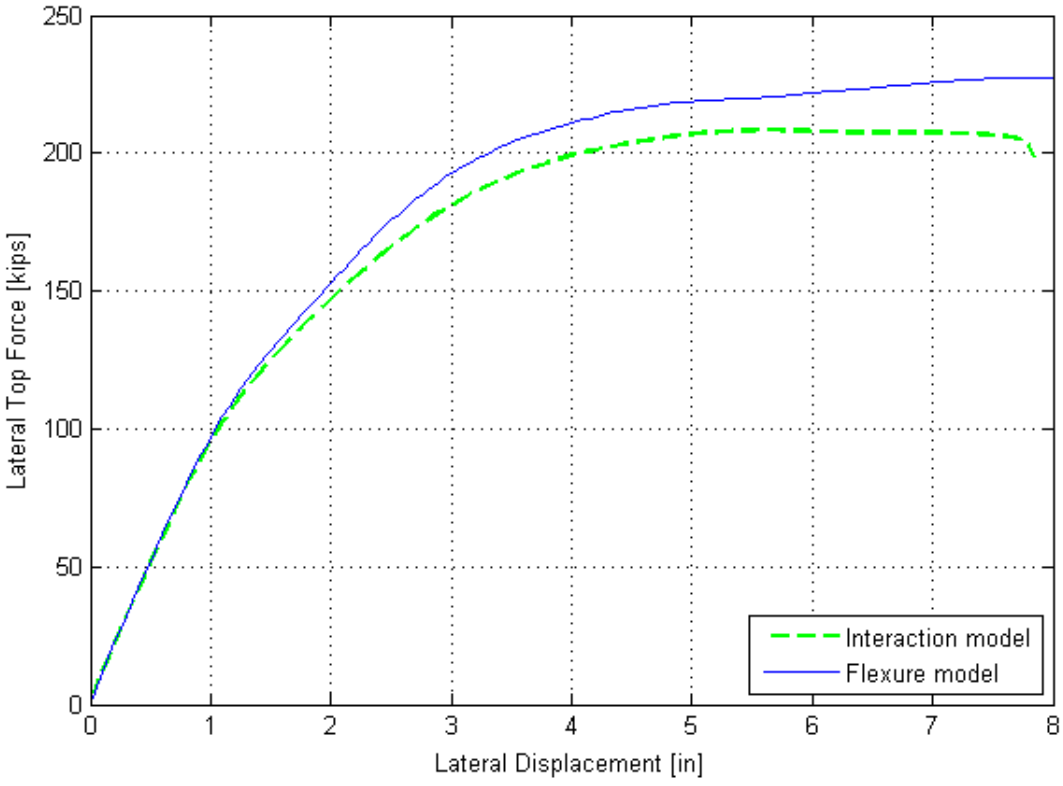

Figure 5.19: Load – displacement responses for sensitivity analysis of soil quality.

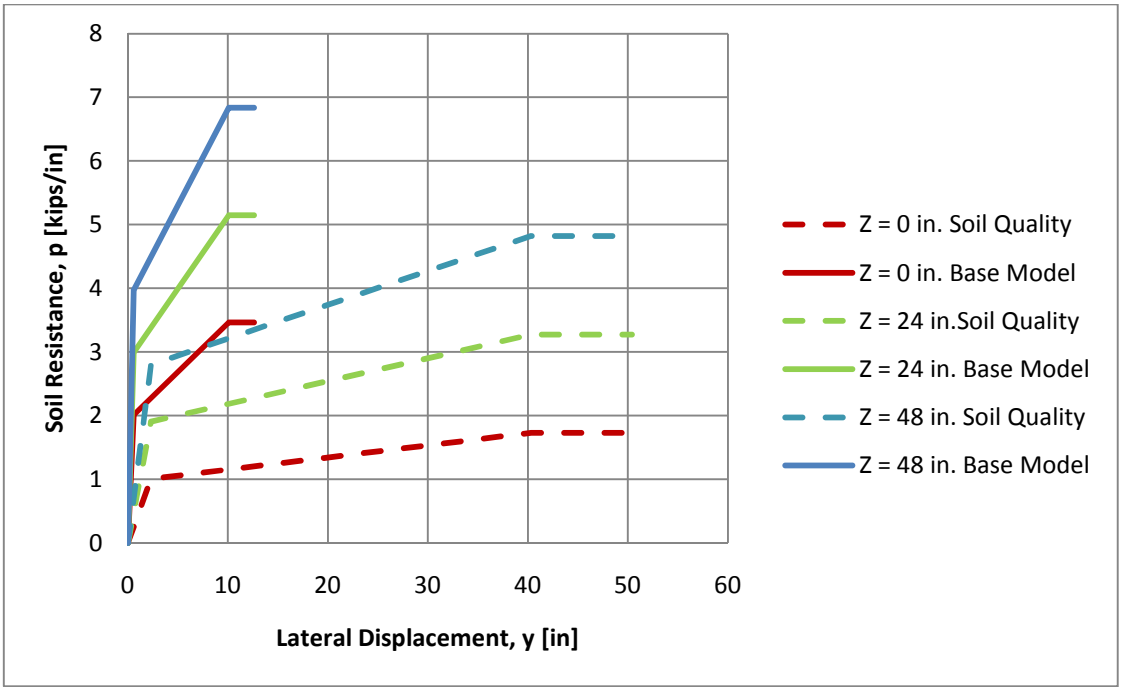

Figure 5.20: Comparison of p – y curves for Base Model (Flexure) and p – y curves used in sensitivity analysis of soil quality.

5.5.4. Pile Diameter

A pile diameter of 48 in was used in this study, which is twice the original pile diameter used in the base model. All other parameters remained constant, nevertheless, the reduction of confinement effectiveness, due to reduction of transverse reinforcement ratio, is considered, obtaining the parameters of concrete shown in **¡Error! No se encuentra el origen de la referencia.**. When increasing the pile diameter, the shear strength is increased (2573 kN or 578 kips, calculated using equations 5.4.1, 5.4.2 and 5.4.3) and so do the yielding and nominal moments (10412 kips-in and 12930 kips, respectively, based on a sectional analysis for the new configuration). Load – displacement response of interaction model showed strength degradation and lower strength than flexure response. This suggests that, even when the degradation occurs at a higher displacement level and shear strength is higher, the shear displacements are still influencing the response. Results showed that shear displacements are contributing up to 27% of total displacements, for a lateral displacement of 5.2 in, and concentrated between the ground line and a pile depth of 1 diameter. Therefore, it is expected similar effect on p – y curves than the other cases.

Table 5.11: Parameters of concrete used in the sensitivity analysis of pile diameter.

f'_c [ksi]	4.7
f'_{cc} [ksi]	6.1
ε_c	0.00230
ε_{cc}	0.00580

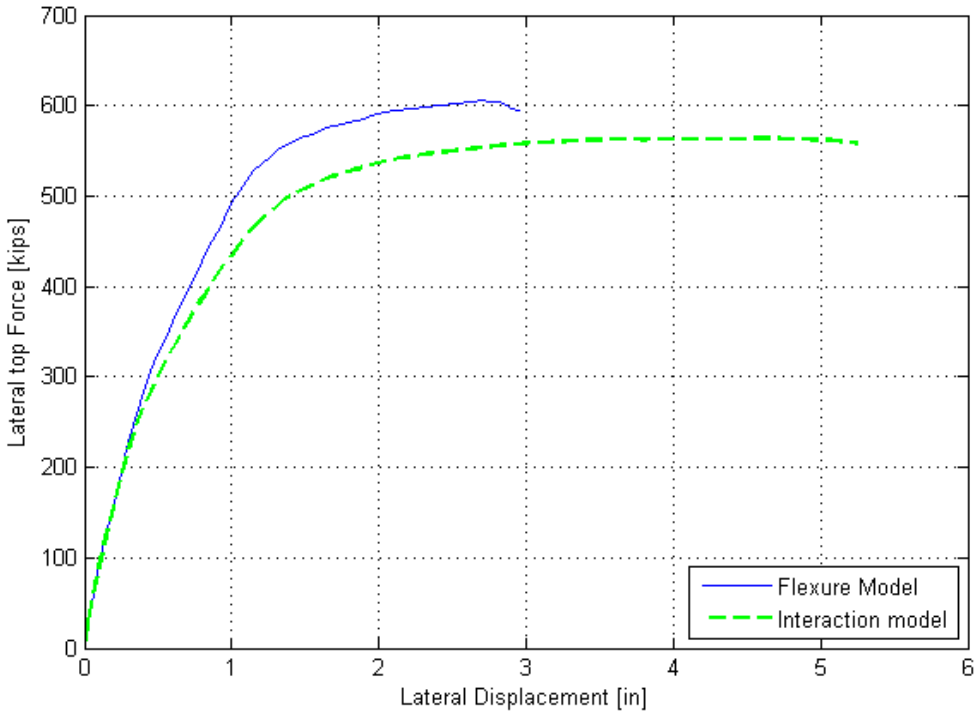

Figure 5.21: Load – displacement responses for sensitivity analysis of pile diameter.

5.5.5. Pile cap – interface rigidity

Interface cracks formed during post – tensioning of anchor bars and micro – cracking caused by differential shrinkage of concrete at the interfaces might produce lateral stiffness reduction during loading. To assess this effect, the procedure proposed by Massone, 2009, in walls is used. First, a moment – curvature analysis of the cross section was performed, and an equivalent rotational stiffness was calculated given by the following expression:

$$K_s = K_\phi \cdot \frac{2}{l_d} \tag{5.6.1}$$

$$K_\phi = \frac{M_y}{\phi_y} \tag{5.6.2}$$

Where, K_s is the equivalent stiffness of the rotational spring shown in Figure 5.22, l_d is the development length of the anchor bars estimated as $40d_b$ (d_b is the longitudinal bar diameter). Finally, M_y and ϕ_y are the yielding moment and the rotation of the cross section, respectively, obtained from the moment – curvature diagram. A value of $K_s = 1.55 \cdot 10^6 [\text{kips} \cdot \text{in}]$ was finally calculated, and the results were compared to the ones obtained in the base model.

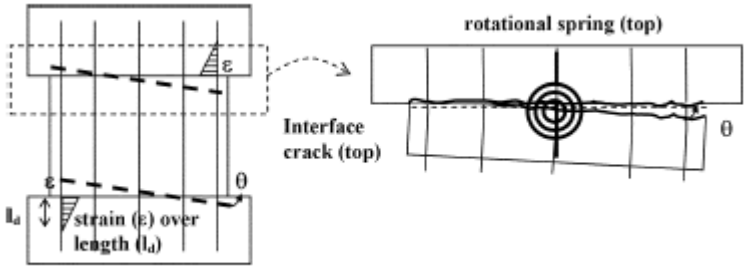

Figure 5.22: Interface crack and rotational spring model (Massone et al, 2009)

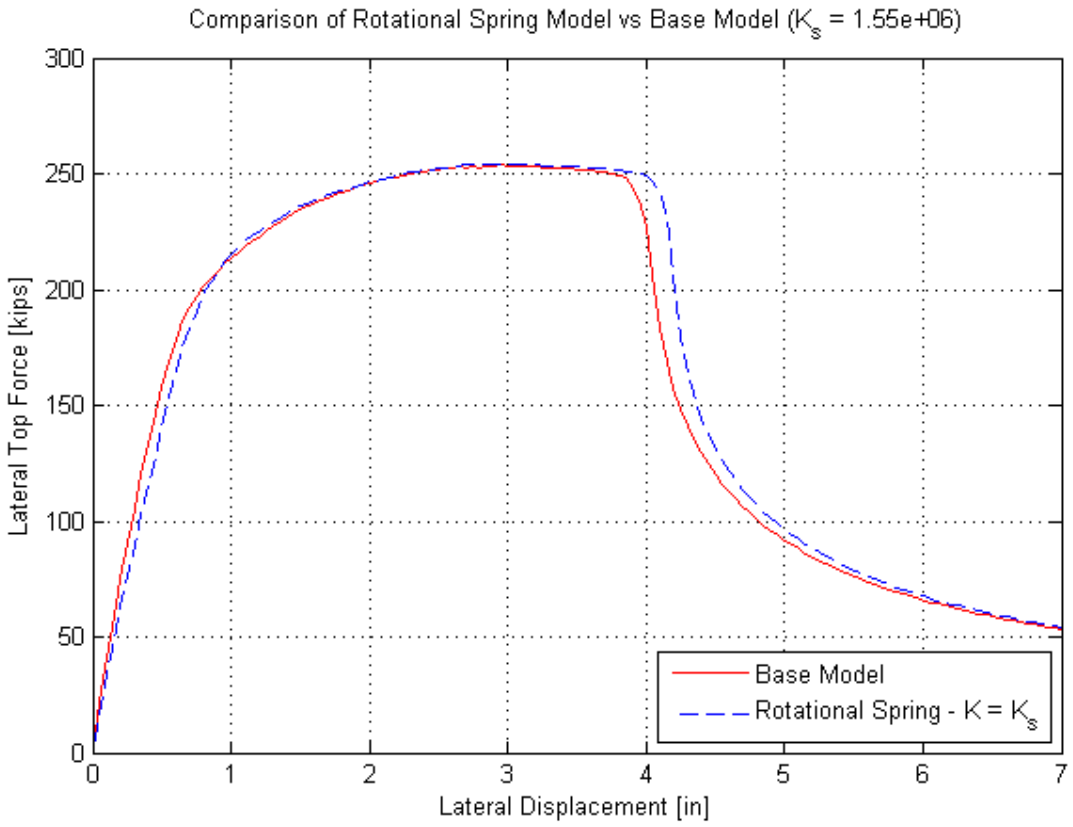

Figure 5.23: Comparison of Rotational Spring model vs Base model. Load - displacement responses.

The load – displacement responses (Figure 5.23) show that the addition of a rotational spring has little effect on stiffness and strength degradation. Nevertheless, there is no difference on strength prediction. Besides, shear displacements contributed up to 35% of the total displacements, for a lateral top displacement of 4.2 in, where strength degradation is observed, that is the same contribution obtained for the base model. Thus, the results suggest that the influence of the rotational spring on p – y relations should be negligible.

A different value of rotational spring stiffness was used, in order to assess the sensitivity of the response to this parameter (K_s). A 10% of K_s was used in this case. Load – displacement responses show that interaction and flexure models show little differences in terms of initial stiffness and strength until a lateral displacement of about 4.2 in (Figure 5.24). Results showed that shear displacements are contributing up to 12% of total displacements, for a lateral top

displacement of 4.2 in. The p – y curves are calibrated in order to fit the interaction and flexure responses until a lateral displacement of 4.2 in. The p – y relationships are compared in Figure 5.25.

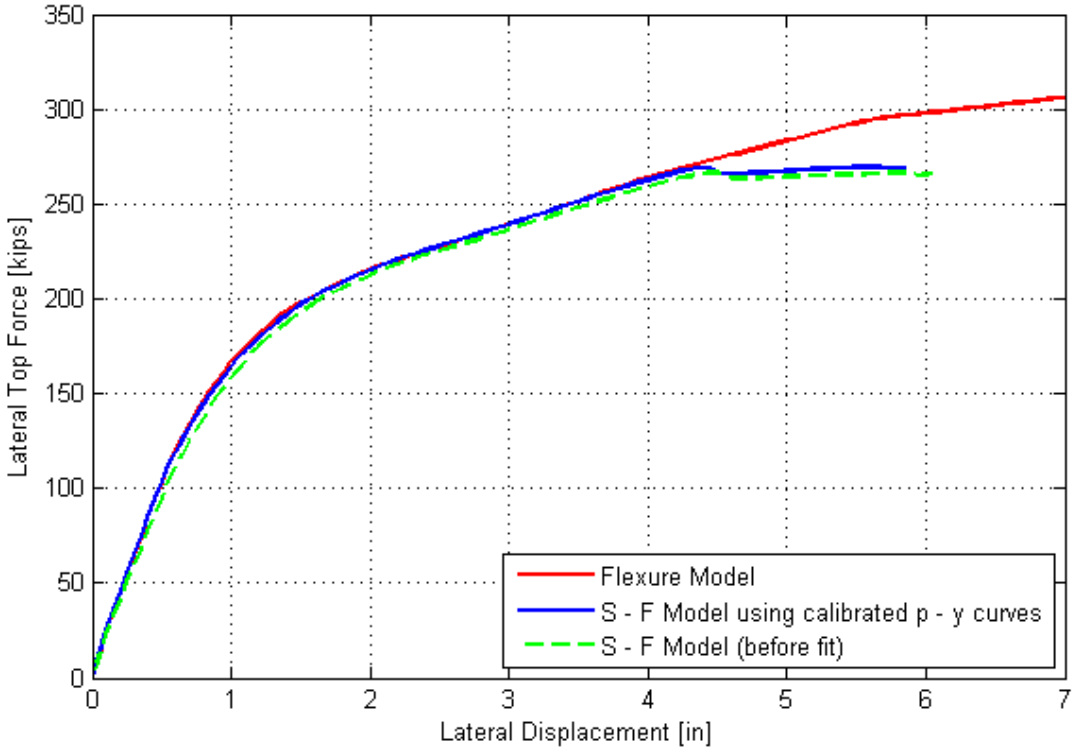

Figure 5.24: Load – displacement responses for sensitivity analysis of 10% of $\mathbf{K_s}$.

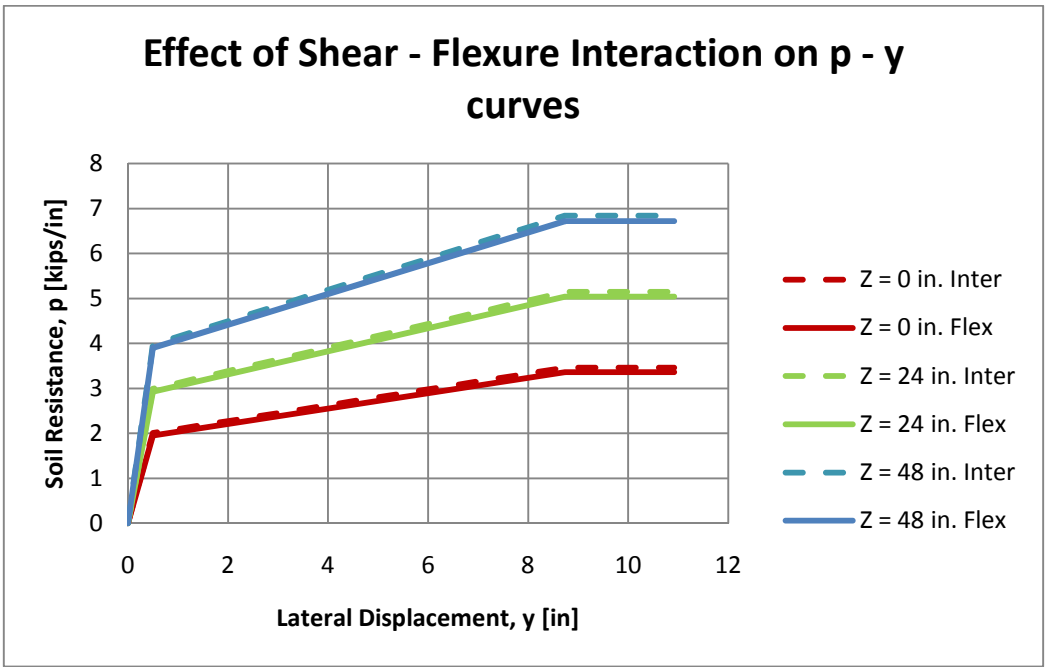

Figure 5.25: Comparison of p – y curves for interaction and flexure models. Sensitivity analysis of 10% of $\mathbf{K_s}$.

Flexure and interaction p – y curves show differences of about 3.0%, for the superficial spring, in terms of initial stiffness and also ultimate resistance, showing that flexure and interaction models give similar results for this configuration.

Table 5.12: Comparison of the initial stiffness and ultimate resistance of the p - y curves obtained by the Shear – Flexure (S-F) and Flexure (F) Models. Sensitivity analysis of 10% of $\mathbf{K_s}$.

Z [in]	K (***S – F***) [kips/in^2]	K (***F***) [kips/in^2]	pu (***S – F***) [kips]	pu (***F***) [kips]	K (***S – F***)/K (***F***) [%]	pu (***S – F***)/pu (***F***) [%]
0	4.0	3.9	3.5	3.4	103.0	103.0
24	6.0	5.9	5.1	5.0	102.2	102.2
48	8.0	7.9	6.8	6.7	101.8	101.8

5.5.6. Lateral reinforcement

The shear displacements have been observed between ground line and a depth of 1 pile diameter. Besides, according to the results of section 5.4.6, the impact of p – y curves are concentrated on a depth of 2 pile diameters below ground line. Thus, it is proposed an analytical study on the amount of lateral reinforcement. The transverse reinforcement ratio is duplicated in this portion of the pile (between ground line and a depth of 2 pile diameters), by decreasing the hoop pitch to one half the original value ($s = \frac{114}{2} = 57$ mm). Therefore, the shear strength is increased to a value of 1631 kN or 367 kips, according to equations 5.4.1, 5.4.2 and 5.4.3.

Load – displacement responses are shown in Figure 5.26. It is observed that the addition of lateral reinforcement enhances the response of the pile in terms of strength and ductility. The strength is increased in about 7%, at a lateral displacement of 3 in, and degradation is observed at a lateral displacement of 6 in, instead of 4 in of the base model. The interaction response approaches the flexure response when increasing the amount of lateral reinforcement in this zone.

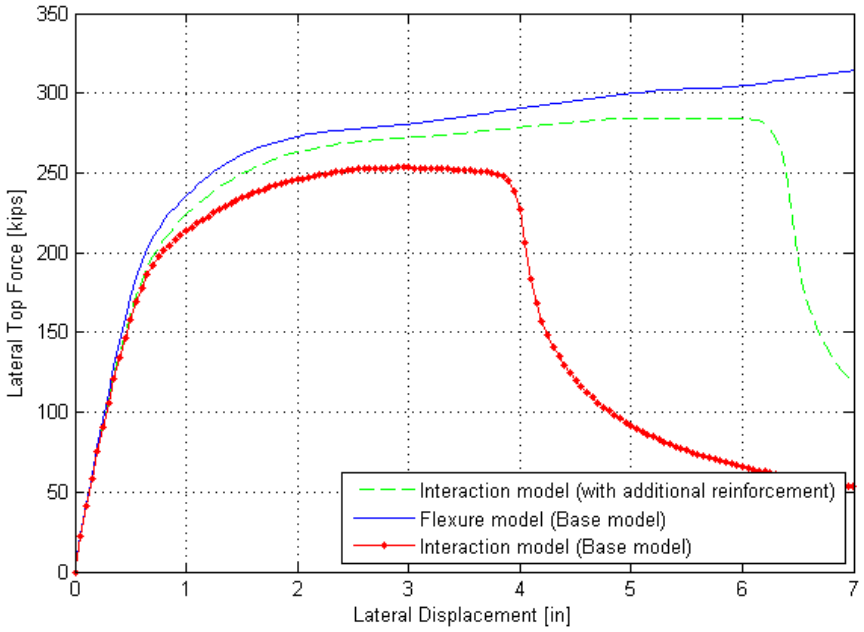

Figure 5.26: Load – displacement responses for sensitivity analysis of lateral reinforcement.

The shear displacements are contributing up to 13% of total displacements, for a lateral top displacement of 6.0 in, that is about one third of the contribution observed in the base model where strength degradation is observed.

CHAPTER 6. Summary and Conclusions

6.1 Column Analysis

A biaxial fiber model that couples shear and axial – bending behavior was studied and validated for the analysis of columns with circular section, uniform distribution of longitudinal reinforcement and spiral transverse reinforcement. In order to achieve this, a set of column tests provided by the PEER (Pacific Earthquake Engineering Research) and Kawashima Earthquake Engineering Laboratory was used, with different shear – span, reinforcement and axial load ratios. The specimens were selected to show strength degradation caused by shear. Thus, different implementations of the so called Shear – Flexure Interaction model were used to compare the load – displacements responses obtained by the different models to the test responses provided in the database.

The models were implemented in OpenSees, using constitutive laws of materials (for plain and confined concrete, and reinforcement steel) from the literature and adjusting them to the ones available in the program. The interaction model, developed by Massone et al, 2006, for walls, and extended for beams (Galleguillos, 2010; Gotschlich, 2011) was now updated for column analysis via a rectangular discretization of the column cross section; proposing 8 fibers and 16 fibers discretizations.

Different implementations were analyzed, comparing the model responses to the test responses. First, the Shear – Flexure (S – F) Interaction model was studied assuming zero transverse stress along the column length ($\sigma_x = 0$), with two different longitudinal discretizations: 1) a constant number of 8 elements along the column length (recommended by Massone et al, 2006, for better predictions on post – peak curve for walls), and 2) a constant $D/h_{st} = 2$ ratio, where D is the column diameter and h_{st} the element length (discretization used due to the observations on post – test excavations performed by Stewart et al, 2007). Both discretizations show similar results in terms of maximum capacity and initial stiffness (the model over test ratio show values of about (V_{mod}/V_{exp}) 0.84 for maximum capacity and (K_{mod}/K_{exp}) 1.7 for initial stiffness). However, it was found that an 8 elements discretization led to fast strength degradation (the model over test ratio ($\delta_{mod}/\delta_{exp}$) showed values below 0.5 for most of the specimens) whereas a $D/h_{st} = 2$ discretization showed a mean value of ($\delta_{mod}/\delta_{exp}$) 0.83.

The S – F model with calibrated ε_x profile showed better results than $\sigma_x = 0$ model for estimating maximum capacity and initial stiffness (the model over test ratio showed values of about (V_{mod}/V_{exp}) 0.90 for maximum capacity and (K_{mod}/K_{exp}) 1.3 for initial stiffness with standard deviations of 0.09 and 0.18, respectively). Nevertheless, ε_x calibrated model has a fixed number of 8 elements along the element length so it has been not considered in analysis of degradation due to the observations with the $\sigma_x = 0$ model. It is also important to note that the ε_x calibrated model needs a calibrated profile and the transverse strain would depend on the type of element and the boundary conditions. Thus, in the case of columns, the ε_x profiles proposed by Massone et al, (2010) for walls were used. Ongoing work should be focused on the implementation of a $D/h_{st} = 2$ discretization and determining proper ε_x profiles for the analysis of columns.

The Flexure (F) model was also analyzed in order to compare the results against the interaction models. The F model showed good prediction of the maximum capacity (the model over test ratio showed a mean value of (V_{mod}/V_{exp}) 1.00 with standard deviation of about 0.19), however, initial stiffness is highly overestimated (the model over test ratio showed a mean value of (K_{mod}/K_{exp}) 1.9 with standard deviation of about 0.25). The analysis of ($\delta_{mod}/\delta_{exp}$) is not considered, because shear degradation was not observed in 6 of 10 cases at large displacements ($\delta_{mod}/\delta_{exp} \gg 2$).

The transverse strain (ε_x) was studied for the $\sigma_x = 0$ model at three different stages of loading: 1) ultimate displacement, 2) maximum capacity and 3) 1% of lateral drift. At ultimate displacement it was found that a lower shear – span ratio gives a higher percentage of fibers with $\varepsilon_x > 0.0021$, where less than a third of fibers are yielding and only the fibers near to the support. At maximum capacity it was found that for 7 of 10 cases transverse reinforcement is not yielding ($\varepsilon_x < 0.0021$ for all fibers). At 1% of lateral drift it was observed similar results than ultimate displacement. These results suggest that, for these specimens, the importance of transverse reinforcement is to provide ductility and not to provide strength to columns.

Sensitivity analyses were undertaken on confinement effectiveness and lateral reinforcement, because transverse reinforcement contributes to both confinement and shear strength. Confinement was reduced to 50%, and threw differences of 1% of maximum capacity. Lateral reinforcement was taken as 50% and 150% of the transverse reinforcement ratio, and threw differences below 1% for all cases in terms of capacity and degradation. The low impact on these parameters is associated with the low amount of transverse reinforcement on the specimens.

6.2 Pile Analysis

In the second section was analyzed the effect of shear on the calculation of the p – y curves for a 0.61 m. diameter fixed – head RC pile embedded in clayey soil. For the study it was used the data of a full – scale test performed by Stewart et al, 2007, on a fixed – head pile. The $\sigma_x = 0$ model with constant $D/h_{st} = 2$ ratio was used for the analysis, in order to represent the field observations on post test excavations. Also, good prediction of strength and strength degradation was observed on columns, essentially on specimen 7 (with similar longitudinal and transverse reinforcement ratios, 1.90% and 0.60%., respectively). The cross section was discretized in 16 fibers. The p – y curves were based on the API (1993) recommendations, implementing them in OpenSees as tri – linear responses, using a least squares procedure. The pile was also modeled using the F model, in order to make comparisons.

A fitting procedure was proposed in order to adjust the load – displacement response of the model to the test response. To achieve this, two parameters were selected: the undrained shear strength of the soil (c), and the displacement at one – half of ultimate resistance (y_c). Both parameters were multiplied by factors (N_c and N_y, respectively), and a fitting procedure was used to find the values in order to match graphically the overall load vs. displacement response. No degradation was possible to match in the case of the flexure model.

The p – y curves were calculated for the F model and compared with the p – y curves used by Lemnitzer et al, 2013. It was found a difference of 10% between the p – y curves of the

superficial layer ($Z = 0$ in) until 3.5 in of lateral displacement, which is the maximum lateral top displacement of the test. Besides, both models (present and Lemnitzer et al, 2013, models) showed good correlation for maximum capacity and initial stiffness of the response, however, they do not show strength degradation beyond 3.5 in of lateral displacement.

Then, the p – y curves were calculated for the S – F model. The model response showed good correlation for maximum capacity, initial stiffness and strength degradation. Also, the F and S – F responses are practically identical for the ascending branch, however, S – F response show strength degradation beyond 3.0 in, whereas F response do not show degradation.

The ***S – F*** p – y curves were compared to ***F*** p – y curves. It was found that a difference of 10% of strength between the flexure and interaction model responses at 3.0 in (using ***F*** p – y curves for both cases) led to a difference of about 47% of ultimate capacity and a difference of about 30% of initial stiffness for the superficial p – y curves (the flexure over interaction model ratio is (p_{u_Flex}/p_{u_inter}) equal to 0.67 for ultimate capacity and (K_{Flex}/K_{inter}) equal to 0.77 for initial rigidity, at ground line), i.e., the ***S – F*** p – y curve is harder than the ***F*** p – y curve for the superficial layer. The difference for the soil resistance at 3.0 in of lateral displacement is about 40%. Similar behavior is observed for deeper layers; however, sensitivity analyses established low contribution of p – y curves for depths below 2 pile diameters.

The displacement profiles showed that the shear displacements significantly influence the overall top displacement response, for top displacement exceeding 0.25 in (0.63 cm). When the top displacement reaches the 3.00 in (start of strength degradation), the shear displacements are contributing up to 35% of total displacements and they are concentrated on a shallow layer of approximately 1 pile diameter. Flexural deformations are contributing up to 65% of the total displacements, at the same displacement level, and they are observed between the ground line and a pile depth of approximately 5 pile diameters, and they are nearly zero for lower depths.

The moment profiles showed two plastic hinges located just below ground line in negative bending and at 66 in (roughly 3 pile diameters) in positive bending, for a lateral displacement of 3.0 in (start of strength degradation). This was confirmed by the stress – strain response of the extreme fibers for both sections. Nominal capacity is reached at 66 in depth, at 3.0 in of lateral displacement. Bending moment approaches zero at depths below 200 in (about 8 pile diameters). In addition, it was observed that the moment profiles obtained using the F model along ***F*** p – y curves are similar to the moment profiles obtained using the S – F model along the ***S – F*** p – y curves.

The shear profiles showed that nominal shear strength is reached at ground line for a lateral displacement of 3.0 in, which is consistent with the field observations of shear cracks at pile – cap interface. In addition, it was observed that the shear profiles obtained using the F model along ***F*** p – y curves are similar to the shear profiles obtained using the S – F model along the ***S – F*** p – y curves.

In order to give more general information about the effect of shear on p – y curves, some sensitivity analyses were undertaken.

To assess the depth of influence of p – y curves, the S – F p – y curves were used between ground line and different depths, and the responses were compared. The results suggest the

following: 1) The initial stiffness of the pile response is controlled by the p – y curve located at Z = 0 in, 2) the effect of shear on p – y curves is concentrated between ground line and a depth of 2 pile diameters (48 in) and 3) the contribution of p – y curves of deeper levels is negligible.

Longitudinal reinforcement was studied using 50% and 150% of longitudinal reinforcement ratio. When using 50% of longitudinal reinforcement, the yielding and nominal moments are lower, thus a more flexural response was expected. Load – displacement response for the S - F model along ***F*** p – y curves showed 10% lower strength than F model, and showed strength degradation at 5.5 in of lateral displacement. The ***S – F*** p – y curve, for $Z = 0$ in, showed about 33% higher ultimate capacity and 33% higher initial stiffness than ***F*** p – y curve at the same location. Shear displacement contributed up to 30% of lateral displacements, for a lateral displacement of 4.5 in. When using 150% of longitudinal reinforcement, the shear displacements contributed up to 35% of total displacements, for a lateral displacement of 2.3 in, resulting in differences of of about 50% of ultimate capacity and 30% of initial stiffness, for the superficial spring.

Soil quality was also studied by reducing p_u by one half and raising y_c by four times the original values obtained using the flexure model. Load – displacement responses show differences of 10% in strength, between S - F and F models along ***F*** p – y curves, and S – F model showed strength degradation beyond 7.8 in. Shear displacements are contributing up to 19% of total displacements, for the same lateral displacement, thus it is expected similar effect on p – y curves than the other cases.

Pile diameter was duplicated in order to raise the shear strength of the pile and obtain a more flexural response. In this case, the interaction model shows lower strength than flexure (about 10% lower) and also showed strength degradation beyond 5.2 in of lateral displacement. Shear displacements are contributing up to 27% of total displacements for the same lateral displacement. Thus, similar effect on p – y curves is expected.

A rotational spring proposed by Massone, 2009, for walls, was used to assess the effect on the response. The effect of adding a rotational spring at the pile – cap interface is reducing the stiffness of that section. It was observed little difference between the load – displacement responses of the base model (S – F model along ***F*** p – y curves), and the response using the rotational spring. Also, shear displacements contributed up to 35% of total displacements, for a lateral displacement of 4.2 in. Thus, the results suggest that the addition of a rotational spring on p – y curves is negligible.

A 10% of the calculated stiffness was used on the rotational spring in order to force the model to reduce de shear displacements. S – F model and F model responses showed little differences and also shear displacements contributed up to 12% of total displacements, for a lateral displacement of 4.2 in. ***S – F*** p – y curves showed differences of about 3%, on ultimate capacity and stiffness, respect to the ***F*** p – y curves. The results suggest that when shear displacements are expected to be low (about 12% or lower) the ***S – F*** p – y curves and ***F*** p – y curves are similar.

The effect of lateral reinforcement was also studied by duplicating the amount of reinforcement between ground line and a pile depth of 48 in. The addition of reinforcement enhanced the response in terms of strength and ductility. Load – displacement responses show that strength is raised in about 7%, compared to the S – F model with the original configuration, and strength degradation is observed beyond 6.0 in, instead of the 3.0 in of the base model. Shear

displacements are contributing up to 13% of total displacements that is about one third of the shear displacements of the base model. Thus, the results suggest that the effect of shear should be lower by adding transverse reinforcement in the zone where maximum shear displacements are expected.

6.3 Future Work

Future work should be focused on the following aspects:

1) Column tests should be performed with different shear – span, longitudinal and transverse reinforcement and axial load ratios; where longitudinal, transverse and shear strains are measured, in order to validate the strains given by the S – F model on columns, and also, verify the hypothesis of transverse strain distribution according to Massone et al, 2010, for columns. Columns should be designed to show shear failure.

2) Since the S – F model with ε_x calibrated showed better results for columns, a transverse strain distribution should be proposed in order to use the S – F model with ε_x calibrated in pile analysis.

3) Since the $^{D}/_{h_{st}} = 2$ discretization showed better prediction of strength degradation on columns, S – F model with ε_x calibrated should be extended in order to use a longitudinal discretization of $^{D}/_{h_{st}} = 2$.

REFERENCES

1. American Concrete Institute (ACI 318 – 08). “Building Code Requirements for Structural Concrete and Commentary”, Committee 318, American Concrete Institute.

2. American Petroleum Institute (API), (1993). “Recommended Practice for Planning, Designing and Constructing fixed offshore platforms”. API recommended practice 2A (RP 2A).

3. ATC-32 (1996). “Improved Seismic Design Criteria for California Bridges: Provisional Recommendations”. Applied Technology Council”. http://www.atcouncil.org/pdfs/ATC32toc.pdf

4. Belarbi, H., Hsu, T.C.C., 1994. “Constitutive Laws of Concrete in Tension and Reinforcing Bars Stiffened by Concrete”, ACI Structural Journal, V.91, No. 4, pp. 465 – 474.

5. CODUTO, Donald P. Foundation Design: principles and practices. 2nd ed. Upper Saddle River, New Jersey, Prentice Hall, 2001. 883p.

6. Evan C. Bentz, Frank J. Vecchio, and Michael P. Collins; “Simplified modified compression field theory for calculating shear strength of reinforced concrete elements”; ACI Structural Journal, 2006, Title no. 103-S65, pp. 614-624.

7. Galleguillos, Tito; 2010; “Modelamiento de Vigas de Hormigón con Fibras de Acero”, Memoria para optar al título de ingeniero civil, Universidad de Chile.

8. Gotschlich, Nicolás; 2011; “Modelamiento de Vigas de Hormigón con Refuerzo de Acero y Cables Pretensados Variando la Relación de Aspecto de Corte”, Memoria para optar al título de ingeniero civil, Universidad de Chile.

9. Kawashima Research Group. Database with the results of cyclic lateral – load tests of reinforced concrete columns. http://seismic.cv.titech.ac.jp/.

10. Lemnitzer, A., Massone, L. M., Wallace, J. W., 2013 “Effect of Shear – Flexure interaction on the response of RC Bridge Pile Foundation Systems”. J. Bridge Eng.,ASCE, (under review).

11. Massone, L. M., Orakcal, K., and Wallace, J. W., “Shear - Flexure Interaction for Structural Walls” SP-236, ACI Special Publication – /Deformation Capacity and Shear Strength of Reinforced Concrete Members Under Cyclic Loading/, editors: Adolfo Matamoros & Kenneth Elwood, 2006, pp. 127-150.

12. Massone, L. M., 2010; “Strength Prediction of Squat Structural Walls via Calibration of a Shear-Flexure Interaction Model,” Engineering Structures, V. 32, No. 4, Apr. 2010, pp. 922-932.

13. Matlock,H. and Reese, L.C. (1970). “Correlations for design of laterally loaded piles in soft clay.” Proc. 2nd Off. Tech. Conf. OTC 1204, Houston, 577-594

14. OpenSees Development Team (Open Source Project). OpenSees: Open System for Earthquake Engineering Simulation. http://opensees.berkeley.edu.

15. PEER. SPD (Structural Performance Database). Database with the results of cyclic lateral – load tests of reinforced concrete columns. http://nisee.berkeley.edu/spd/.

16. Saatcioglu, M., Razvi, S., 1992; “Strength and Ductility of Confined Concrete”. Journal of Structural Engineering, 118(6), 1590-1607.

17. Stewart, J.P. (2007). “Full Scale Cyclic Large Deflection Testing of Foundation Support Systems for Highway Bridges”. Pile Report, Structural & Geotechnical Laboratory, UCLA. Report 2007/01, pp 209. http:// http://escholarship.org/uc/item/5mt9q0m6.

APPENDIX A

The following table summarizes the parameters used in the column models, according to the constitutive laws discussed in section 2.1.

Table A.1: Parameters for columns

	Plain Concrete				Confined Concrete				α Compression	Concrete in Tension				Longitudinal Reinforcement			Transverse Reinforcement		
ID N°	$f'c$ [ksi]	ε0	n	k	$f'cc$ [ksi]	ε1	n	k		fcr [ksi]	εcr	β	α Tension	E [ksi]	Fy [ksi]	b	E [ksi]	Fy [ksi]	b
SPEC1	4.35	0.0018	2.56	1.15	4.94	0.0031	1.98	1.00	0.20	0.25	0.00008	0.40	0.20	29000.00	66.99	0.008	29000.00	52.35	0.008
SPEC2	4.35	0.0018	2.56	1.15	4.72	0.0026	2.10	1.00	0.20	0.25	0.00008	0.40	0.20	29000.00	66.99	0.008	29000.00	52.35	0.008
SPEC6	4.32	0.0018	2.55	1.15	4.50	0.0022	1.95	1.00	0.20	0.25	0.00008	0.40	0.20	29000.00	65.83	0.008	29000.00	29.00	0.008
SPEC7	3.88	0.0018	2.38	1.10	4.06	0.0022	1.95	1.00	0.20	0.23	0.00008	0.40	0.20	29000.00	65.83	0.008	29000.00	29.00	0.008
SPEC8	4.52	0.0018	2.64	1.17	4.70	0.0022	1.96	1.00	0.20	0.25	0.00008	0.40	0.20	29000.00	63.45	0.008	29000.00	29.00	0.008
SPEC9	5.21	0.0019	2.91	1.25	5.99	0.0033	1.95	1.26	0.20	0.27	0.00008	0.40	0.20	29000.00	34.80	0.008	29000.00	34.80	0.008
SPEC10	4.99	0.0019	2.82	1.22	5.77	0.0034	1.66	1.00	0.20	0.27	0.00008	0.40	0.20	29000.00	34.80	0.008	29000.00	34.80	0.008
SPEC11	5.37	0.0019	2.98	1.27	6.18	0.0034	1.80	1.00	0.20	0.28	0.00008	0.40	0.20	29000.00	68.88	0.008	29000.00	49.30	0.008
SPEC13	4.35	0.0018	2.56	1.15	4.92	0.0030	2.00	1.00	0.20	0.25	0.00008	0.40	0.20	29000.00	54.23	0.008	29000.00	52.64	0.008
SPEC14	4.35	0.0018	2.56	1.15	4.67	0.0025	2.08	1.00	0.20	0.25	0.00008	0.40	0.20	29000.00	54.23	0.008	29000.00	52.64	0.008

APPENDIX B

The following figures show the overall load – displacement responses obtained with the different analyses along the test response, for all the different column specimens studied in CHAPTER 4.

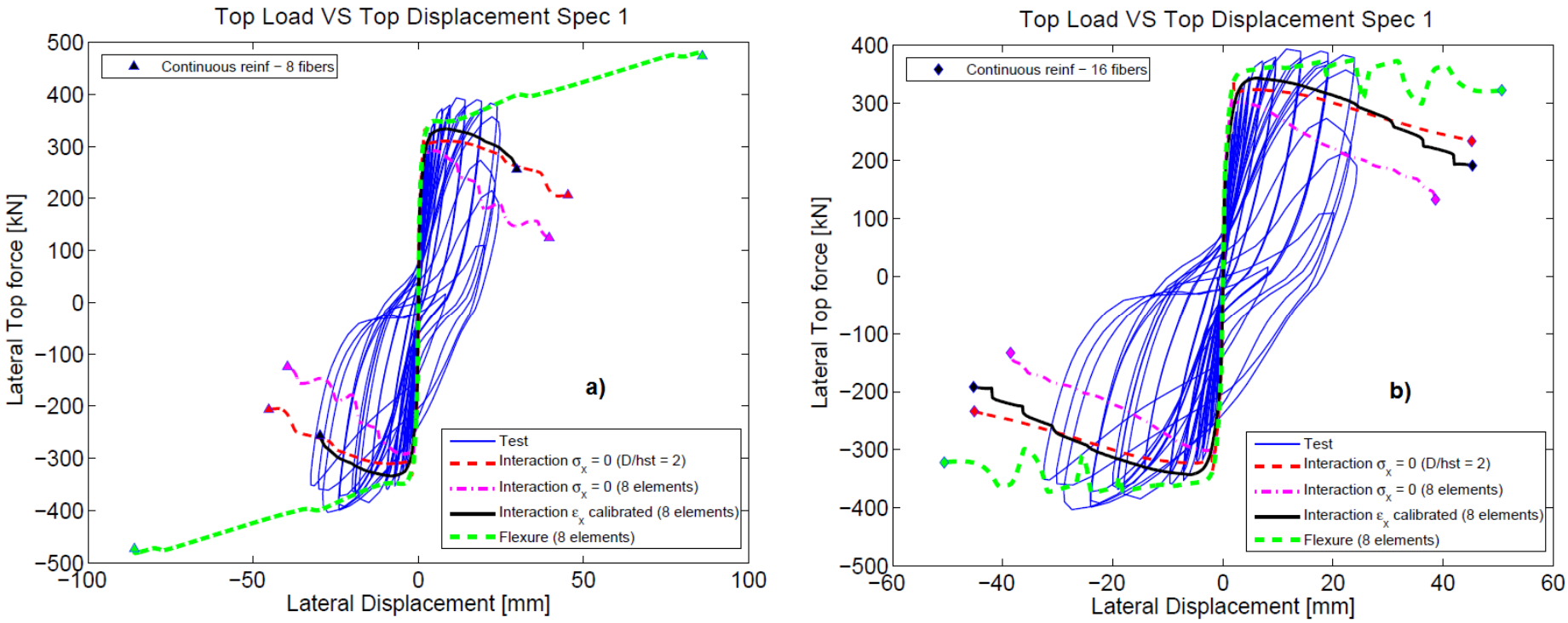

Figure B.1: Load - Displacement responses for all models using a) 8 fibers and b) 16 fibers. Specimen 1.

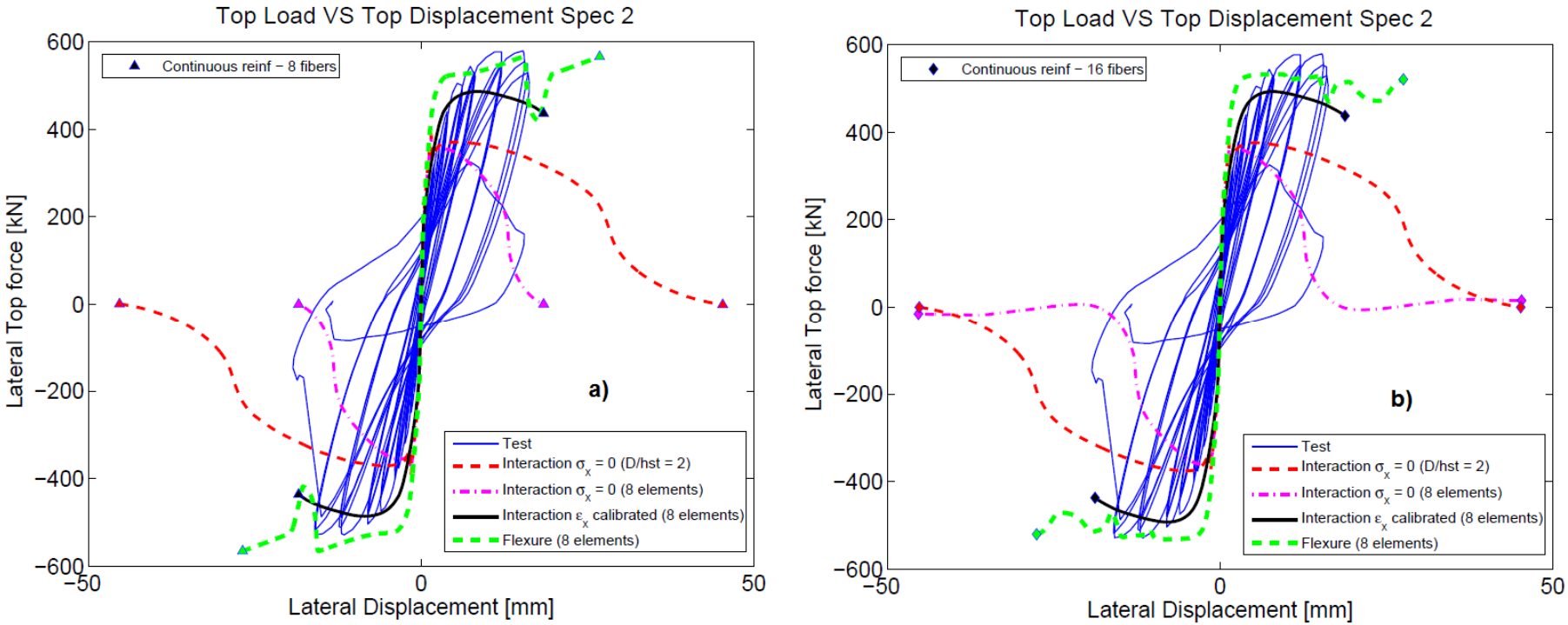

Figure B.2: Load - Displacement responses for all models using a) 8 fibers and b) 16 fibers. Specimen 2.

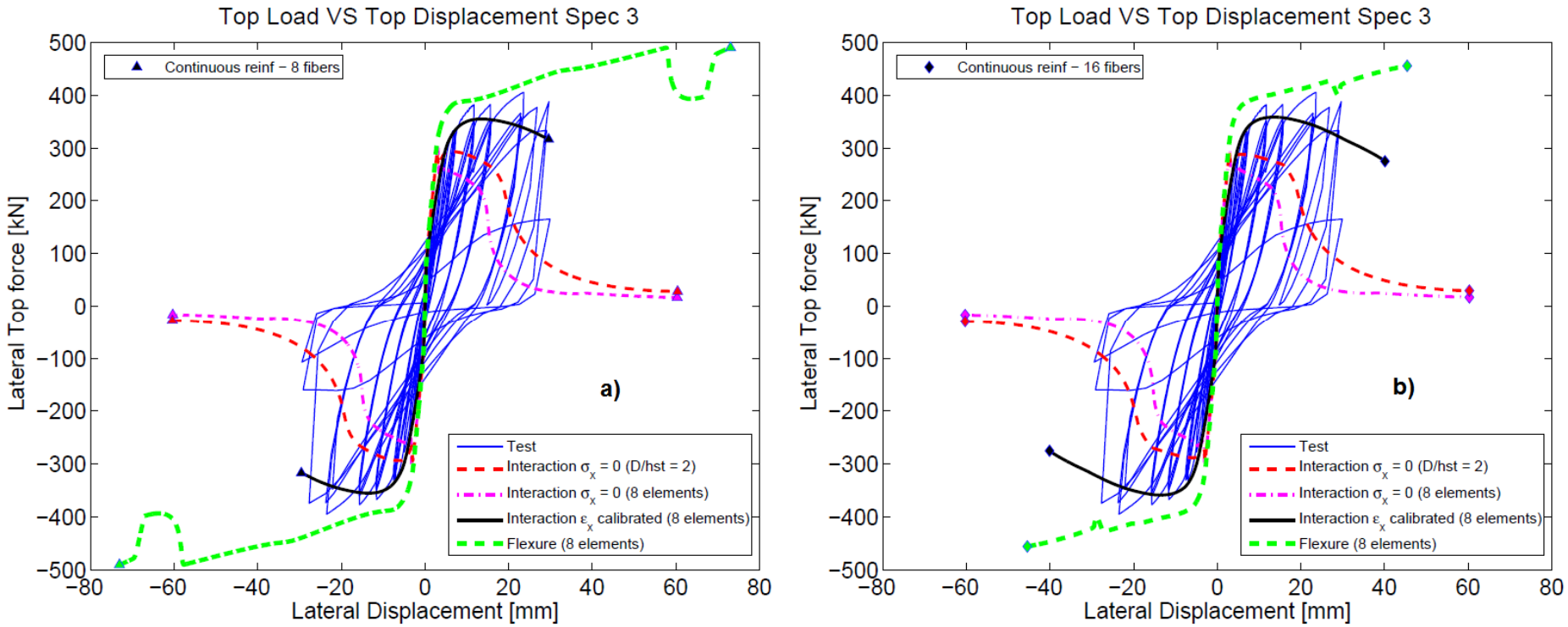

Figure B.3: Load - Displacement responses for all models using a) 8 fibers and b) 16 fibers. Specimen 3.

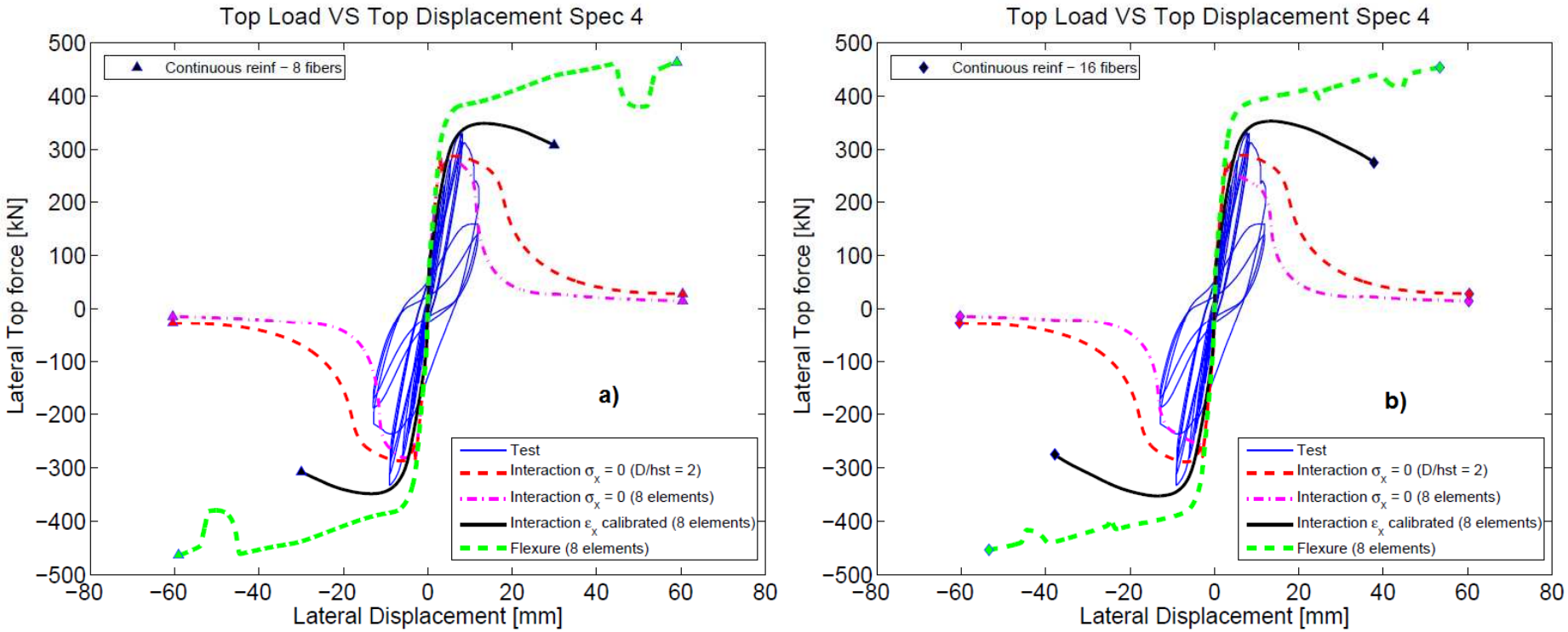

Figure B.4: Load - Displacement responses for all models using a) 8 fibers and b) 16 fibers. Specimen 4.

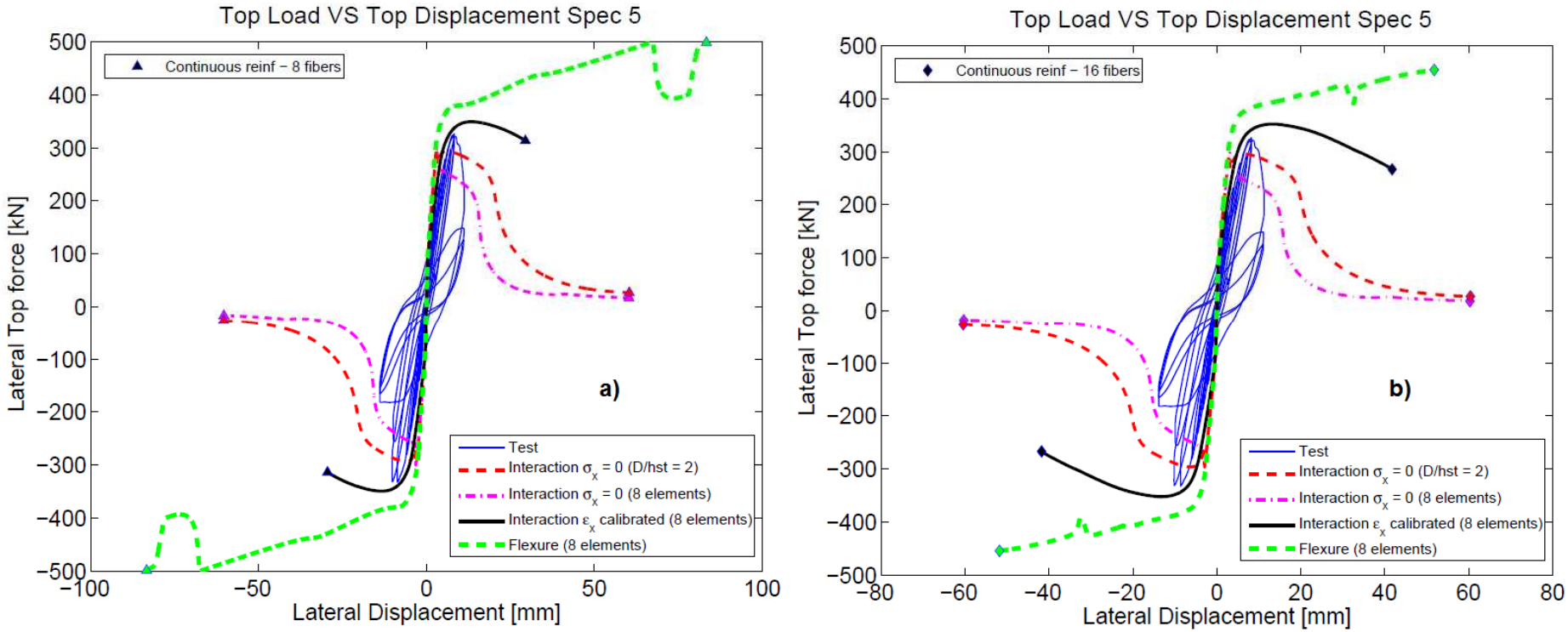

Figure B.5: Load - Displacement responses for all models using a) 8 fibers and b) 16 fibers. Specimen 5.

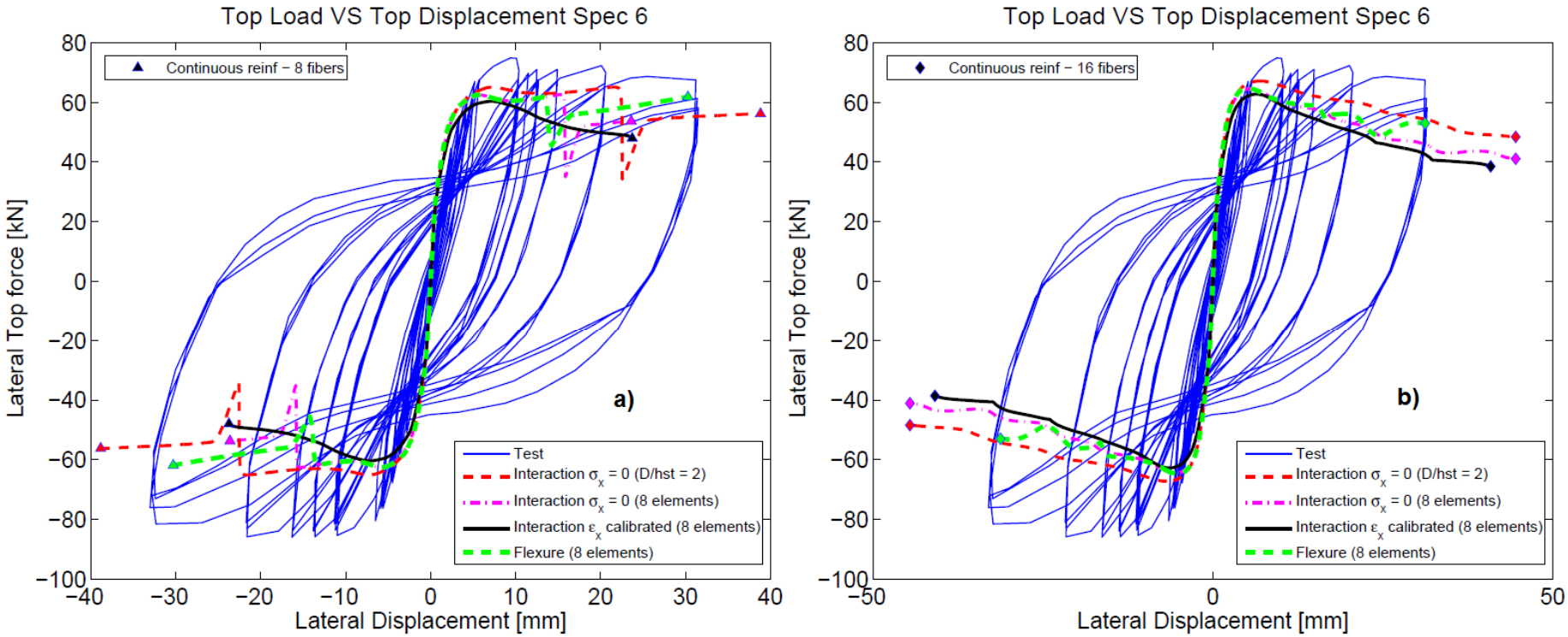

Figure B.6: Load - Displacement responses for all models using a) 8 fibers and b) 16 fibers. Specimen 6.

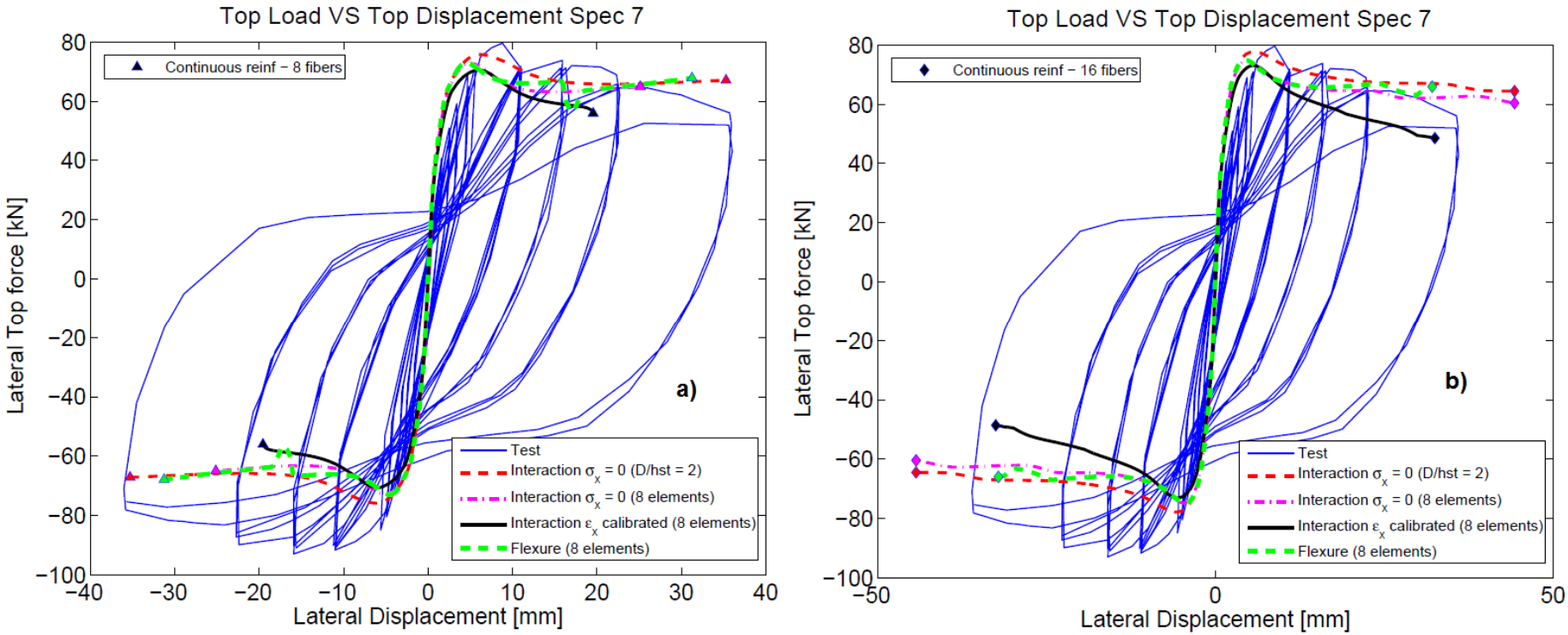

Figure B.7: Load - Displacement responses for all models using a) 8 fibers and b) 16 fibers. Specimen 7.

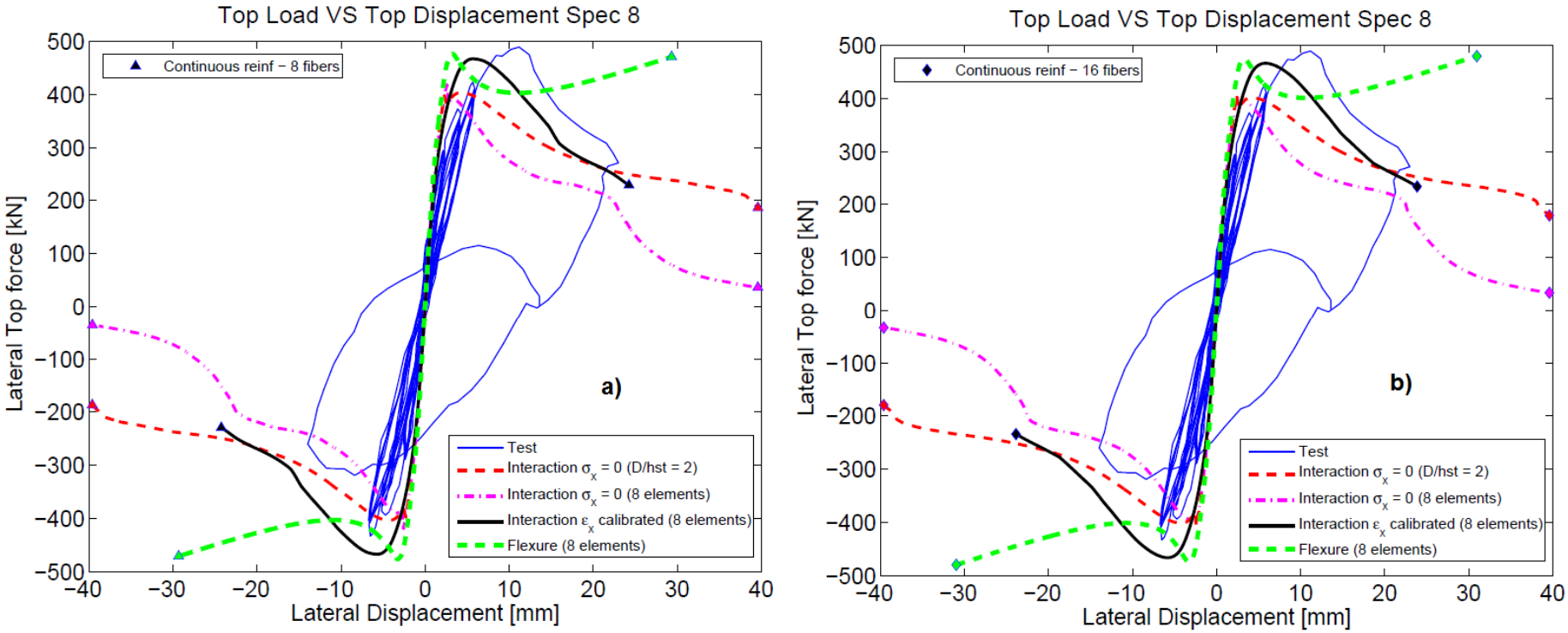

Figure B.8: Load - Displacement responses for all models using a) 8 fibers and b) 16 fibers. Specimen 8.

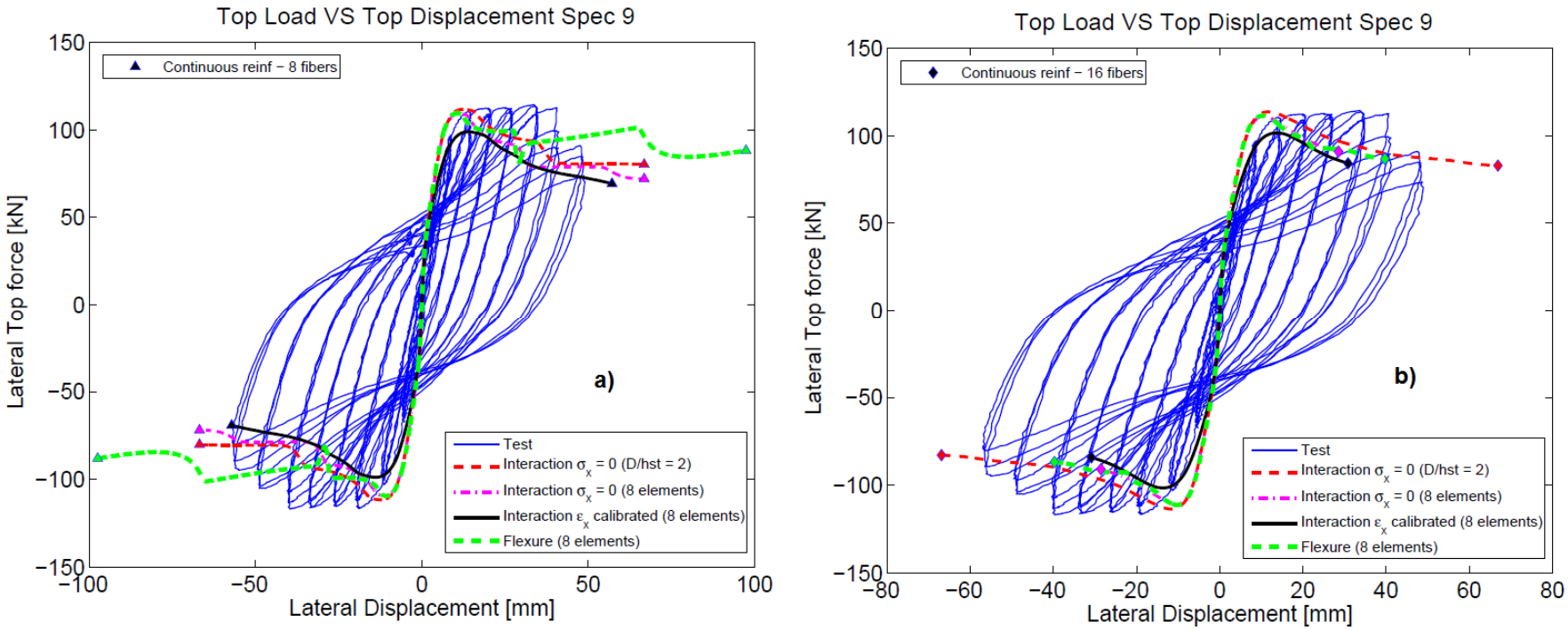

Figure B.9: Load - Displacement responses for all models using a) 8 fibers and b) 16 fibers. Specimen 9.

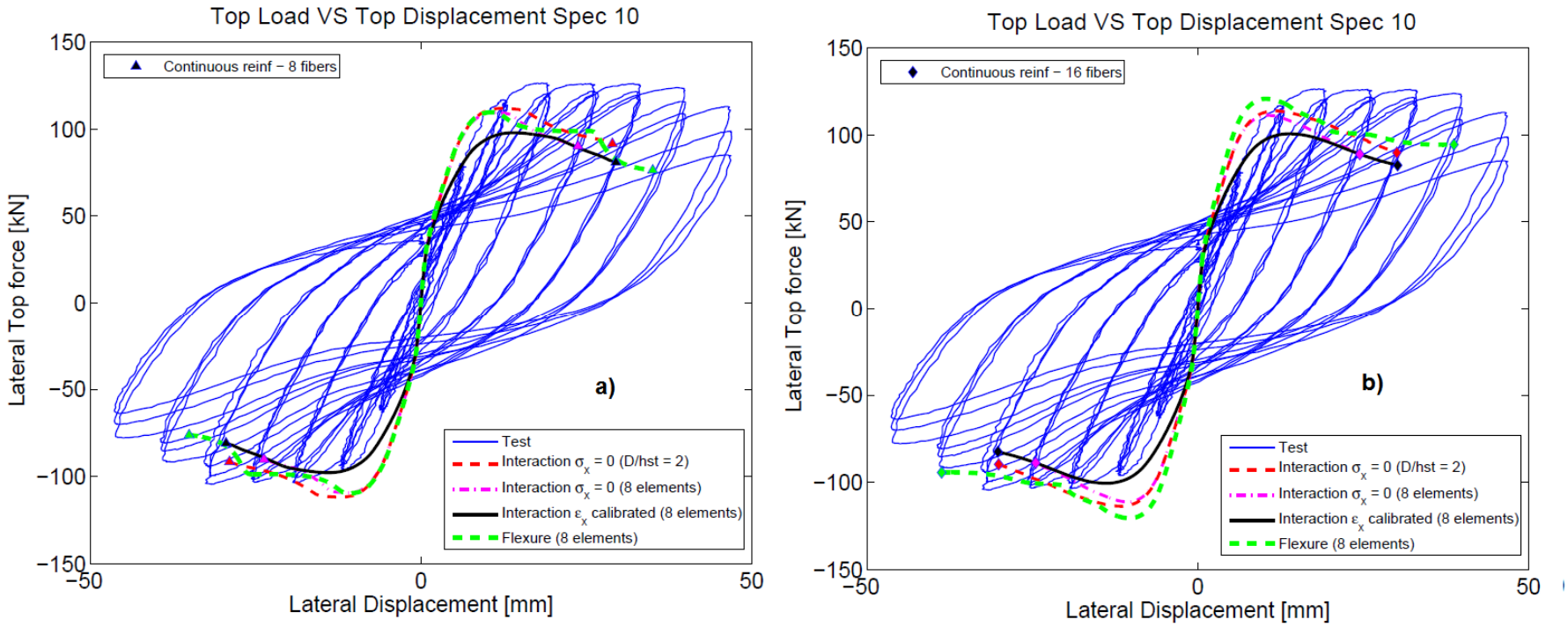

Figure B.10: Load - Displacement responses for all models using a) 8 fibers and b) 16 fibers. Specimen 10.

APPENDIX C

The following figures show the confined concrete material curves used in modeling columns. The confined concrete response incorporated is the Thorendfeldt base curve, calibrated to the Saatcioglu and Razvi (1992) model.

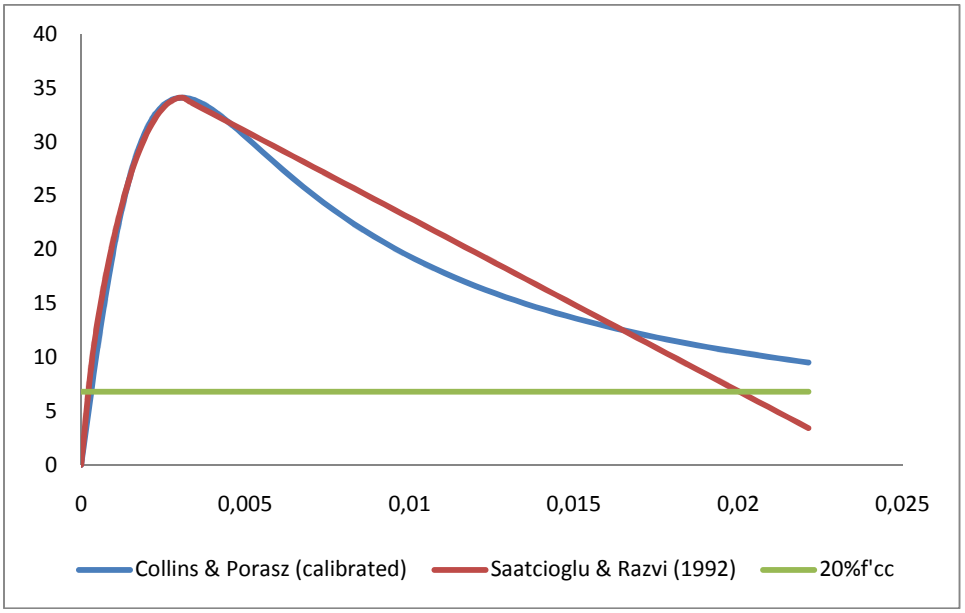

Figure C.1: Collins & Porasz model calibrated to Saatcioglu and Razvi (1992). Specimen 1.

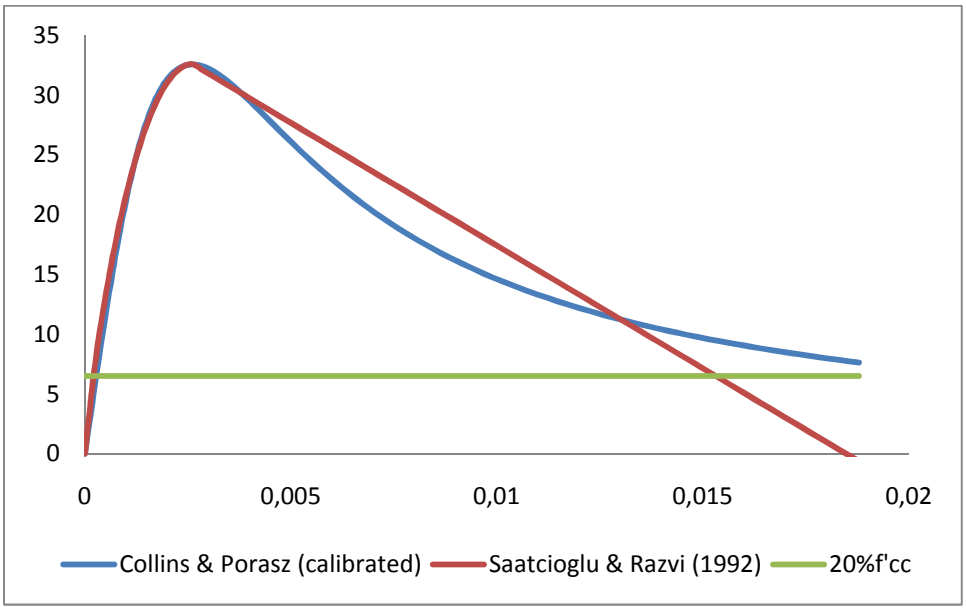

Figure C.2: Collins & Porasz model calibrated to Saatcioglu and Razvi (1992). Specimen 2.

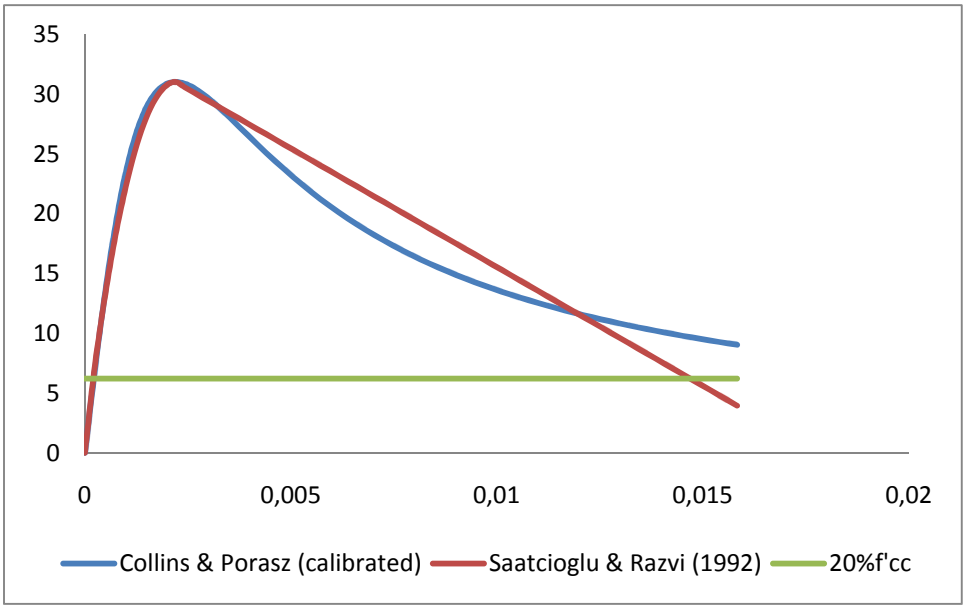

Figure C.3: Collins & Porasz model calibrated to Saatcioglu and Razvi (1992). Specimen 3.

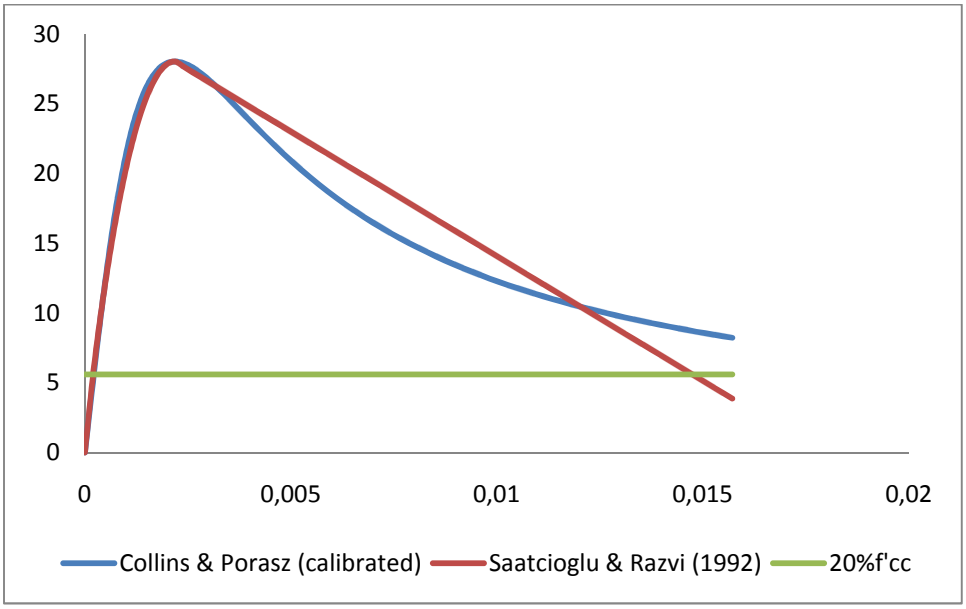

Figure C.4: Collins & Porasz model calibrated to Saatcioglu and Razvi (1992). Specimen 4.

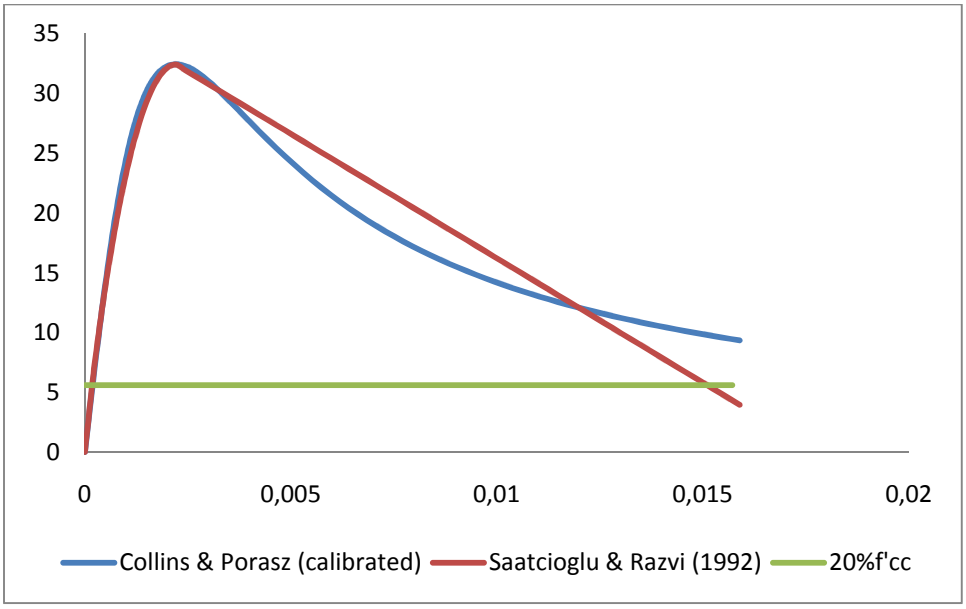

Figure C.5: Collins & Porasz model calibrated to Saatcioglu and Razvi (1992). Specimen 5.

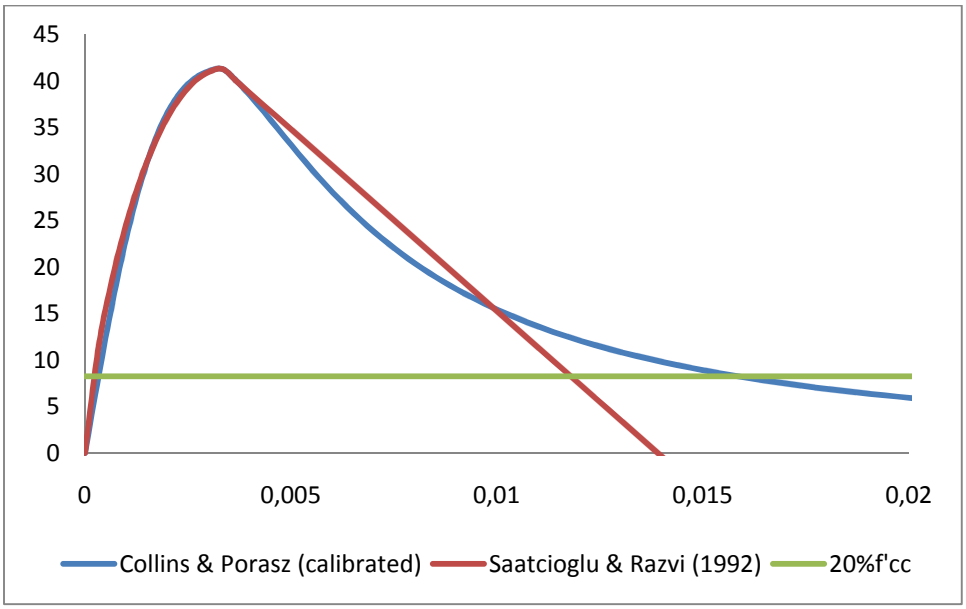

Figure C.6: Collins & Porasz model calibrated to Saatcioglu and Razvi (1992). Specimen 6.

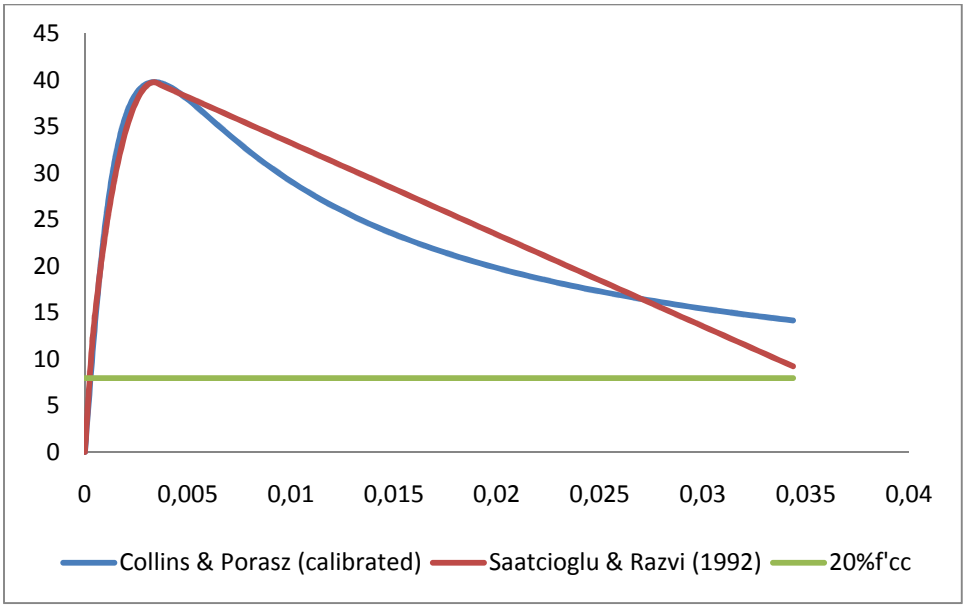

Figure C.7: Collins & Porasz model calibrated to Saatcioglu and Razvi (1992). Specimen 7.

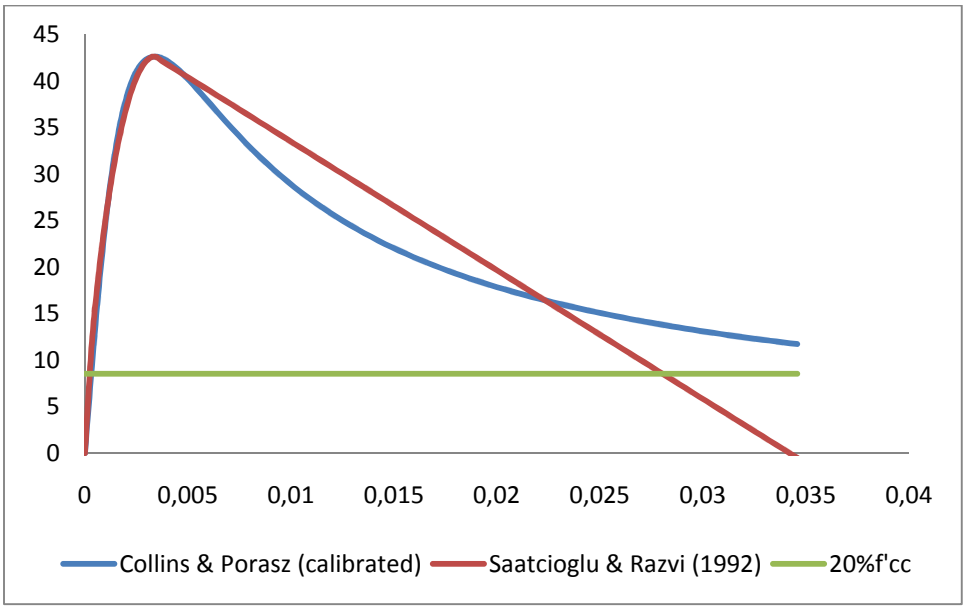

Figure C.8: Collins & Porasz model calibrated to Saatcioglu and Razvi (1992). Specimen 8.

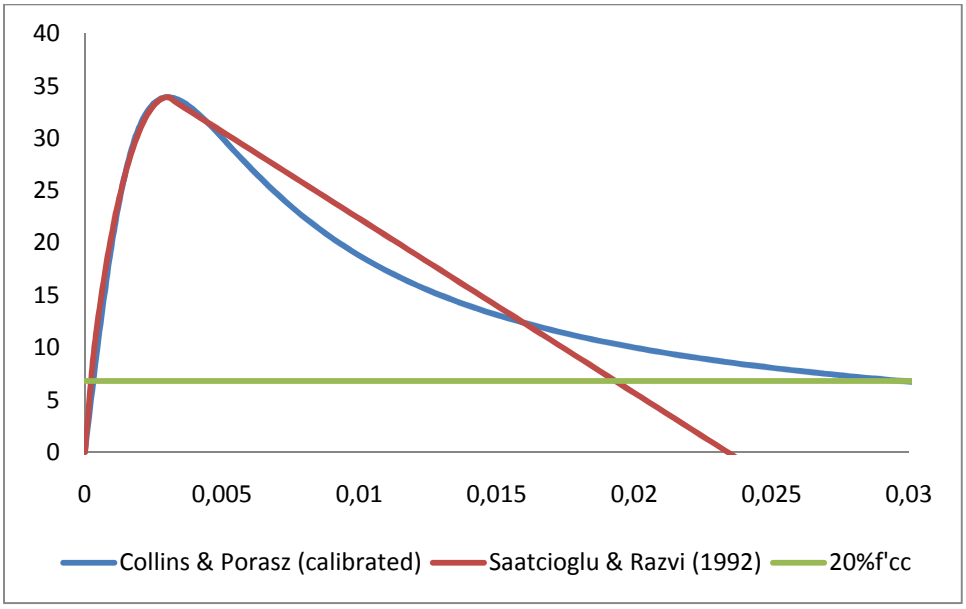

Figure C.9: Collins & Porasz model calibrated to Saatcioglu and Razvi (1992). Specimen 9.

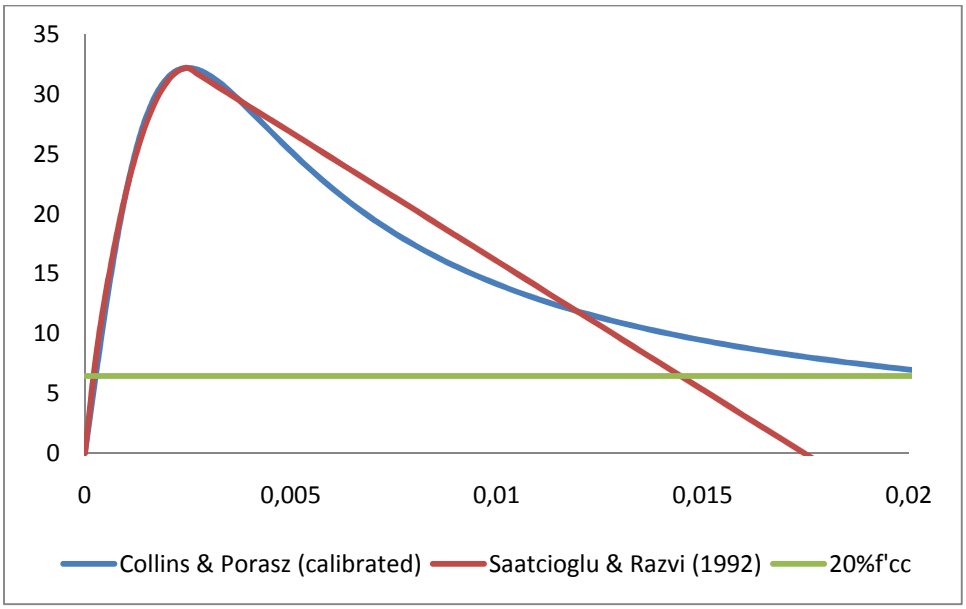

Figure C.10: Collins & Porasz model calibrated to Saatcioglu and Razvi (1992). Specimen 10.

APPENDIX D

The following figures show the load – displacement responses of the column specimens for the sensitivity analysis of confinement effectiveness and sensitivity analysis of lateral reinforcement.

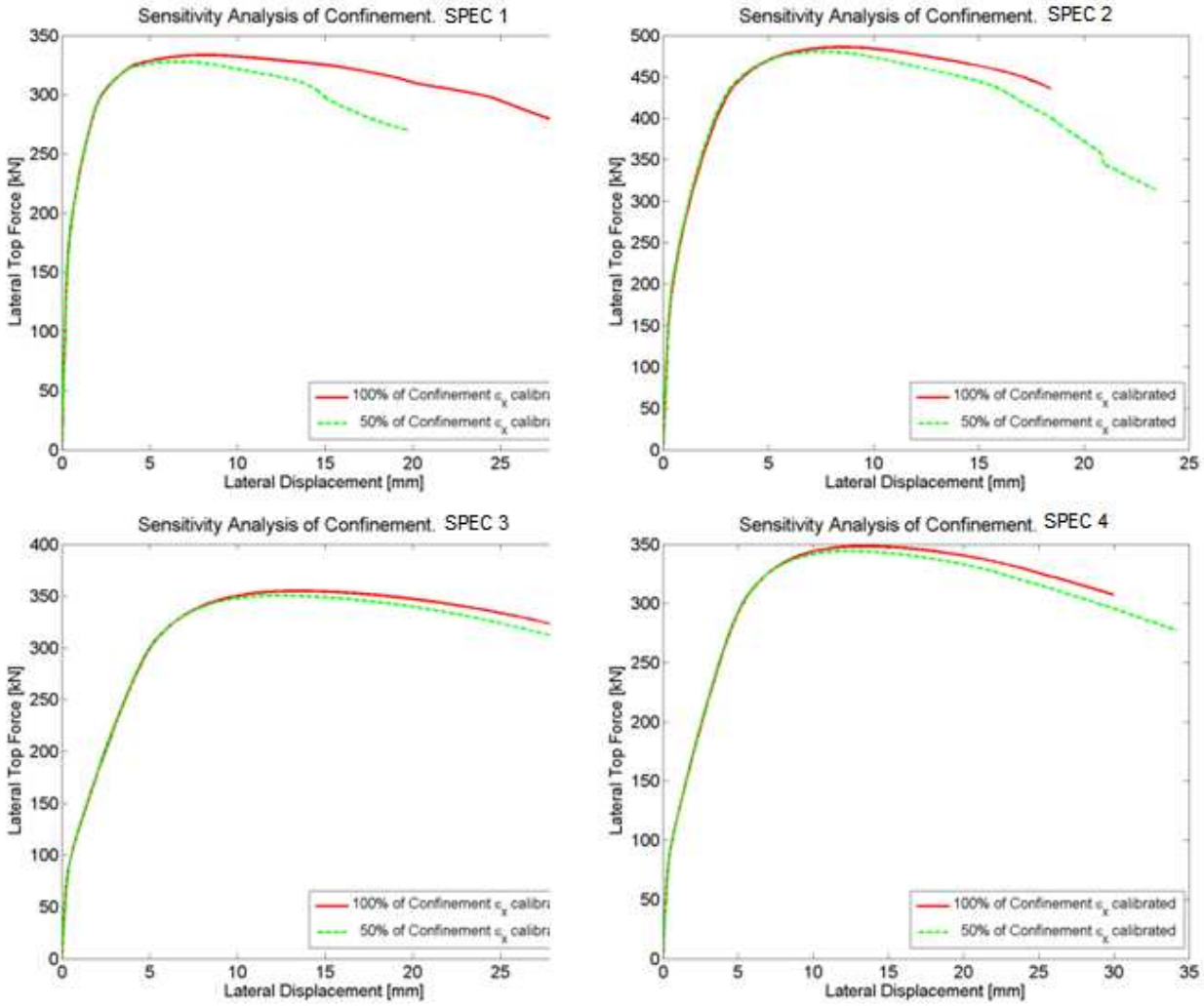

Figure D.1: Load – Displacement responses for specimens 1, 2, 3 and 4. Sensitivity analysis of confinement.

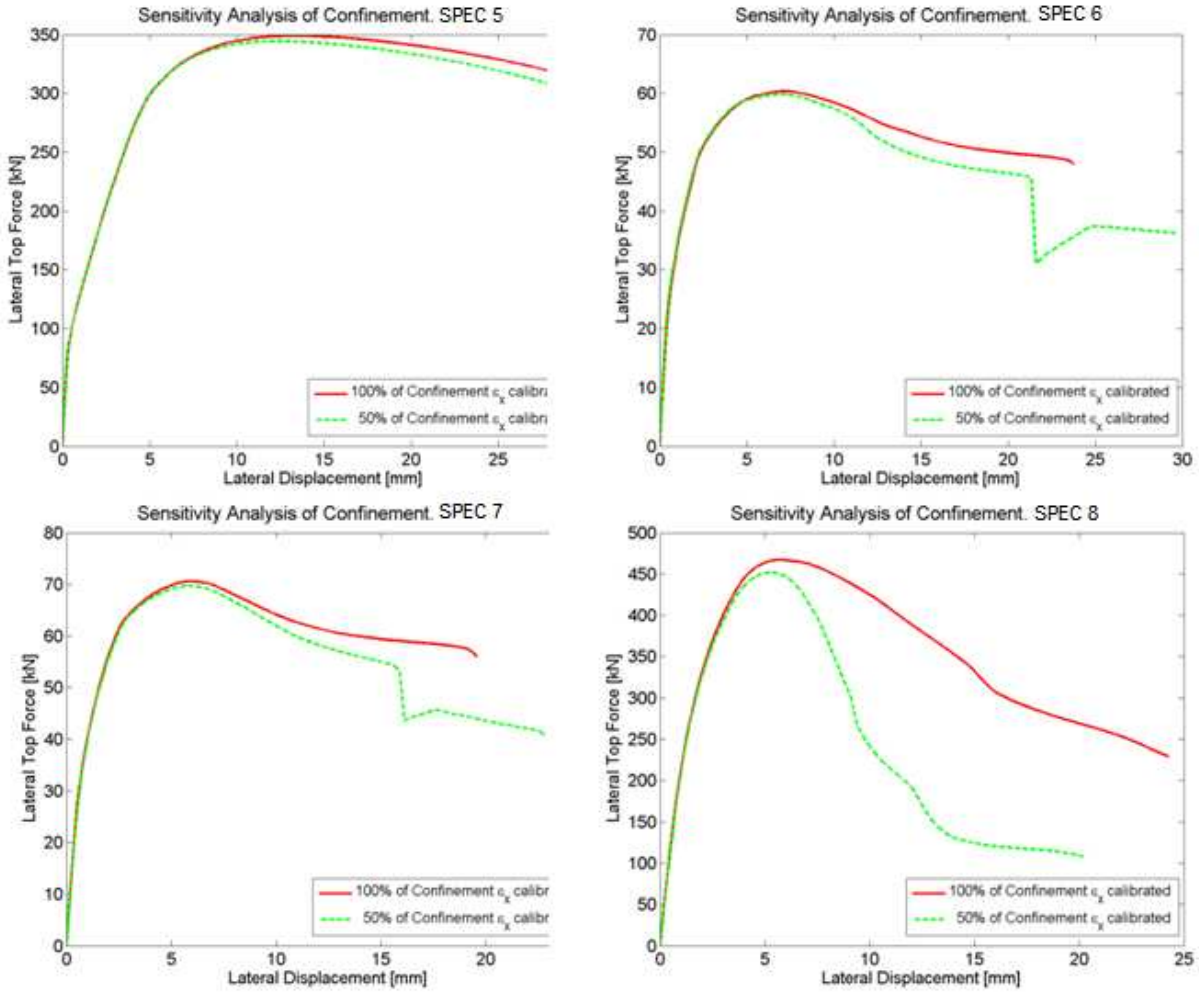

Figure D.2: Load – Displacement responses for specimens 5, 6, 7 and 8. Sensitivity analysis of confinement.

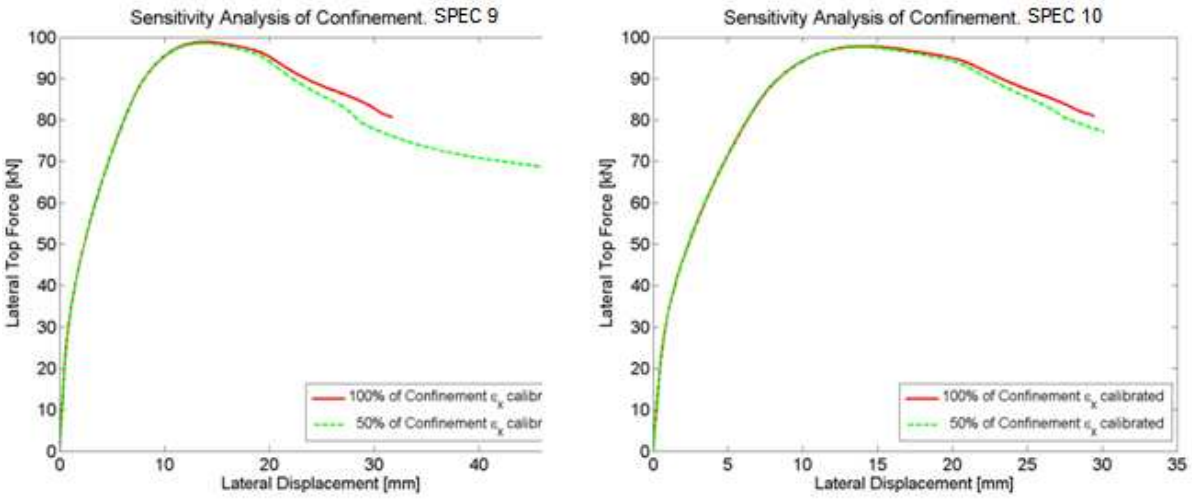

Figure D.3: Load – Displacement responses for specimens 9 and 10. Sensitivity analysis of confinement.

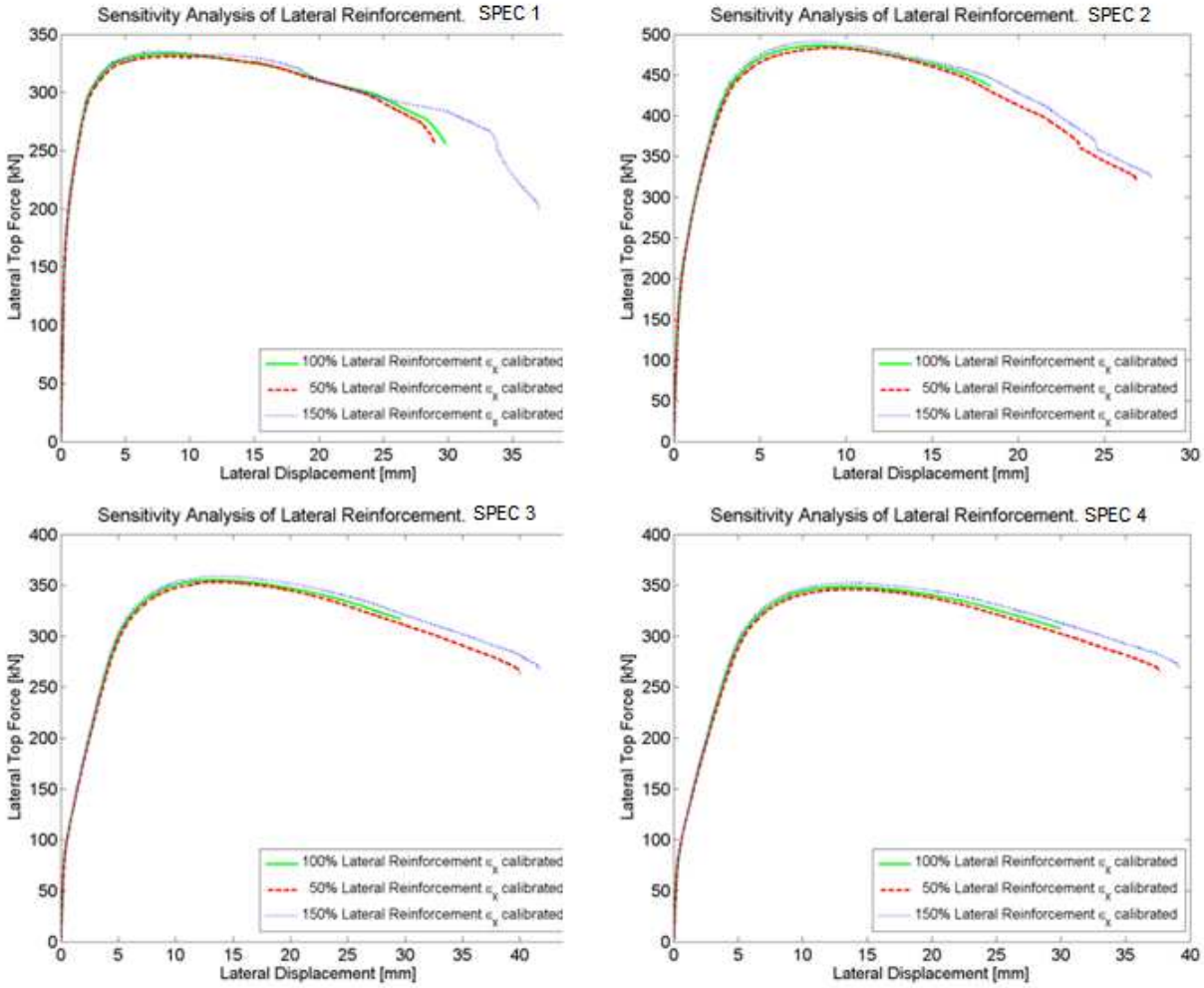

Figure D.4: Load – displacement responses for specimens 1, 2, 3 and 4. Sensitivity analysis of lateral reinforcement.

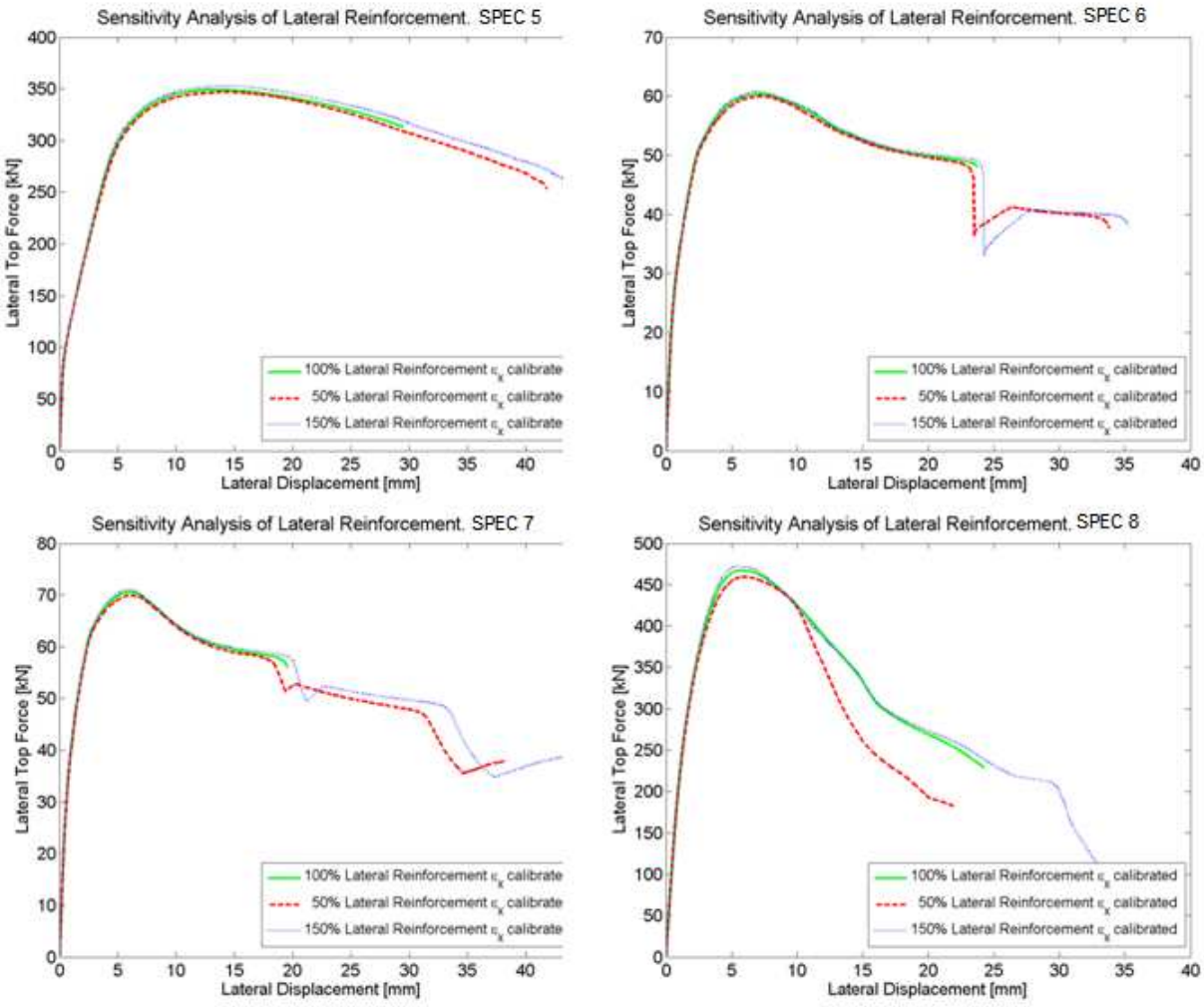

Figure D.5: Load – displacement responses for specimens 5, 6, 7 and 8. Sensitivity analysis of lateral reinforcement.

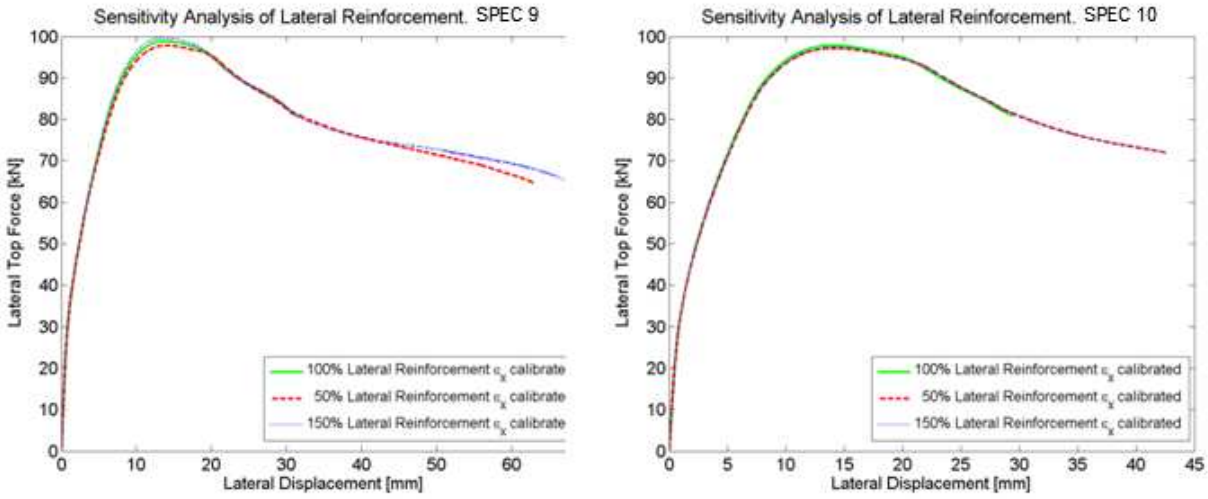

Figure D.6: Load – displacement responses for specimens 9 and 10. Sensitivity analysis of lateral reinforcement.

APPENDIX E

In this section, the load – displacement responses obtained in each step of the fitting procedure described in section 5.3, are shown for flexure and interaction models.

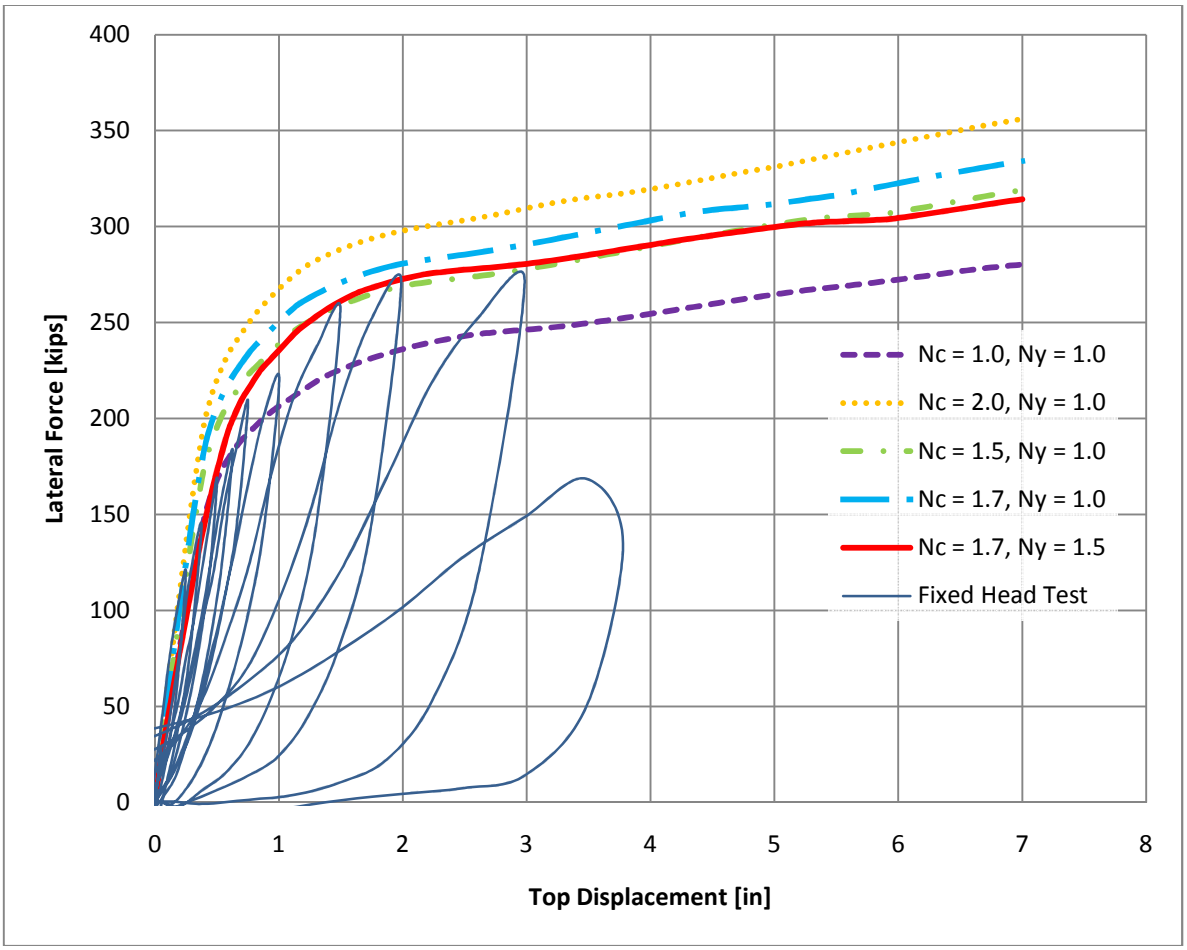

Figure E.1: Load – displacement responses obtained in each step of the fitting procedure for the flexure model. The values of $\mathbf{N_c}$ and $\mathbf{N_y}$ are shown.

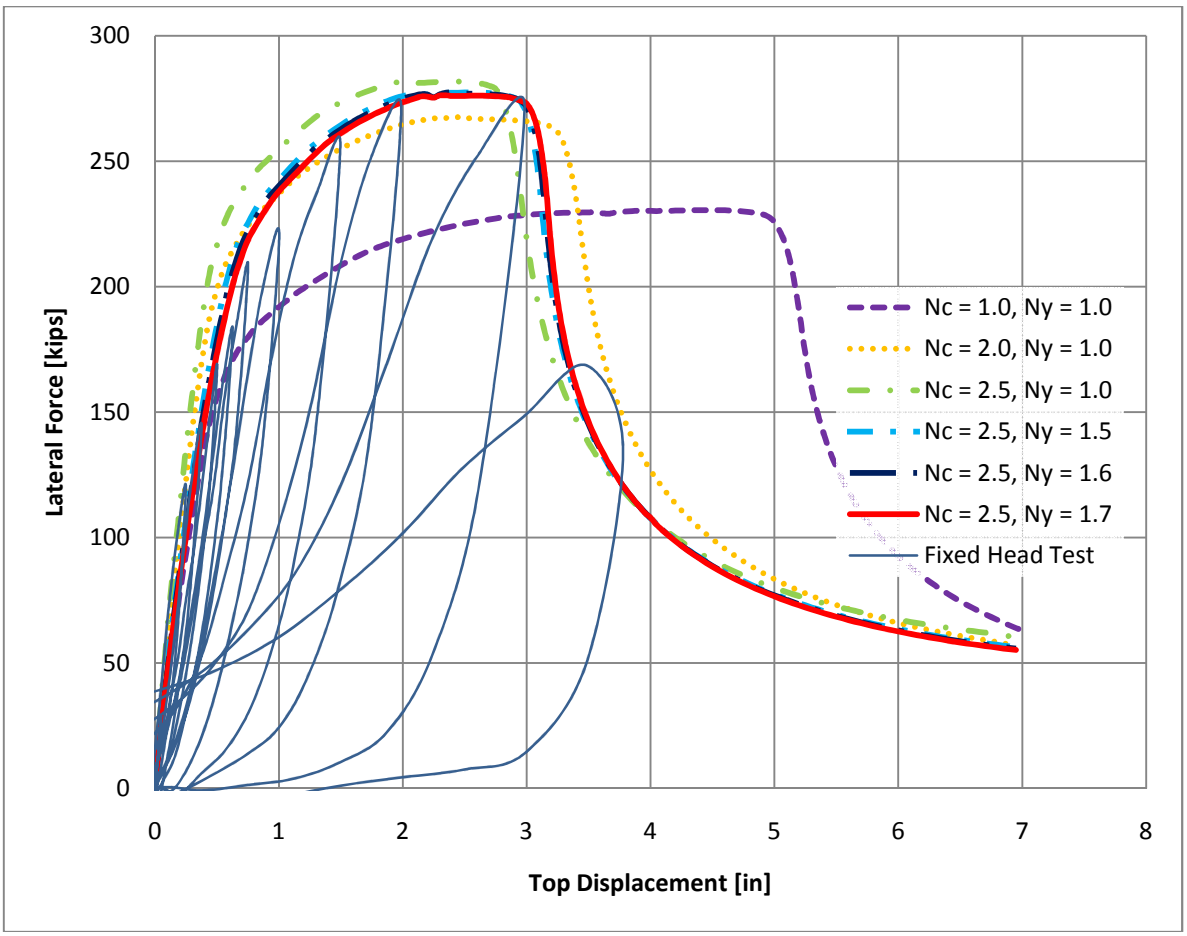

Figure E.2: Load – displacement responses obtained in each step of the fitting procedure for the interaction model. The values of $\mathbf{N_c}$ and $\mathbf{N_y}$ are shown.

APPENDIX F

The results of sensitivity analyses performed for the Fixed – Head pile are shown in this section.

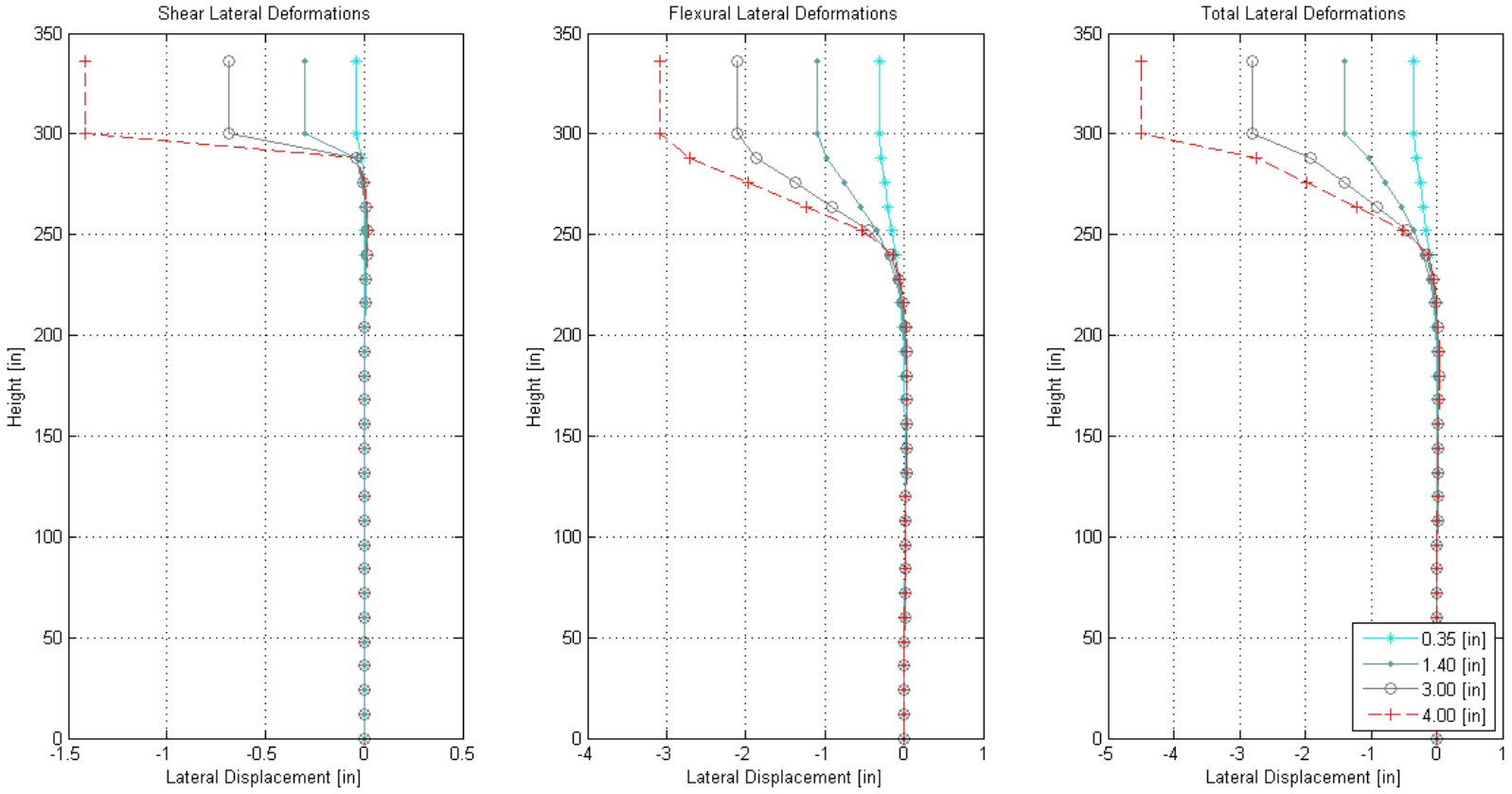

Figure F.1: Displacement profiles for different top displacements. Sensisivity analysis of 50% of longitudinal reinforcement.

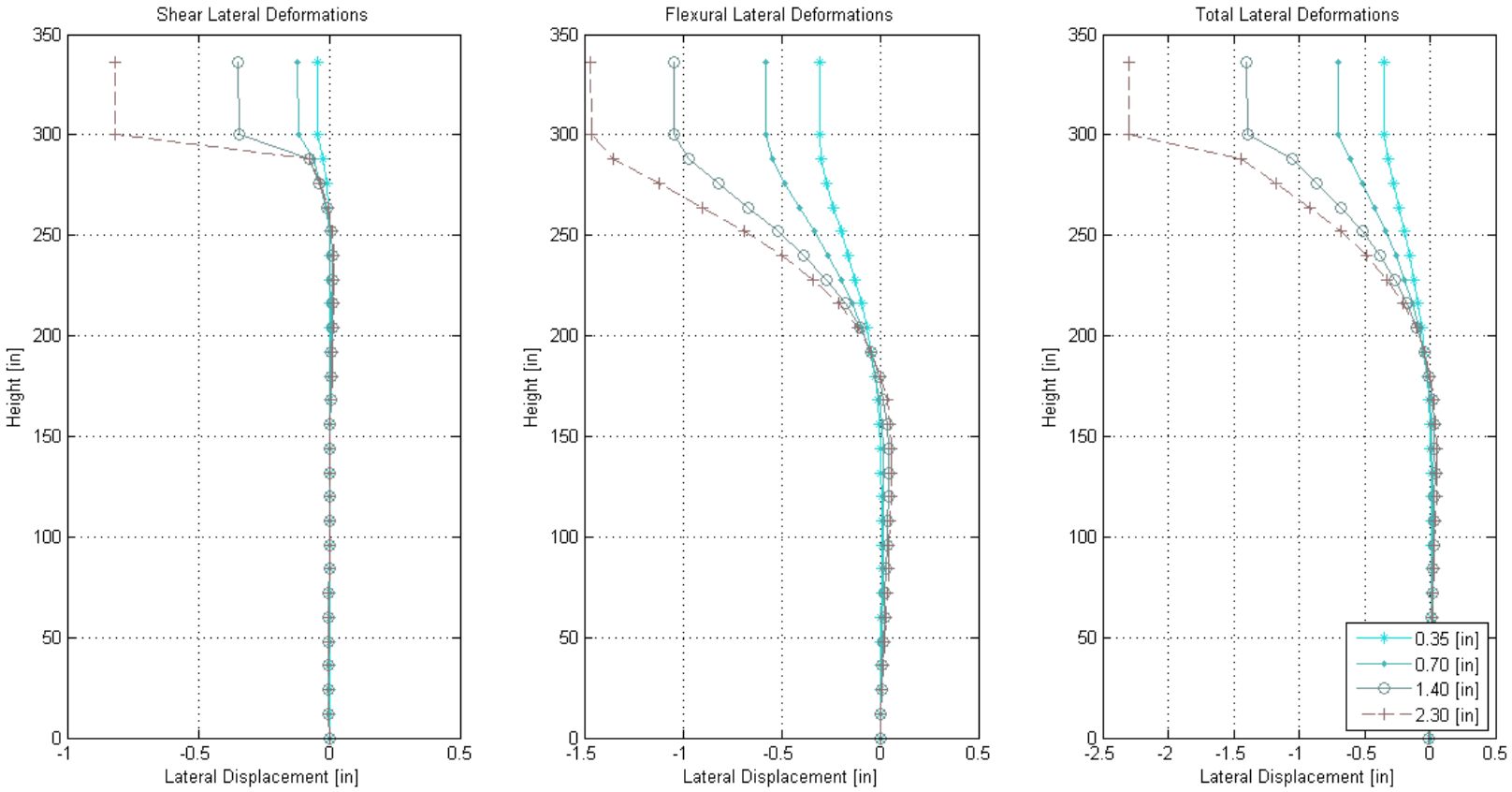

Figure F.2: Displacement profiles for different top displacements. Sensisivity analysis of 150% of longitudinal reinforcement.

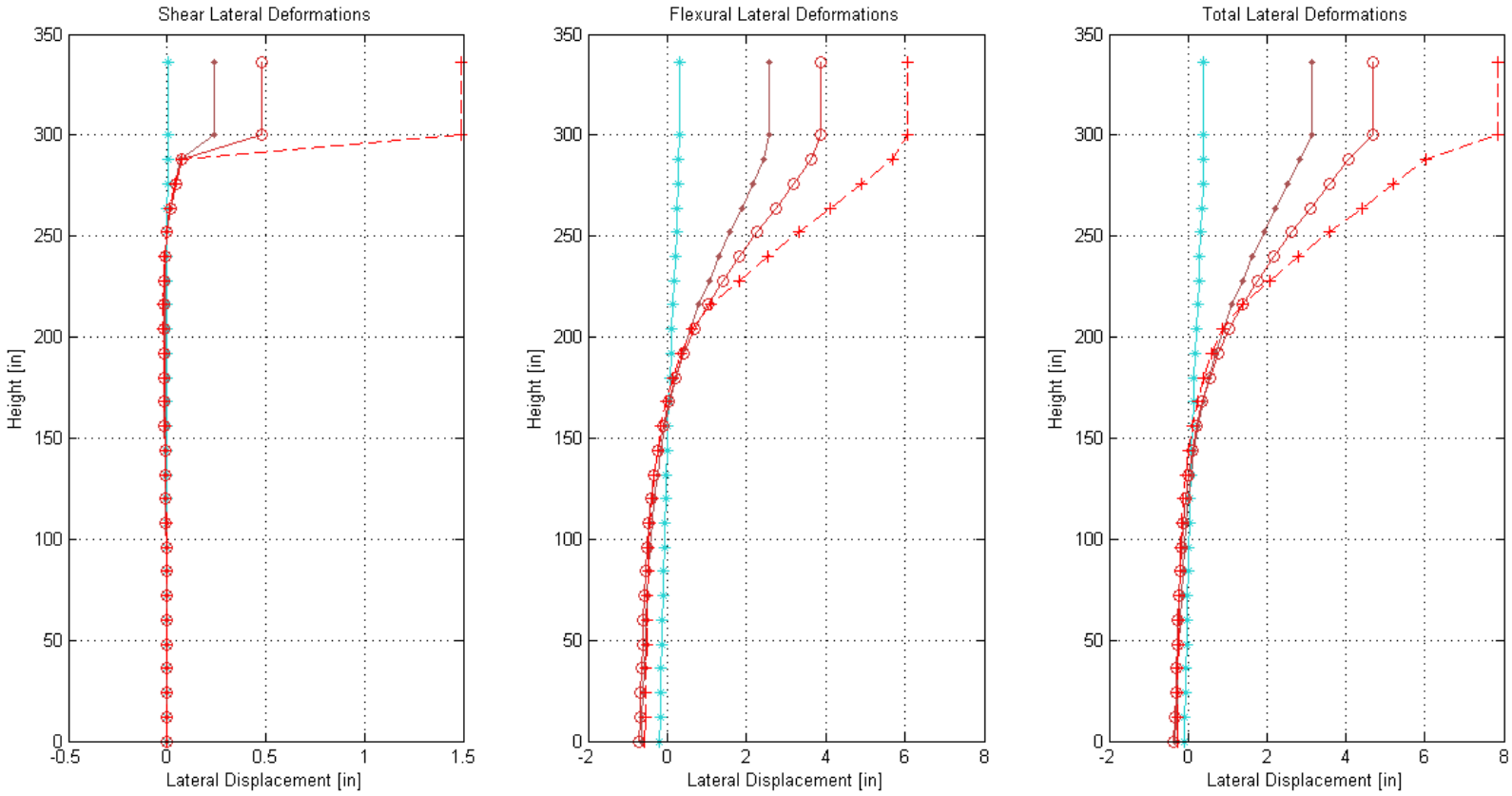

Figure F.3: Displacement profiles for different top displacements. Sensisivity analysis of soil quality.

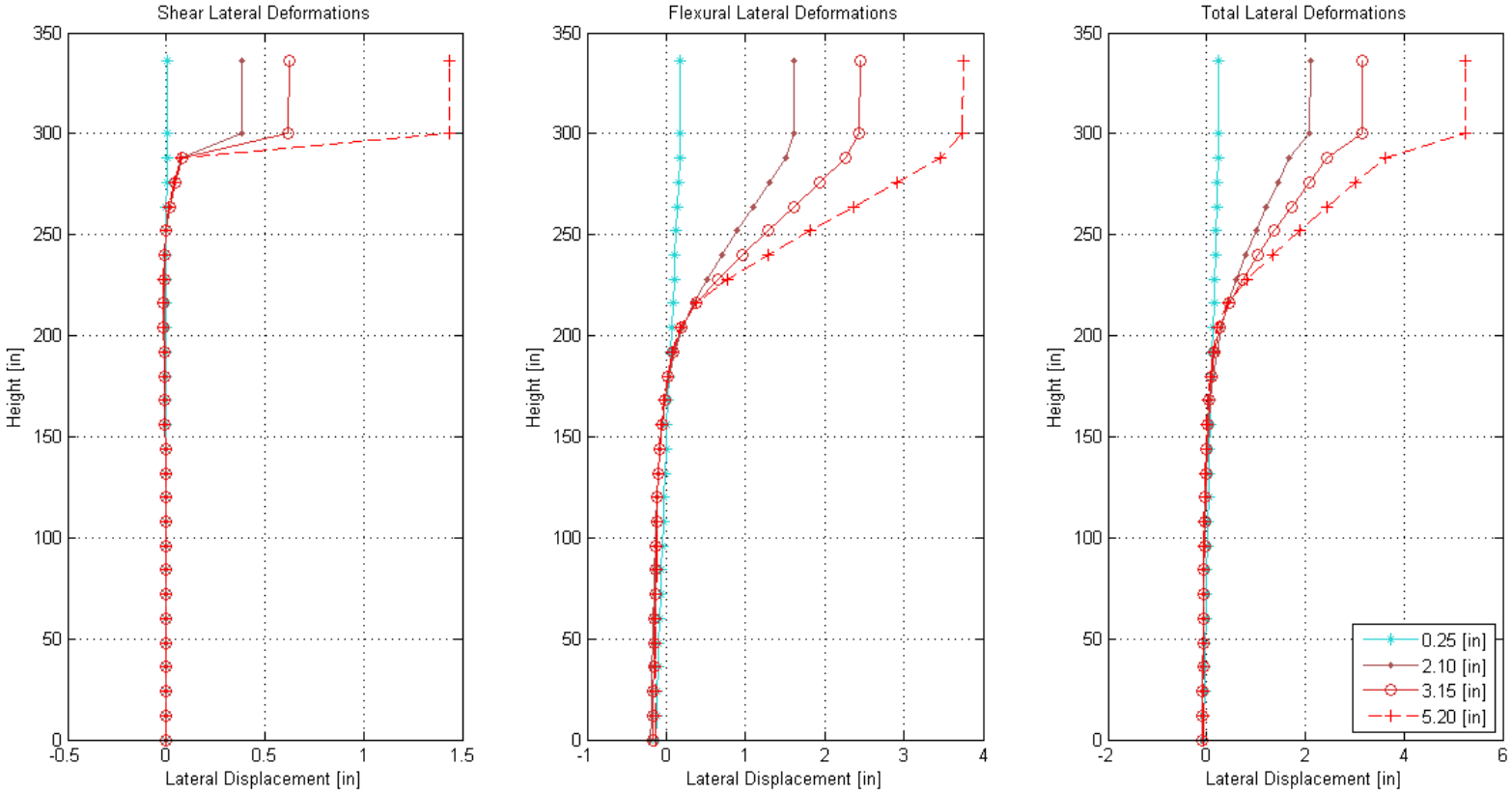

Figure F.4: Displacement profiles for different top displacements. Sensisivity analysis of pile diameter.

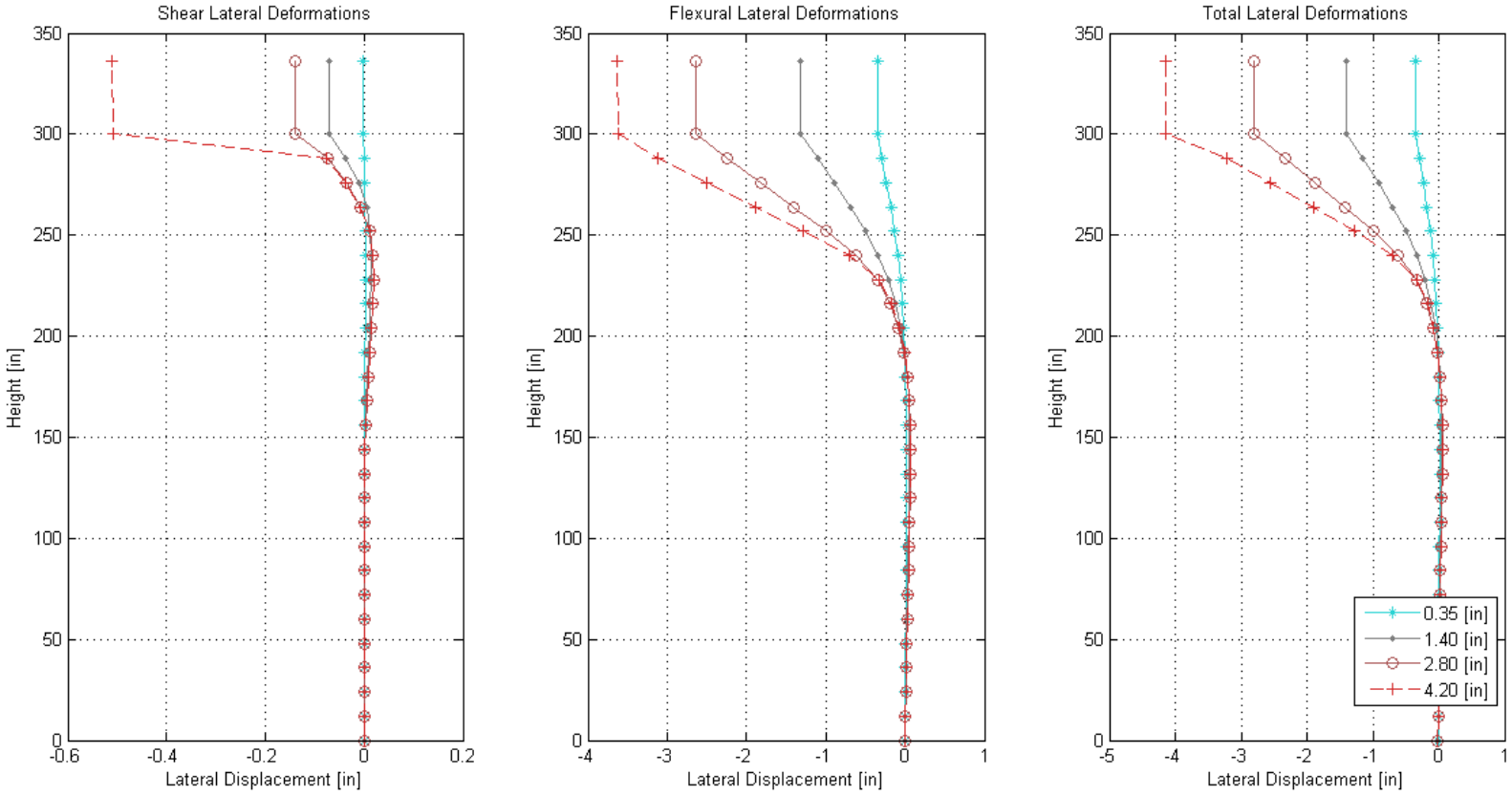

Figure F.5: Displacement profiles for different top displacements. Sensisivity analysis of 10% of $\mathbf{K_s}$, rotational spring analysis.

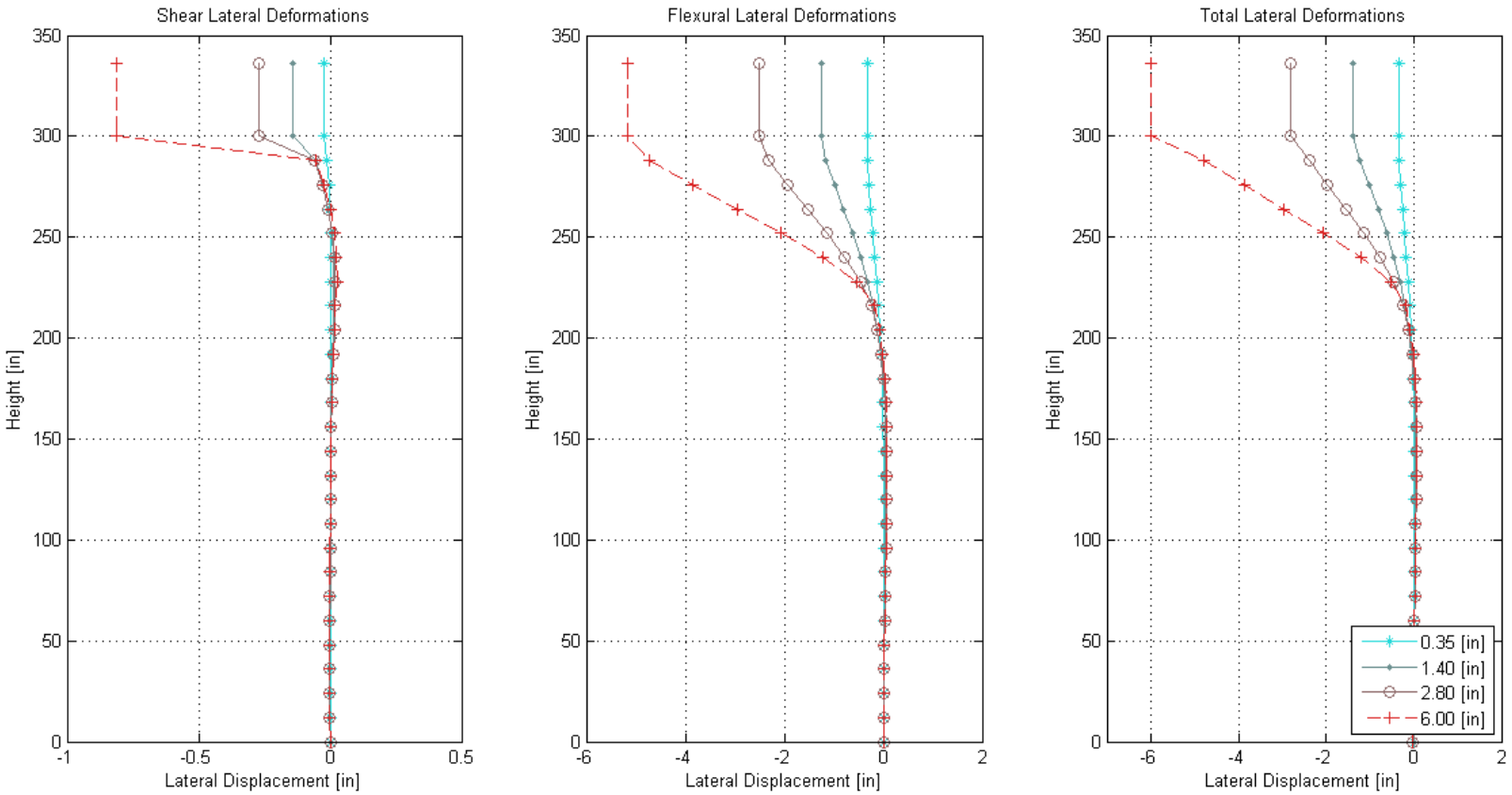

Figure F.6: Displacement profiles for different top displacements. Sensisivity analysis of lateral reinforcement.